



School of Applied Sciences

Department of Environmental Science and Technology
Centre for Automotive Technology

Localised low velocity impact performance of FLAX/PLA biocomposites

Nassiopoulos Elias

Supervisor: Dr. James Njuguna
Co-Supervisor: Dr. James Brighton

Cranfield,
June 2015

Abstract

Natural fibre composites are fast emerging as a viable alternative to traditional materials and synthetic composites. Their low cost, lightweight, good mechanical performance and their environmentally friendly nature makes them an ideal choice for the automotive sector. The automotive industry has already embraced these composites in production of non-structural components. At present, however, research studies into composites made of natural fibres/bio-sourced thermoplastic resins are at infancy stage and such works are rare in the literature.

This study therefore focuses on the mechanical properties of poly(lactic) acid (PLA) flax reinforced composites for structural loaded components. The aim was to investigate the performance of flax/PLA biocomposites subjected to localized low velocity impacts. To start with, a detailed literature study was conducted covering biocomposites and PLA in particular. Next, a series of composite samples were manufactured. Morphological and thermal studies were also conducted in order to develop an in-depth understanding of their thermo-mechanical properties, including crystallinity, thermal response and their related transition temperatures. This was followed by localized impact studies. The influence of temperature, water uptake and strain rates to the material tensile strength and modulus, as well as the damage characteristics and limits that lead to failure were studied. Furthermore, in the present work different methods and existing material models to predict the response of biocomposites were assessed. A case study was then performed using these models to understand, develop and improve the side crash performance of a superlight city car prototype.

The strength and stiffness of flax/PLA samples studied indicated a very promising material to replace traditional choices in load bearing applications. Strength of 72 MPa and a 13GPa tensile modulus were obtained. However, changes in temperature significantly affected the flax/PLA properties. At 50°C the stiffness was reduced 52%, and the ultimate strength was reduced significantly. Strength and modulus were found to increase with increasing strain rates, while elongation at break were reduced respectively.

II

Low velocity impact study of the flax/PLA bio-composite samples using a 20g flying projectile at different impact energies shows very interesting results. At 10 m/s impact velocities the absorbed energy in the specimens was 20%, whilst for the 20 m/sec tests, approximately 52% and 68% respectively. This caused damage of the composite through cracking, fibre and matrix failure, visible through the visual inspection. Ultrasonic C-scanning showed no delamination for the samples tested, as the material failure is vertical to the plate surface. In contrast with the reference samples, the samples tested at higher temperatures showed only micro-cracking and discoloration. Ultrasonic inspection, however, revealed significant internal damage of the samples tested at 45 and 65°C. For the samples submerged into water, cracks did not form initially, but a significant deformation of the whole sample was observed.

The impact energy absorbed during the impact increased with increasing testing temperature. Also at already 5% moisture content the energy absorbed increased from 50 to 70%; however this number did not increase further at higher moisture contents. The testing temperature had no effect on the compressive modulus of the material, explained by the fact that as the damage was localized and did not affect the in-plane properties, the loading was transferred through the unaffected areas. In contrast, the higher the moisture content was, the lower was the remaining material modulus.

FE analysis gave accurate representation of the material behaviour under different loading conditions. Modelling at component level showed that flax/PLA biocomposites can be used as structural components in the automotive sector offering high specific modulus and strength, as well as impactability, and can therefore replace man-made composites. The design however has to take into account the non-linear stress-strain behaviour of the material caused by material viscosity and internal damage accumulation.

To my mother

Acknowledgments

I would like to thank Dr. James Njuguna for his excellent supervision and support throughout these years. His support and belief were essential to face the challenges. Thanks for making this your personal commitment James.

I would like to acknowledge the European Commission for funding this study under the Project Ecoshell, and all the project partners that were involved in this project, for sharing their experience and knowledge. Special thanks to Christophe Avril from MahyTec for all the samples, his great advice and help, Christoph Keckl from ICT Franuhofer for his advice and the walks around Madrid, and Dr. Kambiz Kayvantash for pushing, questioning and steering me towards a better work.

Further, I would like to thank Dr. James Brighton for his support these last years, not giving up on me, and for his always simply great advice; A truly special thanks to Clive Temple for all his trust, the opportunities he gave me, and for including me in his group and activities. Dr. Kim Blackburn for being always next to me in all the hard technical matters and for not just solving them but giving me the knowledge to tackle them; Savina Velotta for all her help with my traveling and papers, and for being always smiley.

I would also like to dedicate a very special thanks to Laura Gendre for being the best colleague I could ever ask for, for the help with my work, for the understanding and our time in the lab. Thanks also to Ian Butterworth for being a great friend, Jinchun Zhu and Rishi Abhyankar, for being great colleagues.

A big thanks to my Greek gang, for spending an unforgettable time together besides the difficulties and peculiarity of the place. Perikli, Paulo, Pano, Kosti,, Xristara, Giorgo, Taso, Ntino, Stelio, Dimitra, Andrea, Xristo, Stefania, thanks to all of you for giving me good memories. Asteri and Gianni, I couldn't have made it without you.

Thanks also to Joe for his support and help through those very hard last months.

I would finally like to thank my family for always being behind me; without their continued encouragement and support I could not have completed this thesis. My last and biggest thanks to my mother, for sculpturing my life with her thought.

Nomenclature

Symbols

E	Elastic modulus
σ	Stress
ε	Strain
$\dot{\varepsilon}$	Strain rate
T_g	Glass transition temperature
T_m	Melting temperature
T_{cc}	Cold crystallisation temperature
X_c	Degree of crystallinity

Acronyms

EU	European Union
ELV	End-of-life-vehicle directive
SMC	Sheet moulding compound
RTM	Resin transfer moulding
BMC	Bulk moulding compound
MAPP	Maleic anhydride grafted polypropylene

VII

LDPE	Low density polyethylene
PP	Polypropylene
PLA	Poly(lactic) acid
DMA	Dynamic mechanical analysis
DSC	Differential scanning calorimetry
SEM	Scanning electron microscope
ASTM	American Society for Testing and Materials
EVO	Epoxidized vegetable oils
GHG	Greenhouse gases

Chemical symbols and compounds

NaOH	Sodium hydroxide
CH ₃ COO-	Acetyl
C ₆ H ₅ C=O	Benzoyl chloride
C ₃ H ₃ N	Acrylonitrile

Units

MPa	Megapascal
GPa	Gigapascal
°C	Degree Celsius
cm	Centimeter
mm	Millimeter

VIII

h	Hour
min	Minute
g	Gram
kg	Kilogram
l	Litre
J	Joule
%	Percentage

Table of Content

Abstract.....	I
Table of Content.....	IX
List of Figures.....	XIII
List of Tables.....	XVIII
Chapter 1. Introduction.....	1
1.1 Background.....	1
1.2 Motivation.....	2
1.3 Aims and Objectives.....	4
1.4 Methodology.....	5
1.5 Thesis Structure.....	7
Chapter 2. Literature Review.....	9
2.1 Historical overview.....	9
2.2 Advantages and disadvantages.....	11
2.3 Natural fibres.....	12
2.3.1 Structure.....	13
2.3.2 Chemical composition.....	15
2.3.3 Mechanical properties.....	18
2.3.4 Fibre Modifications.....	19

2.3.5	Flax fibres	24
2.4	Resins	26
2.4.1	Poly (lactic acid).....	28
2.5	Characterization of natural fibre composites.....	29
2.5.1	Stiffness & Strength	29
2.5.2	Impact performance	31
2.6	Modelling natural fibre composites	32
2.6.1	Modelling composite materials.....	33
2.7	Applications of biocomposites	36
2.8	Conclusions and scope for research in light of literature review	40
Chapter 3.	Structural performance of flax/PLA natural fibre biocomposites	42
3.1	Introduction.....	42
3.2	Materials and methods.....	44
3.2.1	Materials	44
3.2.2	Characterisation.....	45
3.2.3	Mechanical testing	46
3.3	Results and discussion.....	47
3.3.1	Microscopy.....	47
3.3.2	DMA	49
3.3.3	DSC	51
3.3.4	Tensile tests.....	54
3.3.5	Degree of crystallinity.....	58
3.3.6	Influence of temperature.....	61
3.3.7	Strain rate effect.....	65
3.4	Conclusions.....	67
Chapter 4.	Low velocity impact properties and strength after impact performance of flax/PLA biocomposites	70

4.1	Introduction.....	70
4.2	Materials and methods.....	73
4.2.1	Materials	73
4.2.2	Impact testing.....	74
4.2.3	Compression after Impact (CAI).....	76
4.3	Results and discussion.....	77
4.3.1	Impact properties.....	77
4.3.2	Strength after Impact.....	87
4.4	Conclusions.....	89
Chapter 5. Influence of temperature and moisture on the impact performance of flax/PLA biocomposites		91
5.1	Introduction.....	91
5.2	Materials and methods.....	93
5.2.1	Materials	93
5.2.2	Water absorption test.....	93
5.2.3	Impact testing	94
5.3	Results and discussion.....	95
5.3.1	Absorption behaviour.....	95
5.3.2	Impact testing	98
5.3.3	Strength after impact.....	103
5.4	Conclusions.....	105
Chapter 6. Flax/PLA biocomposites application for superlight city car - a case study on side impact analysis to meet EuroNCAP Regulation.....		107
6.1	Introduction.....	107
6.2	Modeling Natural fibre composites - an overview.....	110
6.3	Experiments.....	114
6.3.1	Materials and samples preparation.....	114

6.3.2	Tensile and impact testing.....	114
6.4	Modelling.....	115
6.5	Models set up.....	116
6.5.1	Tensile and gas gun impact modelling.....	116
6.5.2	Side impact car model.....	118
6.6	Results and discussions.....	121
6.6.1	Model Calibration results.....	121
6.7	Car side impact performance.....	125
6.8	Conclusions.....	130
Chapter 7.	Conclusions and future work.....	132
	Achievements.....	137
	Bibliography.....	139
	Appendix A.....	i
	Appendix B.....	viii
	Appendix C.....	xvii

List of Figures

Figure 1-1: Schematic illustration of the gap in current knowledge on flax/PLA biocomposites	4
Figure 1-2: Workflow of thesis methodology	6
Figure 2-1: Henry Ford testing with an axe soy-bean based plastics [7]	10
Figure 2-2: Quantity of natural fibres used in the European industry per year and prediction for 2020 [9]	11
Figure 2-3: Use of natural fibres in the German automotive industry between 1999 and 2005 [9]	11
Figure 2-4: Classification of natural fibres	13
Figure 2-5: Schematic representation of flax fibre – from stem to elementary fibres.....	14
Figure 2-6: Structure of an elementary plant fibre.....	15
Figure 2-7: Representation of plant fibre [16].	15
Figure 2-8: Chemical structure of cellulose	16
Figure 2-9: Young modulus and specific Young modulus of the most commonly used natural fibres	19
Figure 2-10: Tensile and specific tensile strength of the most commonly used natural fibres	19
Figure 2-11: Classification of polymers with respect to their source of origin and their degradability.....	27
Figure 2-12: (a) Macro-, (b) meso- and (c) micro-scale modeling approach	34

Figure 2-13: Mercedes C-class components made of different natural-fibre composites (www.dottal.org)	37
Figure 2-14: Four Motors GmbH green racer; the body-shell is made of plant fibre reinforced composites.....	37
Figure 2-15: The Grasshopper	38
Figure 2-16: Fiat EcoBasic (www.fiat.co.uk)	38
Figure 3-1: Laser extensometer method: experimental setup [58]	47
Figure 3-2: Overview of the fracture surfaces of flax/PLA tensile specimens	48
Figure 3-3: DMA runs for flax/PLA; Storage modulus and tan delta [tests performed at 1Hz frequency].....	50
Figure 3-4: Comparison of storage modulus and tan delta from DMA runs of flax/PLA and flax/epoxy composites [tests performed at 1Hz frequency].....	51
Figure 3-5: Effect of heating rate on DSC curves of flax/PLA	52
Figure 3-6: DSC thermograms with repetitive heating-cooling cycles.....	53
Figure 3-7: Heat flow as a function of time for repetitive heating-cooling cycles of flax/PLA.....	53
Figure 3-8: Tensile strength (a), and young modulus (b) for flax/PLA and flax epoxy composites.....	54
Figure 3-9: Stress-strain curve from tensile testing of flax/PLA and flax/epoxy	56
Figure 3-10: (a) Cyclic test for flax/PLA and (b) tensile modulus reduction as a function of strain due to damage accumulation during testing.....	57
Figure 3-11: Stress strain curve of annealed flax/PLA samples compared to original samples (as a function of X_c).....	58
Figure 3-12: Weight loss of flax/PLA due to drying for 1h at 50 °C and 110 °C	60
Figure 3-13: Detailed SEM photographs from (a) original flax/PLA samples compared to the surface of (b) annealed samples. The formation of cracks and the deterioration of the PLA's surface is visible. During testing, the crack growth results in breakage of the PLA (c). Poor interfacial adhesion was observed as the fibre surfaces were clean (d)....	61
Figure 3-14: Stress-strain curves of flax/PLA tested in room temperature (25 °C), 50 °C, 65 °C and 110 °C and nominal strain rate.....	62
Figure 3-15: Tensile modulus and ultimate strength of flax/PLA specimens as a function of temperature	64
Figure 3-16: Elongation at break as a function of temperature.....	64

Figure 3-17: Detailed SEM micrograph of flax fibres after testing of flax/PLA samples at 110 °C.....	65
Figure 3-18: Stress-strain curve of flax/PLA tensile specimens, tested in three different crosshead velocities.....	67
Figure 4-1: (a) The 0/90 ⁰ woven flax fabric and (b) impact sample dimensions.....	73
Figure 4-2: Road stone, projectile and impactor [80].....	75
Figure 4-3: Test fixture used for the impact assessment of the material.....	76
Figure 4-4: Low velocity gas gun setup	76
Figure 4-5: Compressive residual strength support fixture (ASTM D 7137)	77
Figure 4-6: Fractographs of the samples subjected to gas gun impact testing at 4.5 J (left) and 5.8J (right). The upper images show the front face of the samples, while the lower images the back face.	79
Figure 4-7: Impact sequence for the 23m/sec test of flax/PLA samples (high speed camera imaging).....	80
Figure 4-8: Time histories of the contact forces of the composite specimens conducted at three different impact velocities.....	81
Figure 4-9: Comparison of the maximum impact load observed during testing of the Flax/PLA samples subjected to different impact velocities	84
Figure 4-10: Energy time histories for the drop-weight impact tests of the composite specimens conducted at different impact velocities	85
Figure 4-11: Comparison of the absorbed energy during testing of the Flax/PLA samples subjected to different impact velocities.....	86
Figure 4-12: Typical C-scan images for the Flax/PLA samples subjected to gas gun impacts at 20 m/s	87
Figure 4-13: CAI average load and strengths of the composite specimen subjected to different impact velocities.....	87
Figure 4-14: Residual strength of the Flax/PLA samples as a function of the impact energy.....	88
Figure 5-1: Tensile modulus and ultimate strength of flax/PLA specimens as a function of temperature [113]	93
Figure 5-2: Low velocity gas gun setup with environmental chamber.....	95
Figure 5-3: Water absorption curves for the Flax/PLA samples ($t[sec]$).....	96

Figure 5-4: (a) Average flax/PLA water absorption curve and (b) Fick's law describes matches nicely experimental results.....	97
Figure 5-5: Average impact load recorded for different temperatures and impact velocities.....	98
Figure 5-6: Fractographs of the samples subjected to gas gun impact testing at 20m/sec	99
Figure 5-7: Fractographs of the samples subjected to gas gun impact testing at different temperatures	99
Figure 5-8: C-scan and A-scan images for the Flax/PLA samples subjected to gas gun impacts at 20 m/s for the different temperatures.....	100
Figure 5-9: Average impact load recorded for the samples with different moisture contents	101
Figure 5-10: Force-time histories for the samples tested at (a) different temperatures and (b) with different moisture content.....	102
Figure 5-11: Average energy absorption for the tested samples at different environmental conditions	103
Figure 5-12: CAI average strengths of the composite specimen subjected to different temperatures and moisture content.....	104
Figure 6-1: The Citi-Zen Concept. Vehicle proposed by the Ecoshell project.....	109
Figure 6-2: Schematic of the (a) the tensile test model and (b) the impact plate model with constraints and boundary conditions.....	118
Figure 6-3: Meshed model showing all the different components designed flax/PLA and foam sandwich structures	119
Figure 6-4: Stress versus volumetric strain of the PVC foam used (45 kg/m^3)	120
Figure 6-5: side impact models prepared for the Ecoshell Citi car	121
Figure 6-6: Comparison of experimental and simulated stress-strain curves.....	123
Figure 6-7: Experimental and simulated load time histories for (a) 9 m/sec and (b) 20 m/sec impact velocities.....	124
Figure 6-8: (a) Crack on sample tested at 20 m/sec and (b) Deleted elements representing crack formation on the simulated impact sample at 20 m/sec	125
Figure 6-9: Predicted resulted damage from the side impact runs of design 1.....	126
Figure 6-10: Impact sequence from the side impact runs of design 1	126

Figure 6-11: Energy time histories through the side impact of the initial design (design 1) of the Ecoshell Citi Car 127

Figure 6-12: Comparison of the force-time histories for the initial and final design 128

Figure 6-13: (a) Side impact damage of the final design of the Ecoshell Citi vehicle and (b) damage of the barrier after the impact 129

Figure 6-14: Energy time histories through the side impact of the final design iteration of the Ecoshell Citi Car 130

List of Tables

Table 2-1: Chemical composition of the most known natural plant fibres	17
Table 2-2: Mechanical properties of the most known natural plant fibres.....	18
Table 2-3: Main failure mechanisms in composite material.....	35
Table 3-1: Tensile properties for flax/PLA composites; Comparison with flax/epoxy (standard deviation).....	55
Table 3-2: Tensile properties of annealed and non-annealed flax/PLA samples	59
Table 3-3: Tensile properties of flax/PLA for all four temperatures tested (standard deviation).....	63
Table 3-4: Tensile properties of flax/PLA as a function of the crosshead displacement tested at room temperature (standard deviation).....	66
Table 4-1: Average impact loads recorded at specific impact energies and their corresponding velocities (standard deviation).....	78
Table 4-2: Damage assessment of the tested samples after gas gun impact at different conditions.....	80
Table 4-3: Tensile properties of flax/PLA as a function of the crosshead displacement [88]	83
Table 5-1: Summary of the average recorded load and energy absorption for the tested samples and conditions	103

Table 6-1: Material properties of the different PVC foams tested	115
Table 6-2: Tensile properties of flax/PLA [88].....	121
Table 6-3: Values of the input parameters for Mat58, T=testing, F=fitted, L=literature	122
Table 2-4: Most famous failure criteria for composite macroscopic modelling.....	ix
Table 7-1: Available composite models in LS-DYNA.....	xix

Chapter 1. Introduction

1.1 Background

The automotive industry is gearing towards more eco-friendly technologies to reduce the negative environmental impact especially the greenhouse emissions. This covers a wider scope from fuel consumption to materials used, associated manufacturing processes and the recyclability of the vehicles and their assemblies [1].

Among the main targets of the automotive industry are vehicle weight reduction that will help reduce the fuel consumption and consequently emission levels. To achieve this objective, composites using both long and short fibres have increasingly been used in a wide range of components. These offer distinct advantages over more conventional engineering materials, such as aluminium and steel, including higher specific strength and stiffness and superior corrosion resistance. Historically, starting with glass fibres and thermosetting resins allied to very low cost, the automotive sector now uses a wide range of materials, both for the fibres and the resins, as well as a number of manufacturing techniques that allow fast production rates and deliver top quality products at relatively low cost.

Composite materials, such as aramid, carbon and glass fibre reinforced plastics, are today widely deployed, with glass fibres being the most widely used due to their low cost and good mechanical properties [2]. However, these composites come with a series of drawbacks, as they are not easily (if not at all) recyclable and/or renewable, or biodegradable. Composites with synthetic fibres rely on non-renewable resources, introducing a high environmental cost with respect to their production. Furthermore, there are a number of health risks associated with the use of petrochemical based composites, both through direct exposure or inhalation of debris, and indirect from pollution of the soil, water and air. Another relatively new group of composites,

developed to address the problems of weight reduction, while combining very high specific properties and good corrosion properties, are the nano-composites. However, these composites exhibit similar drawbacks with additional health risks associated with the nano-phase particles emission and exposure [3].

Biocomposites are fast emerging as a viable alternative to traditional materials and synthetic composites. Their low cost, lightweight and good mechanical performance, as well as their environmentally friendly nature - biodegradability, recyclability and reusability - make biocomposites attractive. In addition, their very low energy consumption for production and the CO₂ balance ensure biocomposites as a viable alternative. Over the last decade, intensive research has been devoted to the development of bio-composites based on vegetable and mineral fibres, embedded in resins also deriving from natural sources. Presently, Mercedes, Audi, Toyota, Renault, Peugeot, Volvo and Lotus are among the car manufacturers using natural fibre composites for non-structural components, such as dashboards, door panels, seat backs and package trays [4].

It is worth noting that this turn to natural eco-friendly materials is fully in line with the European (E.U.) regulations released in 2000 [5]. The end-of-vehicle life directive states that by 2015, vehicles must be constructed of 95% recyclable materials, with 85% recoverable through reuse or mechanical recycling and 10% through energy recovery or thermal recycling. Asian countries introduced similar regulations as well, as Japan for example now requires 95% of a vehicle to be recoverable by 2015.

1.2 Motivation

Although natural fibre biocomposites have already found their way to the automotive industry for a wide range of components, their relatively lower properties and several technical considerations not yet resolved, limit their use into structural applications or exterior vehicle components. The study of their mechanical properties in relation to their loading capacity, the deformation behavior and their response under different loading conditions is critical. Understanding the failure process and damage accumulation is vital for the design of reliable structural components that will replace their traditional and less eco-friendly metallic or synthetic-composite equivalents.

Different research groups are currently studying the mechanical properties of biocomposites together with their thermal properties and fatigue behavior. A significant number of studies focus on material modifications for both the fibres and the resins towards improving these properties and achieving performance comparable to that of synthetic fibres, to allow the use of biocomposites in different structural components. However, all these studies concern the properties at the material level and do not include the influence of the structure and loading characteristics of a component. Additionally, all studies look into the properties before and up to the failure point, with the main focus being on the tensile, compression modulus, strength, shear modulus and impact strength. Currently, little is known about the behavior of these materials during and after an impact, the energy a material will absorb during an impact, the way potential cracks will propagate and how the mechanical properties will be affected as a result of the impact.

Flax fibres are considered to be one of the strongest and commercially available plant fibres. Its strength varies between 350 and 1500 MPa whilst its modulus can be as high as 80 GPa [6; 8; 11; 14; 17; 18; 33]. These properties combined with its very low density and excellent damping properties make flax fibres a very good alternative to glass fibres in structural applications. Further, the high availability of flax in the European market makes it the most attractive option for project within Europe. To date, research has shown that flax fibre reinforcements considerably improve the stiffness and strength of the matrix, whether thermoset or thermoplastic [34; 35; 36], with the performance being affected by the fibre length, volume fraction within the composite and the interfacial adhesion between the fibres and the matrix.

In addition poly lactic acid (PLA) is a biopolymer that has garnered significant attention in recent years. Recent research has shown that PLA is a highly suitable polymer matrix for natural fibres –reinforced composites. Studies resulted in good quality composite materials with the presence of a range of natural fibres increasing greatly the structural and thermal properties as well as impact performance [43; 44; 45; 46] .

This study will therefore investigate flax/PLA biocomposites to cover the current gap in current knowledge concerning their structural performance with special focus on the

localized impact behaviour and influencing parameters, failure characteristics, damage and post impact strength as illustrated on Figure 1-1.

Studies as such are very important for exterior vehicle components, where potential localized impacts induce damage to the composite in the form of matrix cracking, delamination, debonding or fibre breakage. Studies with Izod or/and Charpy impact testing revealed that natural biocomposites are capable of absorbing a specific (relatively low) amount of energy, but the way this energy is translated to damage is not well understood. Furthermore, under the influence of environmental factors such as moisture, temperature and salts, this behavior and mechanisms can be potentially altered, causing a negative or positive effect in the component's life.

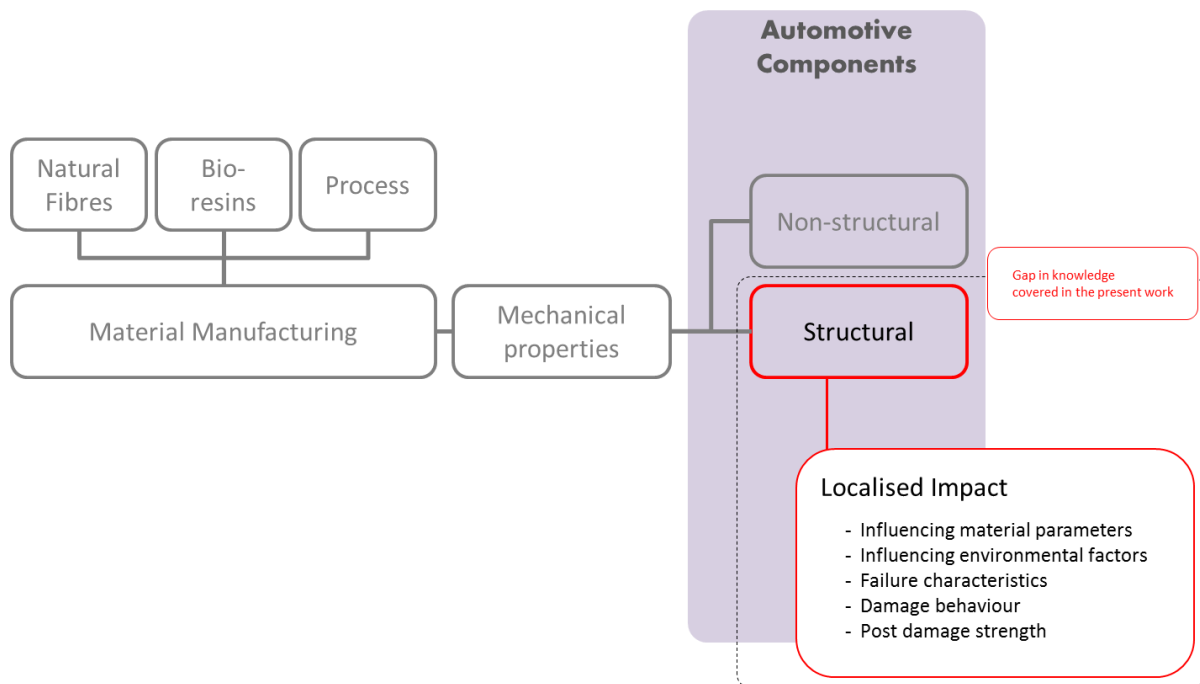


Figure 1-1: Schematic illustration of the gap in current knowledge on flax/PLA biocomposites

1.3 Aims and Objectives

The aim is to investigate and model the performance of flax/PLA biocomposites subjected to localized low velocity impacts, and assess material characteristics and influencing parameters, to allow their further applications in automotive exterior applications.

The study primarily focus on experimental study to develop in depth understanding of the energy absorbing mechanisms, post impact behavior and damage caused. The work will also identify influencing parameters from the material level such as crystallinity, mechanical properties (moduli, strength, strain rates) and environmental factors such as exposure to temperature and moisture.

The following key objectives will be covered:

1. Conduct a detailed literature review to establish the current state of the art
2. Study the thermo-mechanical thermal properties of flax/PLA composites. Evaluate the quasi-static engineering properties of the material to develop the overall understanding of their mechanical response
3. Assess the properties and behavior of flax/PLA biocomposites subject to a localized low velocity impact with a flying projectile, as well as the remaining strength in the material after such impact
4. Understand the influence of different environmental conditions –specifically temperature and moisture – on the impact performance and remaining strength of flax/PLA biocomposites
5. Use finite element analysis and apply the obtained knowledge and results to an application case study, and the design of structural components of a suitable road car

The project addresses some of the current weaknesses of biocomposites, resulting in working solutions for natural fibre biocomposites used for the manufacturing of exterior vehicle components. This project is directly related to the European project ECOSHELL, however the research and outcomes are independent.

1.4 Methodology

The study is divided into three parts, as schematically depicted in the work flow chart of Figure 1-2. Each of the three parts includes a number of studies tailored to contribute to the specific gap in the body of knowledge identified in the literature review conducted. A better understanding of flax/PLA biocomposites and their mechanical response is systematically pursued.

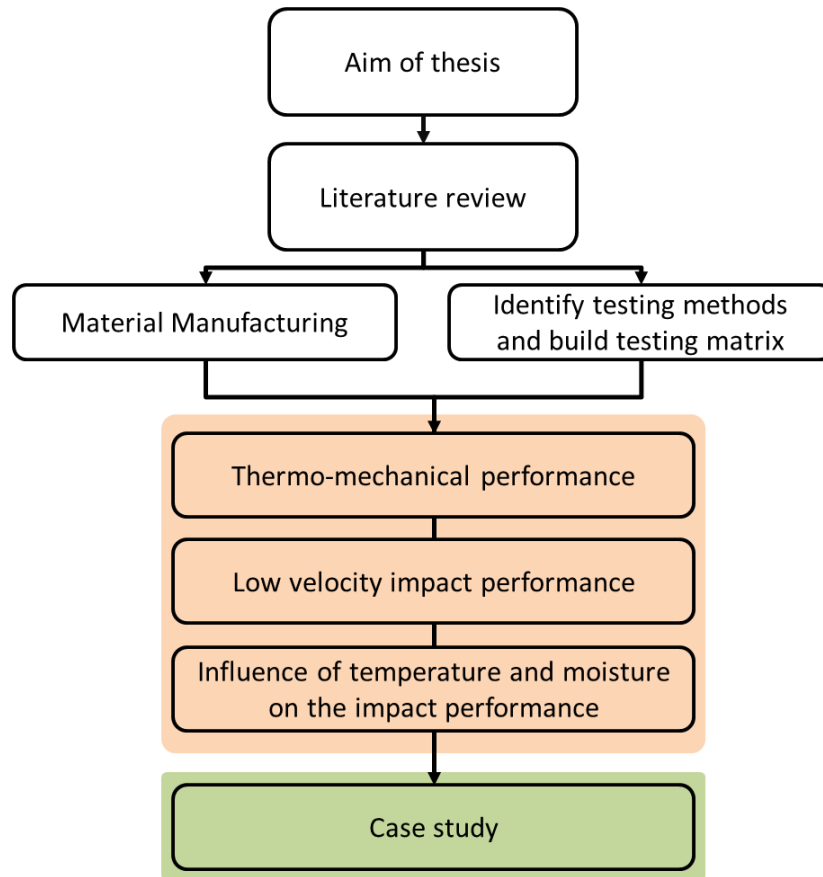


Figure 1-2: Workflow of thesis methodology

Initially, a series of morphological and thermal studies were conducted. It is necessary to be familiar with the composite structure and morphology of the components, and to understand the thermal response and their related transition temperatures, since these properties are related to the behavior of the material under impact loading. These values also set limits for the mechanical performance of the material. These limits help to build the appropriate testing matrix for the impact studies.

The second part of the thesis focuses on the quasi-static behavior of the composite material and determines those mechanical properties which explain the response of the material under loading conditions. The influence of temperature and strain rates on the properties is also studied, together with the damage characteristics and limits that led to failure.

The experimental results are finally complimented by modeling and simulations, and the development of a full model case study of a superlight electric vehicle. The purpose

of this study is to better understand the feasibility of using natural fibre composites in structural automotive components, and provide predictive tools for the design and development of novel natural composite structures. It should be noted here that the testing matrix and experimental procedures are updated continuously in case the chosen measurement, sampling and characterisation techniques were proven to be inadequate for the samples and materials, or the progress of the work and the outcomes dictate more or different testing.

1.5 Thesis Structure

In Chapter 1 the reader is introduced to the subject of the thesis, the aims, objectives and the overall thesis plan. Chapter 2 is a literature review, starting with a historical overview of the use of natural fibres, including the state-of-the-art concerning their structural and chemical properties, their advantages and disadvantages and a series of applications and examples of current use. An extensive presentation of some of the most popular natural resins follows, together with the current knowledge concerning them. The state-of-the-art of natural fibre reinforced biocomposites is then presented and factors affecting their mechanical properties are described. This concludes with a focus on flax/PLA biocomposites, including a review of past research into these materials and limitations within the present research.

In chapter 3 systematic studies on flax/PLA biocomposites are presented. The aim of this work is to determine the phenomena dominating the mechanical behavior of these materials and their potential use in structural automotive applications. The mechanical properties are evaluated through tensile testing in different environmental and loading conditions. To support and understand the outcomes, thermal studies with dynamic mechanical thermal analysis (DMA) and differential scanning calorimetry (DSC) are conducted. Fracture surfaces and fibre/matrix interactions are investigated with scanning electron microscopy (SEM).

Chapter 4 aims to assess the properties and understand the behavior of flax/PLA natural composites subject to a localized low velocity impact with a flying projectile, as well as the remaining strength in the material after such impact. As exterior automotive components are often subjected to impacts with road debris, knowledge of the behavior and limits of the material under such loading conditions is crucial. Flax/PLA samples are

subjected to gas gun testing using a 20g projectile, at different impact energies. Focus of the studies is the assessment of the damage and the mechanisms in which it occurs, failure thresholds, as well as the remaining strength in the material after such impact.

Chapter 5 investigates the influence of environmental conditions on the impact performance of flax/PLA biocomposites. Samples are subjected to localized impact testing with the specific objective to characterize the effect of moisture absorption (water content) and temperature in the low velocity impact performance and post impact strength of these composites, and study the mechanisms of those effects.

In Chapter 6 different modelling methods are assessed and the capability of existing material models to predict the response of natural composites are reviewed. A case study is then performed using these models to understand, develop and improve the side crash performance of a superlight city car prototype.

Chapter 7 concludes the thesis work, summarising the current understanding of flax/PLA biocomposites in terms of structural and mechanical performances. This research project contributed in the understanding of the mechanical performance and impact properties of flax/PLA biocomposites, and has also been beneficial to the development of structural components and the use of natural composite for automotive applications. Further investigations and improvements are also suggested.

Chapter 2. Literature Review

2.1 Historical overview

The history of natural fibres has its origins in the distant past, when mankind started developing and using continuous yarns. Archaeological artifacts suggest that humans used these materials in fabrics thousands of years ago. In Egypt flax fibres were used in textiles at least 7,000 years ago. Prehistoric hunters were making cords of flax to build tools more than 3,000 years ago [6]. Lines, ropes, textiles, clothes, baskets, paper, as well as early suspension bridges and rigging for naval ships are some of the applications where natural fibres were used.

Natural fibre composites are not new either. As early as 1908 the first composite materials were applied to the fabrication of large quantities of sheets, tubes and pipes for electronic purposes. In the 1930s and 1940s, Henry Ford strongly advocated the use of natural materials, experimenting with compressed soybeans to produce composite plastic-like components for exterior body panels [7](Figure 2-1). In 1986 airplane seats and fuel-tanks were made of natural fibres with a low percentage of polymeric binders [8].

After decades of development of artificial fibres such as carbon, aramid and glass, natural fibre composites have received an increasing interest. Their intrinsically beneficial environmental properties compared to artificial fibres make natural fibres emerge as the only viable alternative to the man-made fibres that are compromised by their poor environmental performance.



Figure 2-1: Henry Ford testing with an axe soy-bean based plastics [7]

In the past decade the European car manufacturers and suppliers have demonstrated an increasing interest in natural fibre composites. Door panels, seat backs, dashboards and package trays are among many of the components where natural fibre composites have been applied.

The “End of Life Vehicle” (ELV) Directive (established in 2006 by the European Union [5]) offers an excellent opportunity for the development and improvement of bio-composites. The Directive states that by January 1st 2015 for all end-of life vehicles the reuse and recovery target is increased to a minimum of 95% of the average weight per vehicle. Within the same time limit, the reuse and recycling is increased to a minimum of 85%. According to the Kyoto Protocol, Europe is also committed to reduce its overall emissions of greenhouse gases (GHG) during the period 2008 - 2012 by 8% compared to the level of emissions in 1990. The very low density, and thus the overall weight, is a second clear advantage of using natural fibre composites in automotive applications.

According to the German Nova-Institute at least 315.000 tonnes of bio-composites, including flax, hemp, jute, kenaf, sisal and coir, are currently used in Europe per year, mainly in the automotive and construction sectors [9]. This is predicted to rise to 830.000 tonnes by 2020 (Figure 2-2), 40.000 tonnes of which are used in compression moulded composites, with 95% of current applications being in the automotive industry. To place these numbers in context, it is worth noting that in 1996 the total reported use of natural fibres in the car industry did not exceed 4.000 tonnes (Figure 2-2).

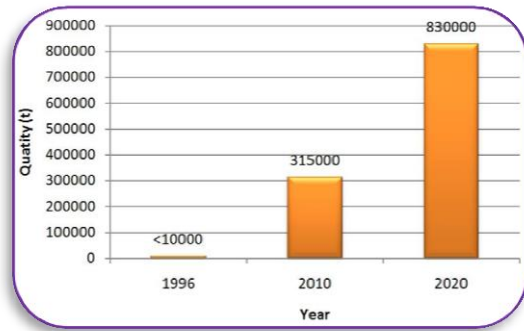


Figure 2-2: Quantity of natural fibres used in the European industry per year and prediction for 2020 [9]

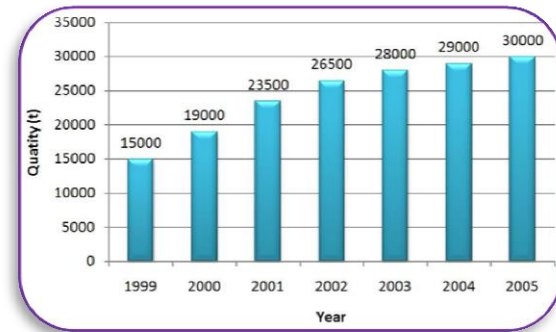


Figure 2-3: Use of natural fibres in the German automotive industry between 1999 and 2005 [9]

A major market for natural fibres is Germany, where car manufacturers are aiming to make every component of their vehicles either recyclable or biodegradable. The use of bio-fibres has increased dramatically, from 15,000 in 1999 to 30,000 in 2005 [10] (Figure 2-3).

Of primary importance to the automotive industry are the considerable environmental advantages of natural fibres. Allied to these, a weight saving of up to 30% is possible when using natural fibre composites. Cost savings is another crucial factor.

2.2 Advantages and disadvantages

Combined with the weight reduction benefits and the eco-friendly production and life cycle, the main advantages of using natural fibre composites in comparison with man-made composites can be summarized in the following [1; 2; 11-13]:

- Low density, resulting in high specific strength and stiffness
- Easy degradable (bacteria, enzymes, etc.)
- CO₂ balance kept at a stable level
- Low cost production
- Production/processing benefits
- Highly renewable resource
- Less reliance on foreign oil sources
- Recyclability
- Advantageous thermal and acoustic properties (insulation)

- No skin irritations associated with the processing of the fibres and no health concerns from the inhalation of composite dust.

However, natural fibre composites have also major disadvantages, which is a drawback for their use in structural applications. The most important of these include the fibre-matrix adhesion, the dimensional instability, the scattered fibre properties, influenced by environmental parameters, and the high moisture absorption of the fibres. The relatively high degradation rate of natural fibre composites is another major weakness.

Natural fibre composites will continue to extend their use only if such technical challenges are solved. Studies have shown that it is possible to address these drawbacks with several chemical and mechanical processes. However further studies are required to build confidence in these techniques and introduce green composites into structural applications.

2.3 Natural fibres

All natural fibres can be subdivided into three categories based on their origins: plants, animals and minerals [14]. Plant fibres mainly consist of cellulose, while animal fibres are composed of proteins. Among these, plant fibres are the most suited for the construction of fibre reinforced plastics, as their properties, combined with their very low density, make them ideal for use as reinforcements of different materials. Plants fibres can be divided into bast (stem), leaf, seed, wood fibres and other grass fibres [15]. Figure 2.4 below presents the classification of natural fibres according to their origin, together with examples of the most popular plant fibres currently used in the design of composite materials.

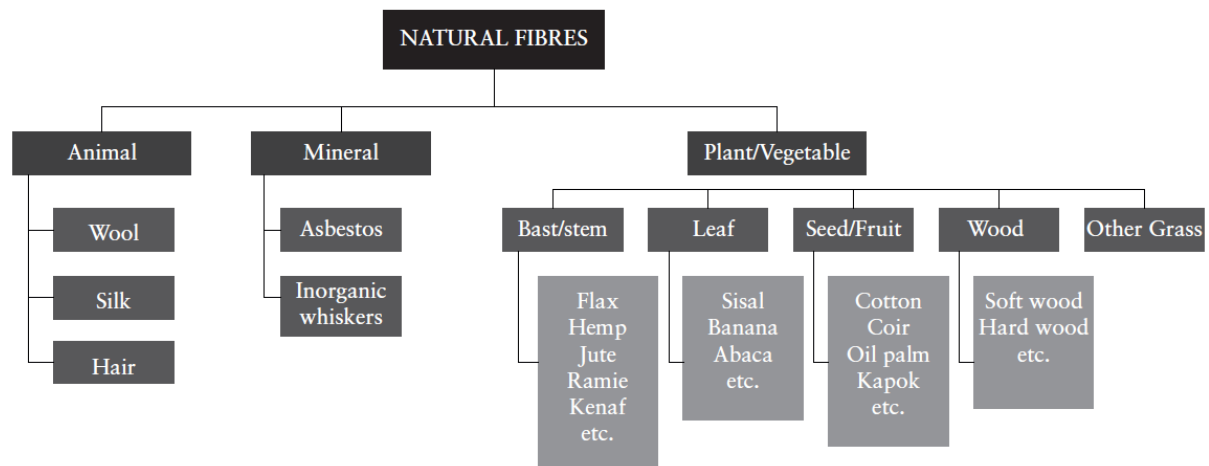


Figure 2-4: Classification of natural fibres

Bast fibres such as hemp, jute, kenaf and flax are fibrous bundles found in the inner bark of the plant stem. Leaf fibres, known also as hard fibres, run in the length of the leaves. Sisal is the most common, while others include banana, abaca and pineapple fibres. The most commonly used fruit fibres in composite applications are coir and oil palm [14-16].

Bast fibres have the highest mechanical properties and this makes them the first choice as reinforcement of polymers in the manufacturing of natural fibre composites. However, which type of fibre is most suitable depends on the specific application, the properties and the performance needed.

2.3.1 Structure

Plant fibres are technically referred to as “elementary fibres” [6; 8]. Depending on the category and nature of the plant, the elementary fibres are located and extracted differently. However they are often grouped to the “technical fibres” (a technical fibre consists of about 10 to 40 elementary fibres), held together mainly by a lignin and hemicellulose matrix. The technical fibres have an average length up to a meter, with a typical diameter between 50 to 100 μm and, in many cases, they also form larger groups, normally referred to as bundles [15]. The characteristic schematic representation of the flax stem in figure 2.5 illustrates the physical form of the fibres as described above. In composites, both elementary fibres and technical fibres or even bundles can be used, depending on the specific requirements and the preferred

production methods. However, in most of today's applications, technical fibres are used as the reinforcing unit for composites, primarily due to the simple extraction techniques, combined with their overall properties [8; 11; 15].

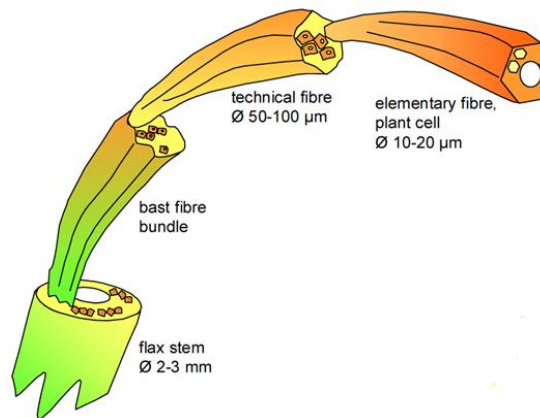


Figure 2-5: Schematic representation of flax fibre – from stem to elementary fibres

The elementary fibres (plant fibres), which are responsible for the overall mechanical properties of the final product, are basically single plant cells, with a typical length of 10 to 50 mm and a diameter between 10-50 µm. Due to their complex structure, which resembles to microscopic tubes made out of layers of different constituents, plant fibres are often considered as composites made by nature.

Each elementary fibre (cell) has four different layers surrounding the lumen, as depicted schematically in Figure 2-6 [11]. The lumen is an open channel in the centre of the fibre. The outer layer is called "primary" and is usually a very thin wall, while the inside cell wall is called "secondary", and consists of three layers (S1, S2, and S3). Among them, S2 is much thicker than the other two, containing large quantities of cellulose and is consequently the major contributor to the overall properties. From the outside to the inside the hemicellulose content remains constant, in contrast to the cellulose content of each layer, which increases steadily. Consequently, the lignin content decreases from the outer to the innermost S3 layer.

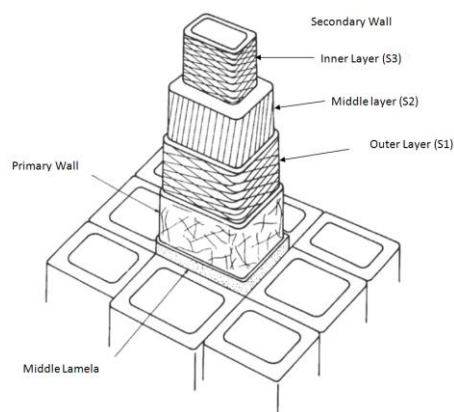


Figure 2-6: Structure of an elementary plant fibre

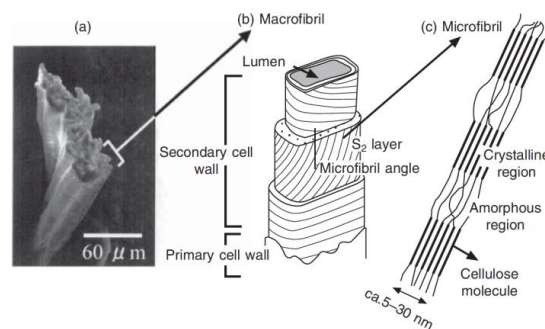


Figure 2-7: Representation of plant fibre [16].

Although the primary wall is porous and is composed of disorderly arranged crystalline cellulose, the secondary layers are formed from orientated cellulose microfibrils, “glued” together in a complex hemicellulose and lignin matrix (pectin is often found in the matrix) [15]. In each layer the microfibrils are fairly parallel to each other and follow a helical arrangement around the cell (fibre axis). They consist of semicrystalline cellulose with alternating crystalline and amorphous regions and their diameter has a typical value from 10 to 30 nm. The angle of the helical arrangement to the normal fibre axis in every layer has a major impact on the mechanical properties of the fibres and is known as the microfibrillar angle (figure 2.7).

The structure, microfibrillar angle, cell dimensions, defects, and the chemical composition of fibres are the most important variables which determine the characteristics of the fibres.

2.3.2 Chemical composition

The chemical composition, as well as the structure of plant fibres, are fairly complicated, with the main polymers involved in the composition of plant fibres being cellulose, hemicellulose and lignin. Other extractives present in plants include pectin and waxes [11; 12; 15].

The major component of most plant fibres is cellulose (α-cellulose). The existence of cellulose as a common material in plant walls was first discovered by Anselm Payen in

1838. Cellulose is a linear macromolecule, consisting of D-anhydroglucopyranose (often abbreviated as anhydroglucose) repeating units ($C_6H_{11}O_5$), joined by β -1,4-glycosidic linkages. The projection formula of cellulose is given in Fig. 2.8:

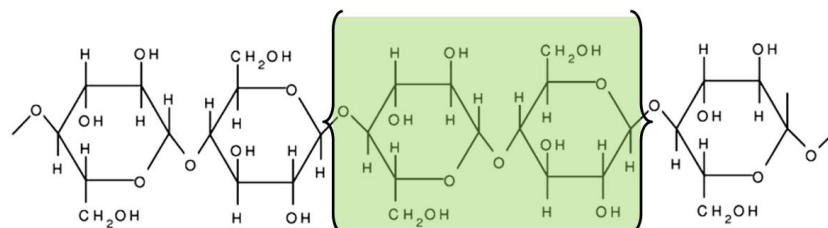


Figure 2-8: Chemical structure of cellulose

The molecular structure of cellulose is responsible for the resulting macromolecular structure, as well as for many of the material's chemical and physical properties. In the fully extended molecule, sequential chain units are orientated by their mean planes at an angle of 180° to each other. Thus, the repeating unit in cellulose is the anhydrocellulobiose unit and the number of repeating units per molecule is half the degree of polymerization. This, in native cellulose, can be as high as 14,000.

Different plants have different types of cellulose, depending on the length of the chain (DP) and the cell geometry. The adjacent chains are linked due to the existence of strong hydrogen bonds between the three hydroxyl groups in each unit and their position. Cellulose has a semicrystalline structure with regions of high order and regions of low order (amorphous). Several different crystalline structures of cellulose are known, depending on the location of hydrogen bonds between and within strands (chains). The crystal structure of naturally occurring (mainly obtained from plants and wood) cellulose is known as cellulose I, with all the cellulose strands parallel and no inter-sheet hydrogen bonding [11]. In nature, cellulose I (naturally occurring) is metastable and can be regenerated irreversibly to the more stable cellulose II. Various special chemical treatments can produce the structures cellulose III and cellulose IV [8].

Hemicellulose, which is not a form of cellulose (the name is misnomer), is made up of polysaccharides, composed of a combination of 5-carbon and 6-carbon ring sugars (glucose, mannose, galactose, etc.) [15]. The chains are much shorter (than in cellulose) (degree of polymerisation ≈ 50 to 300) and branched, containing pendant side groups

giving rise to its non-crystalline nature (amorphous). Hemicellulose is very hydrophilic and soluble in alkali and easily hydrolyzed in acids [14].

Lignin is thought to be a complex, three-dimensional copolymer of aliphatic and aromatic constituents with very high molecular weight [11]. The monomers and their proportions depend on the source in nature. Its chemistry has not yet been precisely established, as there is still no method of isolating lignin in its native state, however hydroxyl, methoxyl and carbonyl groups have been identified. Lignin is a thermoplastic polymer with melting temperature of around 170°, structurally amorphous and hydrophobic in nature [15]. Its mechanical properties are lower than those of cellulose, while lignin is also not hydrolyzed by acids, but soluble in hot alkali, readily oxidized and easily condensable with phenol. Lignin has the advantage to resist attacks by most microorganisms and anaerobic processes that do not attack the aromatic rings at all.

Pectins are a family of complex structural heteropolysaccharides, which consist primarily of polygalacturon acid, whereas waxes are different types of alcohols which are insoluble in water, as well as in several acids.

On average, natural fibres contain 60–80% cellulose, 10-20% hemicelluloses, 5–20% lignin (or pectin) and up to 20% moisture. The chemical composition of some of the most common plant fibres is shown in table 2.1 [1; 8; 11; 15].

Table 2-1: Chemical composition of the most known natural plant fibres

Name	Cellulose (wt %)	Hemicelluloses (wt %)	Lignin (wt %)	Pectin (wt %)
Flax	60 - 81	14 - 20.6	2 - 3	1.8 - 2.3
Sisal	43 - 88	10 - 14	5 - 14	0.8 - 2
Hemp	70 - 78	17.9 - 22.4	3.7 - 5.7	0.9
Ramie	68.6 - 76.2	13.1 - 16.7	0.6 - 1	1.9 - 2
Jute	51 - 72	12 - 20.4	5 - 20	0.2
Oil palm	65		29	
Abaca	56 - 64	21	12 - 13	0.8 - 1
Banana	60 - 65	6 - 19	5 - 10	3 - 12
Coconut (coir)	43	0.3	45	4
Stinging nettle	86	10		
Cotton	82.7 - 92	2 - 5.7	0.5 - 1	5.7
Bamboo	26 - 43	30	21 - 31	
Kenaf	36 - 57	21 - 21.5	8 - 18	2 - 5
Wood	45-50	23	27	

2.3.3 Mechanical properties

The overall properties of the fibres depend on the individual properties of each of their components, their physical and chemical properties, as well as their morphology. The structure, microfibrillar angle, cell dimensions and defects, and the composition are among the most important variables. The increase of the cellulose content generally increases the strength and modulus of the fibres, while the orientation of the microfibrils controls the stiffness, as the more parallel the microfibrils are in respect to the fibre axis, the higher the resulting rigidity of the fibre [8; 15]. Hemicellulose is responsible for the biodegradation, moisture absorption and thermal degradation of the fibres, while lignin (or pectin) on the other hand is thermally stable but is responsible for UV degradation of the fibres. Moisture absorption and the hydrophilic nature of plant fibres results in reduction of the overall mechanical properties. The length of the fibres is another property that has been proven to affect their strength, explained through the degree of homogeneity or amount of defects in the fibre length [6].

The main mechanical properties found in the literature for the most important natural fibres are collected in table 2.2 and compared with those of glass fibres [6; 8; 17-19].

Table 2-2: Mechanical properties of the most known natural plant fibres

Name	Diameter (μm)	Density (g/cm^3)	E-Modulus (GPa)	Tensile Strength (MPa)	Elongation at break (%)
E-GLASS		2.55	70-73	2400	
Flax	40-620	1.45-1.5	27-80	343-1500	2.7-3.2
Hemp	16-50	1.4-1.5	30-90	350-1100	1.3-4.7
Sisal	100-300	1.3-1.5	9-28	300-855	2-5
Jute	30-140	1.3-1.5	20 - 50	187-773	1.4-3.1
Bamboo		0.8-1.4	30-89	391-1000	2
Ramie	40-60	1.5	44-128	400-938	3.6-3.8
Oil palm					
Abaca	17-21	1.5	72	980	10-12
Banana	50-280	1.3-1.35	7.7-32	529-914	3-10
Coconut coir	100-450	1.2-1.5	3-6	106-270	15-47
Stinging nettle					
Kenaf	40-90	1.22-1.4	25 - 50	295-930	1.7-6.9
Cotton	16-50	1.4-1.5	5.5-12.6	287-597	2-10

The scattering of the values for all properties is underlined as one of the major disadvantages of natural fibres, and can be explained by differences in the fibre structure, composition and morphology due to different overall environmental conditions during plant growth (area, climate, age of the plant when harvested). On average the performance of natural fibres in terms of stiffness and strength cannot compete with that of glass fibres. However, their specific properties, especially stiffness, are comparable or even superior compared to those of glass when the density of natural fibres is half that of glass. Figure 2-9 depicts Young modulus and specific Young modulus of the most commonly used natural fibres, while **Error! Reference source not found.** shows the tensile strength of the most commonly used natural fibres.

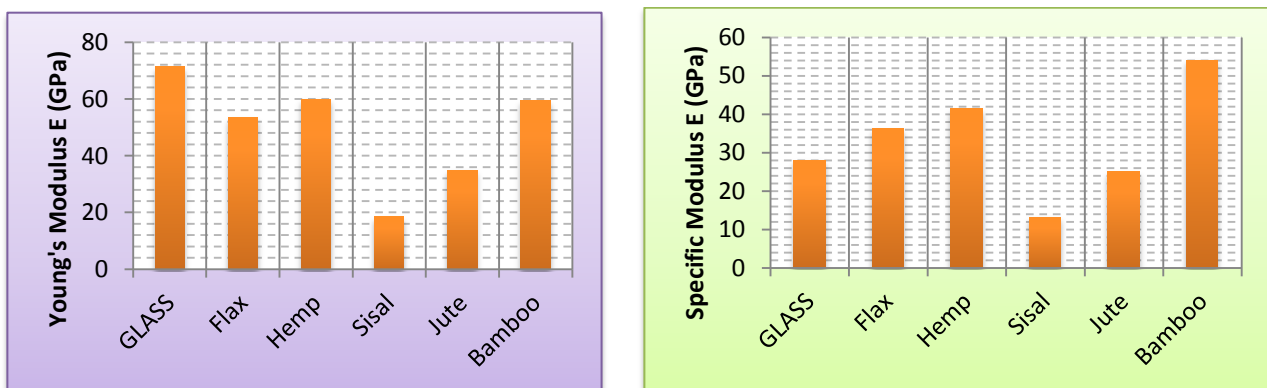


Figure 2-9: Young modulus and specific Young modulus of the most commonly used natural fibres

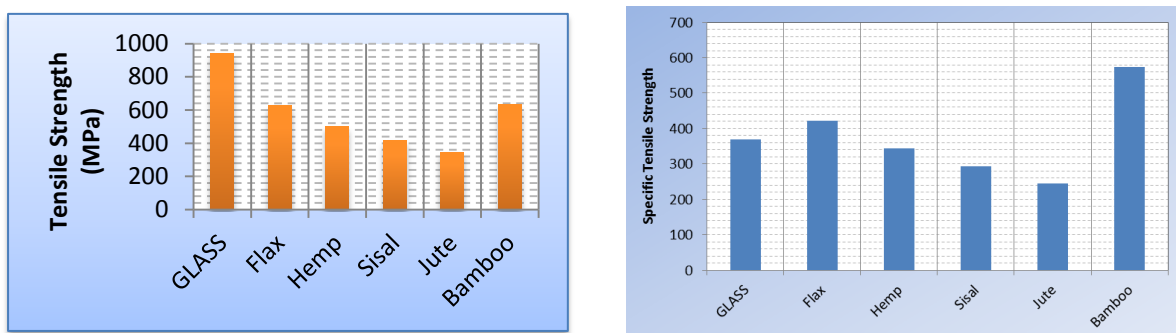


Figure 2-10: Tensile and specific tensile strength of the most commonly used natural fibres

2.3.4 Fibre Modifications

In varying degrees all natural fibres (although in different extent) are hydrophilic in nature. This is attributed mainly to the lignocellulose within their structures, which

contains strongly polarized hydroxyl groups [14]. As a result these fibres are inherently incompatible with many widely used, well-known composite manufacturing resins. Only some thermosets such as the phenolformaldehyde and related polymers are less hydrophilic and thus less problematic.

This discrepancy often leads to the formation of an ineffective interface between the fibres and the matrix. The major limitations of using these fibres as reinforcements in such matrices include poor interfacial adhesion between polar-hydrophilic fibres and non-polar-hydrophobic matrix, combined with difficulties in mixing due to poor wetting of the fibres within the matrix. The role of the matrix in a fibre-reinforced composite is to transfer the load to the stiff fibres through shear stresses at the interface. This process requires a good bond between the polymeric matrix and the fibres [2]. Poor adhesion at the interface means that the full capabilities of the composite cannot be exploited and leaves it vulnerable to environmental attacks that may weaken it, thus reducing its life span. Insufficient adhesion between the polymer and the fibres results in poor mechanical properties of the natural fibre-reinforced polymer composites.

Pre-treatments of the fibres can clean the fibre surface, chemically modify it, stop the moisture absorption process and increase the surface roughness [8; 12]. Physical treatments like cold plasma treatment or corona treatment, chemical treatments such as graft copolymerization, esterification and isocyanates, or use of coupling agents can improve the composite's mechanical properties and protect it from environmental attack.

Physical treatments

Physical treatments change the structural and surface properties of the fibres and thereby influence the mechanical bonding to polymers. Plasma treatment is one of the most popular and effective techniques for surface modification [8]. The plasma discharge can be generated by either corona treatment or cold plasma treatment, two different methods with the same principle of surface oxidation activation through electric discharge which changes the surface energy of the cellulose fibres. Both methods are considered as a plasma treatment when ionized gas has an equivalent number of positive and negative charged molecules that react with the surface of the present material. The distinguishing feature between the two is the frequency of the

electric discharge. High-frequency cold plasma can be produced by microwave energy, whereas a lower frequency alternating current discharge at atmospheric pressure produces corona plasma.

Another traditional physical method is mercerization (or alkali treatment). In this process the fibres are treated with an aqueous solution of a strong base (NaOH) so as to produce great swelling that results in changes of their structure, dimensions, morphology and mechanical properties [20]. Mercerization leads to fibrillation, which causes the breaking down of the composite fibre bundle into smaller fibres and reducing the fibre diameter. Thereby, it increases the aspect ratio, which leads to the development of a rough surface topography, resulting in better fibre-matrix interface adhesion and an increase in mechanical properties [20]. Moreover, mercerization increases the number of possible reactive sites and allows better fibre wetting. Several works on alkali treatment [21-23] were made, which reported that mercerization leads to an increase in the amount of amorphous cellulose at the cost of crystalline cellulose and the removal of hydrogen bonding in the network structure.

Chemical Treatments

Among the most effective methods of chemical treatment is graft copolymerization [8; 14; 20; 24-26]. The cellulose is treated with an aqueous solution with selected ions and is exposed to a high energy radiation. Under the radiation the cellulose molecule cracks and radicals are formed. Using then a suitable (compatible with the matrix) solution, it is possible to create a co-polymer with properties and characteristics of both the fibres and the matrix. For example, the treatment of cellulose fibres with hot polypropylene-maleic anhydride (MAH-PP) copolymers provides covalent bonds across the interface. Gauthier et al. [27] reported that adhesion may be improved by using maleic anhydride to incorporate hydroxyl groups on the matrix through hydrophilization and consequently enhancing the wetting effect of the resin on the fibres. A PP chain permits maleic anhydride to be cohesive and produce maleic anhydride grafted polypropylene (MAPP). Graft copolymers of natural fibres with the presence of vinyl monomers provide also better adhesion between matrix and fibre. The graft copolymerization method is effective, but complex [20].

Acetylation describes a reaction introducing an acetyl functional group ($\text{CH}_3\text{COO}-$) into an organic compound and is a well-known method in which the fibers are usually immersed in acetic acid for 1 h, then immersed in a mixture of acetic anhydride and few drops of concentrated sulphuric acid for a few min, then filtrated, washed and dried in ventilated oven [20; 25]. Acetylation is based on the reaction of cell wall hydroxyl groups of lignocellulosic materials with acetic or propionic anhydride at elevated temperature and is an esterification method which stabilizes the cell walls, especially in terms of humidity absorption and consequent dimensional variation. Another esterification method is treatment with stearic acid, in which acid is added to an ethyl alcohol solution up to 10% of the total weight of the fibers. The aim of the stearic treatment is the reaction of the hydroxyl group of the fibre with the stearic acid group, to hydrophobise the fibre's surface, yielding better compatibility

In benzylation treatment, benzoyl chloride is used in fiber pretreatment and the reaction between the cellulosic $-\text{OH}$ group of the fibers and benzoyl chloride ($\text{C}_6\text{H}_5\text{C}=\text{O}$) is responsible for the decreased hydrophilic nature of the treated fibers [28].

Anhydride treatment is another technique proved to produce significant reduction of water absorption [28]. It is usually carried out by utilizing maleic anhydride or maleated anhydride polypropylene (MAPP) or polyethylene in a toluene or xylene solution, where the fibers are immersed for impregnation and react with the hydroxyl groups on the fiber surface.

Isocyanate group ($-\text{NCO}$) can react with the hydroxyl groups on fiber surface, thus improving the interface adhesion with the polymer matrix. Isocyanate treatment is typically performed with isocyanate compounds at intermediate temperatures (around $50\text{ }^\circ\text{C}$) for approximately 1 h.

Treatments with permanganate is another chemical method conducted by using different concentration of potassium permanganate (KMnO_4) solution in acetone with soaking duration from 1 to 3 min after alkaline pretreatment [20]. As a result of permanganate treatment, the hydrophilic tendency of the fibers is reduced, and thus, the water absorption of fiber-reinforced composite decreases. This effect increases with increased KMnO_4 concentration. Permanganate treatments have been reported to be very effective in improving the interfacial adhesion in natural fibre composites.

Enzymatic treatments are an increasingly interesting option as such, or combined with chemical and mechanical methods for modification and processing of biomaterials [29]. This is due to the fact that enzymes are highly specific and efficient catalysts, so that they work in mild, energy-saving conditions. Oxidative enzymes, such as laccases or peroxidases, can be used to activate and further functionalise lignocelluloses. The primary reaction of laccase is the oxidation of phenolic hydroxyls to phenoxy radicals in the presence of oxygen. Laccases can thus be used to activate lignin, lignans, and different types of lipophilic extractives present in the complex lignocellulosic materials to improve the hydrophobicity or bonding capability between fibres and matrix.

Coupling agents

Coupling agents are based on the concept that when two materials are incompatible, a third material with intermediate properties can bring the compatibility to the mixture [8]. The coupling agents have two functions: to react with -OH groups of the cellulose and to react with the functional groups of the matrix with the aim to facilitate stress transfer between the fibres and the matrix. Numerous studies [8; 20; 25; 27; 28] have been conducted on the use of coupling agents, including organosilanes, triazine and maleic-anhydride (MAH).

Silane is a chemical compound with chemical formula SiH_4 . Silanes (organosilanes) are used as coupling agents to let fibers adhere to a polymer matrix, stabilizing the composite material. Silane coupling agents may reduce the number of cellulose hydroxyl groups in the fiber-matrix interface. Xie et al. [30] used silane coupling agents in natural fibre/polymer composites and concluded that proper treatment of fibres with silanes can increase the interfacial adhesion and improve the mechanical performance of the resulting composites. Gassan et al. [31] improved the tensile and flexural strength and stiffness of jute/epoxy composites by treating the fibres with silane. Proper treatment of fibres with silane can increase the interfacial adhesion to the target polymer matrices and improve the mechanical and outdoor performance of the resulting fibre/polymer composites.

Use of triazine ($\text{C}_3\text{H}_3\text{N}_3$) coupling agents has also been reported to improve moisture absorption of the fibres by reducing the number of hydroxyl groups available on the fibre surface and by creating a cross-linked network due to covalent bonding [8; 25].

2.3.5 Flax fibres

Flax is an erect annual plant growing to 1.2 m tall, with slender stems and glaucous green leaves 20 to 40 mm long and 3 mm broad. Flax (with the latin name *Linum usitatissimum*) is one of the most popular and commonly used natural fibres, but also one of the oldest known textile fibres. The first documented applications date back to 5000B.C., used by the Egyptians to wrap their mummies [6]. Since then, flax has been applied to a vast number of applications and products, from clothing and packaging to the naval and automotive industry.

Presently, two types of flax are grown, fibre flax and seed flax. Fibre flax is optimized for the production of thin strong fibres. Flax grows in moderate climates and is presently cultivated among others in large parts of Europe, Canada, the USA and Russia. World-wide approximately 5 million hectare flax is grown. Especially in the European Union 122 000 tonnes of flax fibre were produced in 2007 [32], making it the world's first producer, followed by China with about 25 000 tonnes. The demand for flax fibres in plastic composites is growing by more than 50% annually in Europe and this trend has now started in North America. By far the largest users are automotive part manufacturers, who are being pressured to make cheaper and lighter weight vehicles with lower gas consumption and use more environmentally friendly materials in their construction. However at present, flax fibres are able to substitute only the lower (mechanically) glass grades (lower price fibreglass), due mainly to the fibre inconsistency.

Flax is harvested for fiber production after approximately 100 days or a month after the plant flowers and two weeks after the seed capsules form [6; 15]. The base of the plant will begin to turn yellow. If the plant is still green the seed will not be useful, and the fibers will be underdeveloped. The fibers degrade once the plant is brown.

Flax belongs to the category of bast fibres and is considered to be one of the strongest and easily available ones. Its strength varies between 350 and 1500 MPa, while its modulus can be as high as 80 GPa [6; 8; 11; 14; 17; 18; 33]. These properties, combined with its very low density, make flax fibres a very competitive contestant against glass. Flax fibres are also generally cheaper, lighter in weight and impart more springiness

than fibreglass. In addition, they take less energy to manufacture and are easier to decompose or burn than fibreglass.

Bos et al [6; 18] conducted a range of studies on the stiffness and strength of flax technical and elementary fibres. Tensile properties of flax fibres depend on the clamping length due to the structure of the technical flax fibres. This also explains the scatter in flax fibre tensile strengths reported in literature. They also concluded that single elementary flax fibres have considerably higher strengths than technical fibres and a strong dependency of the fibre strength on the decortication process. The strength distribution of flax fibres was also studied by Anderson et al., who approximated the trend using a modified Weibull distribution.

Liu et al [34] fabricated flax-epoxy composites using different types of woven and volume fractions, and showed that flax improves up to 4 times the stiffness of the unreinforced epoxy. They also concluded that toughness is dominated by the fiber volume fraction, rather than the architecture of the weave. Another study on the reinforcement of polypropylene with flax nonwovens was conducted by Maya et al [35]. Tensile strength and modulus were found to increase with the increase in fiber loading, while flexural strength and modulus also registered an increase. Zein modification of nonwovens was found to enhance the mechanical properties of the composites due to better interfacial bonding between them. However they also observed a decrease of the impact strength, explained by the presence of fiber breakage in chemically modified composites. Thermoplastic composites based on flax fibres and a polypropylene (PP) matrix were manufactured by Garkhail et al. [36]. The materials stiffness, strength and impact performance were then studied with respect to fibre length, fibre volume fraction and interface modification through the use of a maleic-anhydride grafted PP grade. It was concluded that composites based on a PP matrix and flax fibres can compete with E-glass-based materials in stiffness critical structures, whereas for strength and impact critical applications, these materials still need to be further optimised. Baiardo et al. [37] also studied flax fibre composites with a bio-polyester matrix (bionolle). The study showed again the need for surface modification to improve the adhesion between fibres and matrix. The use of acetylation on the fibre surface remarkably increased the strength of the composite. Many more studies exist for flax

fibre reinforced composites, looking into their properties, their environmental impact and the effect of different treatments and modifications [14].

2.4 Resins

The growing environmental concern has made plastics a target of criticism, due to their lack of degradability [38]. The manufacturing, use and removal of traditional composites have been studied for many years, proving that the disposal of composites after their intended life span is –when possible- very expensive, while the recycling, as well as reuse of composites is not easy, since they are made of two dissimilar materials. Traditional thermoplastics and thermosets are considered non-biodegradable and so there has been a lot of interest in research, committed to the design of biodegradable plastics. The concept of environmentally conscious materials is being rapidly accepted by countries all over the world and biodegradable polymers are now considered as the environmental waste management option.

Bioplastics have a history of about 150 years, since the invention of celluloid in 1860's. There have been some promising attempts to make bioplastic cars out of them, e.g. Henry Ford had the first all Soy plastic based car body at 1941. Consisting of 70% cellulose and 30% resin pressed into cloth, the new plastic was reportedly 50% lighter and 50% cheaper than steel: it could absorb, without denting, and blow ten times higher than steel could stand. As early as 1934, Ford had remarked that 'almost all new cars could be soon made of such things as soybean' [39]. However the promising soy plastic and many new renewable based materials were left in laboratory due to the petroleum industry and new large-scale industrial synthetic polymers in 1950's. The oil crisis in the 1970's brought back the interest towards materials coming from other raw materials than oil. This interest increased in the last 30 years and finally led to new commercial bioplastics in the early 2000's.

The term bio-based here has the meaning of being man-made organic polymers, whose monomers are derived from bio-resources and used for plastic composite product applications. There are three principal ways to produce bio-based plastics:

- make use of natural polymers which may be modified but remain intact to a large extent (e.g. starch and cellulose based plastics);

- to produce bio-based monomers by fermentation or conventional chemistry and polymerize these monomers in a second step (e.g. polylactic acid);
- produce bio-based polymers directly in microorganisms or in genetically modified crops.

However, bio-based (natural) plastics should not be confused with biodegradable polymers. Bio-based polymers can be tailored to be either biodegradable or non-biodegradable according to their end properties, while respectively some oil-derived polymers can also be biodegradable (Figure 2.11).

Biodegradable polymers have been the subject of research and development since the early 1970s and growing pressure on the world's resources, as well as concerns about disposal of plastics, led to intensified interest and commercial activity in the 1990s [40]. Biodegradable polymers, or biopolymers, as they are sometimes known, are now attracting interest for a wide range of applications and became very appealing to the automotive industry. Figure 2.11 shows a classification of polymers with respect to their source of origin and their degradability.

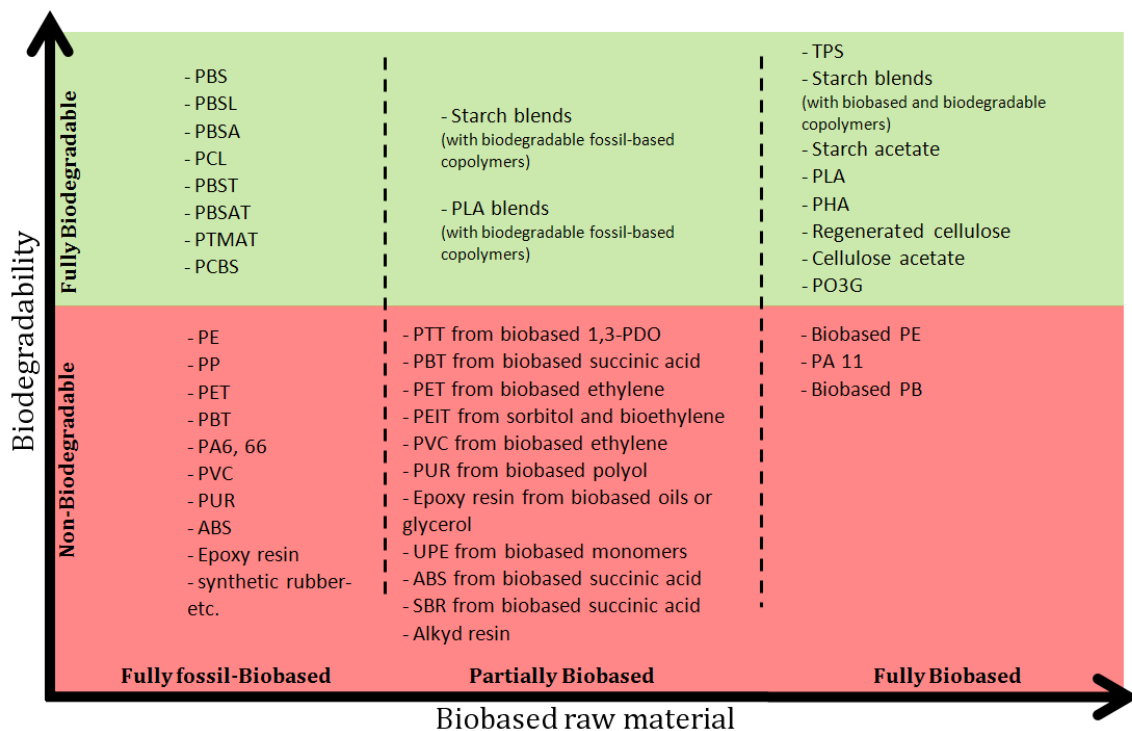


Figure 2-11: Classification of polymers with respect to their source of origin and their degradability

Biodegradable polymers can be obtained from renewable resources, synthesized microbially, or synthesized from petroleum-based compounds. The challenge for the development of biodegradable polymers lies in the fact that such biopolymers should be stable during storage and usage and then degrade once disposed-off after their intended lifetime. Biopolymers, on reinforcement with biofibers, can produce novel bio-composites to replace/substitute glass fiber-reinforced composites in various applications.

2.4.1 Poly (lactic acid)

Poly (lactic acid) or polylactide (PLA) is an aliphatic thermoplastic polyester, derived from lactic acid found in renewable resources, such as corn, wheat, barley, cassava, and sugar cane [41]. Lactic acid is then polymerised to poly (lactic acid), either by gradual polycondensation or by ring opening polymerisation. Due to the chiral nature of lactic acid, several distinct forms of polylactide exist: poly-L-lactide (PLLA) is the product resulting from polymerization of L,L-lactide (also known as L-lactide), while D-lactide is producing poly-D-lactide (PDLA). PLA is among the few polymers in which the stereochemical structure can be easily modified by polymerizing a controlled mixture of the L- or D-isomers to yield high molecular-weight amorphous or crystalline polymers that can be used for food contact and are generally recognized [41]. PLAs are hydrophobic in nature.

The commercially attractive features of PLA include its production from renewable resources, as well as its good mechanical properties [42]. PLA has good tensile strength, low extension and a high modulus (approximately 4.8 GPa). It has hence been considered as ideal biomaterial for load bearing applications. PLA-based polymers are completely degradable and, after use, can be recycled or disposed-off either by incineration or by land-filling. PLA polymers have also a relatively high hardness. In order for PLA to be processed on large-scale production lines, such as injection moulding, compression moulding and extrusion, the polymer must possess adequate thermal stability to prevent degradation and maintain its molecular weight and other properties. Poly(lactic acid) and its polymers have a glass-transition and melt

temperature of about 55°C and 175°C respectively, while they undergo thermal degradation at temperatures above 200°C.

Although PLA has been frequently used for packing, numerous tests have shown that PLA is also suitable as matrix for the embedding of fibres in composites. Tokoro et al [43] mixed three types of bamboo fibres into a PLA matrix to improve its impact strength and heat resistance. Their research resulted in a good quality composite material, with the presence of the bamboo fibres largely improving its impact performance and thermal properties. Ochi [44] investigated kenaf/PLA composites with different fiber proportions. He found that tensile and bending strength, as well as Young's modulus, increase linearly by increasing the fibre content up to 50%. He also concluded that unidirectional biodegradable composites fabricated using an emulsion-type PLA resin and kenaf fibers at a fiber content of 70% have high tensile and flexural strengths, of 223 MPa and 254 MPa respectively. In a comparative study, Shibata et al. [45] fabricated composites with lyocell fabric and PLA by compression moulding. The tensile modulus and strength of lyocell/PLA composites improves with increasing fibre content. Impact strength is considerably higher than that of pure PLA. Pan et al. [46] also fabricated kenaf/PLA composites by injection moulding with fibre contents ranging between 0% and 30%. At 30% a tensile strength improvement of 30% is observed.

2.5 Characterization of natural fibre composites

In a composite the properties of the fibres are combined with those of the matrix, which is responsible to transfer the external loads to the stiffer fibres through shear stresses at the interface, as well as to keep the fibres together in a specific structural form. Thus, the properties of the composite are a combination of the properties of the ingredients, so that their prediction and estimation is difficult.

2.5.1 Stiffness & Strength

The mechanical properties of natural fibre composites are much poorer than those of glass fibres. However, their specific properties, especially stiffness, are comparable to the stated values of glass fibres. Moreover, natural fibres are about 50% lighter than glass, and in general cheaper. It is widely acknowledged that natural fibre composites combine good mechanical properties with a low specific mass and offer an alternative

material to glass fibre-reinforced plastics in some technical applications. For example, Bledzki and Gassan [8] found that the characteristic values of natural fibres are comparable to those of glass fibres. Experimental data giving the tensile strength, flexural strength, modulus, impact and compressive strength, are available in the literature for different types of natural-fibre composites.

The ultimate strength of any composite depends on several factors, most important of which are the properties of the components and the volume fraction. Wambua et al. [2] studied the effect of the volume fraction on the tensile strength of natural fibre composites. They reported that an increase in the fibre weight fraction produces an increase in the tensile strength. Testing different fibre reinforcement, they also found that hemp/ polypropylene (PP) composites with a 30% volume fraction displayed a tensile strength of 52MPa and that the overall mechanical performance of hemp/PP was comparable to that glass reinforced composites with the same volume fraction and hence could potentially be used to replace those composites. Furthermore, hemp and kenaf–polypropylene composites registered a high tensile modulus of 6.8GPa compared to 6.2GPa of equivalent glass composites. The increase of the modulus and the tensile strength with the increase of the volume or weight fraction was also showed by Bos [6; 17] on flax/PP composites with maleic-anhydride grafted polypropylene for improved adhesion.

Studies and results of tensile tests on flax-fibre reinforced PP composites were conducted by Garkhail et al. [36]. They concluded that fibre length affects the strength and modulus of the composites for small fibre lengths, both reaching a constant value after a specific length, explained through the extraction process of the fibres from the plant and the fibre bundles. The stiffness of a flax/PP composite was shown to be comparable to E-glass based composite, especially when the specific properties are concerned, mainly due to the very low density of flax. However, the results also showed a relatively low tensile strength.

Nishino [16] studied the mechanical properties of kenaf/poly-L-lactide (PLLA) composites. He concluded that the modulus of the composites increases with the increase of the volume fraction, but only up to a certain level. When this threshold is reached, further increase of the fibre fraction leads to a dramatic deterioration of the

composite properties due to insufficient impregnation of the fibres by matrix resin and as such the ineffective transfer of stresses.

Water content has also a dramatic effect on the properties of natural-fibre composites. Espert et al. [47] showed this effect on cellulose/PP composites by submerging samples into distilled water under different temperatures. The samples were removed from the water at certain times and the water absorption was measured. The results of tensile tests showed a significant effect of the water content on the Young's modulus of the samples, and an even larger effect on the tensile strength. This drop of mechanical properties was explained through fibre swelling and hydrolysis mechanisms, but also also due to weakening of the interfacial adhesion caused by further loss of compatibilization between the fibres and the matrix due to the water uptake. The studies also concluded that the effect of the water on their properties is highly influenced by the fibre content, the matrix and mainly the temperature. Thwe et al. [48] investigated the same effect on bamboo-fibre composites. They found that both the tensile strength and modulus decrease by aging in water at 25 and 75°C for a prolonged period. The extent of strength and stiffness loss depends on the aging time and temperature. They also concluded that tensile strength and stiffness are enhanced by inclusion of a coupling agent, as for example maleic anhydride polypropylene (MAPP), in the matrix material, as a result of the improved interfacial bonding.

2.5.2 Impact performance

There are only few studies that are known about the impact behaviour of natural fibre reinforced composites. The impact performance of several natural fibre composites was compared and reviewed by Wambua et al. [2]. Using kenaf, coir, sisal, hemp, and jute reinforced polypropylene, their study concluded that natural fibre composites display low impact strengths compared to glass composites, whereas their specific impact strength can be comparable with that of glass mat composites. Among the materials studied, sisal and hemp showed the higher impact strength.

Pavithran et al. [49] determined the fracture energies for sisal, pineapple, banana and coconut fibre-polyester composites in a Charpy impact test. They concluded that

increased fibre toughness results in increased fracture energy. Additionally, fibres with higher fibril angles have higher fracture-toughness than those with small spiral angle.

The fibre content and fibre length have also a contribution to the impact performance of the composite. Tobias et al. [50] examined this influence with banana-fibre composites and concluded that smaller fibre lengths have higher impact strength, which also increases by increasing the fibre content. The fibre length was also studied by Garkhail et al. [36] on flax/PP composites. Contradictorily, their results showed that, as in glass fibre composites, the impact strength increases with increasing fibre length until a plateau level is reached. After that level the impact performance drops due to insufficient impregnation of the fibres, depending also on the pre-treatment of the fibres.

Mueller [51] investigated the effect of several material parameters on the impact strength of compression moulding components of hemp, flax and kenaf–polypropylene composites. The studies showed a strong influence of the thermal process conditions during the moulding. It was concluded that, for every material studied, there is an optimum temperature that results to a peak of the impact strength. Higher and lower processing temperatures result in lower mechanical values that could be explained by a thermal decomposition of the fibres. The effect of temperature and water on the impact properties of natural-fibre thermoplastics were reviewed by Bruijn [52]. No significant effect on the impact properties of the composites is reported. However, it was found that the impact strength is 20 to 25% lower than that of glass reinforced thermoplastics.

A significant contribution of coupling agents on the impact strength has been also reported. When the composites have no coupling agent, a part of the energy is lost in the interface, for example by debonding and friction effects. Maleic-anhydride-treated jute composites show higher impact strength than untreated samples, fabricated using the same process.

2.6 Modelling natural fibre composites

Very little numerical work exists concerning the mechanical performance of bio-composites. Very little is found in the literature on modeling, while the existing few attempts are based on generic assumptions and models initially created for man-made composites (glass, carbon, aramid, etc.).

Depending on the application, the manufacturing process, the type of fibres and finally the required degree of approximation, a number of theoretical models were developed, mainly predicting the stiffness and strength of natural fibre composites. There exist models, validated by different experimental tests [53], based mainly on laws such as the rule of mixture (ROM) or the laminate approach, valid for short and long fibres. Most of them are general models, using mathematical approaches and analytical prediction of the response of composites under mild conditions, with a modification factor to correct for the complexity of natural fibres.

Most reported models include a number of approximations, none of which, however, perfectly matches the natural fibre composites properties. The most important approximations used are [53]:

- The fibres and matrix are linearly elastic
- The matrix is isotropic and the fibres isotropic or transversely isotropic
- The fibres are axi-symmetric and identical in shape
- The fibre and matrix are well bonded at their interface and remain as such during deformation

2.6.1 Modelling composite materials

Micro-, Meso- and Macro-scale approach

The numerical/mechanical approaches for modeling composites can be categorized into three different scales, the micro-, the meso- and the macro-scale [54-56]. These are defined as follows (see also Figure 2-12):

- Micro-scale: fibre fracture, matrix cracking and debonding at the fibre-matrix interface.
- Meso-scale: concerns failures which occur at the ply level, such as debonding between laminates.
- Macro-scale: concerns the overall failure of the laminate.

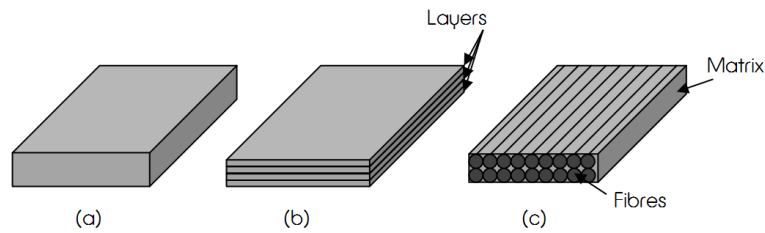


Figure 2-12: (a) Macro-, (b) meso- and (c) micro-scale modeling approach

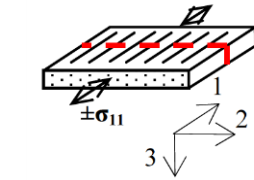
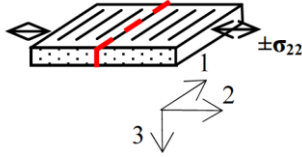
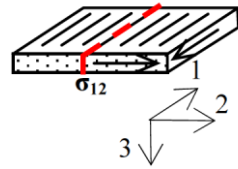
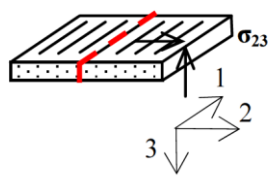
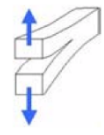
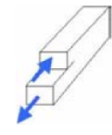
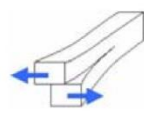
In the first, each phase of the composite is considered and modeled separately. The properties of each phase have to be well defined, and the loading is then applied separately to the resin and the reinforcing material. The overall properties of the composite depend then on the behaviour of both constituents. This approach, compared to the other two, is able to model and give details on the interactions between the different phases, and has been reported to give very good results. However, a larger number of material testing is needed to get separately the properties of all the constituents and to reach a good knowledge of the reinforcements shape and direction within the composite. Furthermore, a major disadvantage of the micro-scale approach is the big computational time needed. Often, results from the micro-scale approach, which requires significantly smaller computational time, are used to extract the properties to be used in meso- and macro-models.

Within the macro-scale approach, the material is considered to be a homogenous and anisotropic continuum. There is no distinction between the matrix and reinforcement and the properties describe the behaviour of the overall material. The mechanics do not treat separately the different phases and the interfacial interactions are neglected. Failure and damage are included, but they concern the material as a whole. Each element represents the composite as one unit and not just as one of the distinctive phases. In the meso-scale approach, the different layers (plies) of the composite (laminate) are considered individually, and the interactions between them are also considered. The ply is then considered as the homogenous continuum, with an orthotropic or transversely isotropic behaviour.

Failure Criteria

The failure mechanisms in a composite laminate can be divided into intra-laminar (within a ply) and inter-laminar (between plies), each with different failure modes, as shown in the table below (Table 2-3) [57; 58].

Table 2-3: Main failure mechanisms in composite material

Intra-laminar Failure	Tension/compression	
	Transverse tension/compression	
	In-plane shear	
	Out-of-plane shear	
Inter-laminar Failure	Delamination Mode I	
	Delamination Mode II	
	Delamination Mode III	

As opposed to metals and isotropic materials, composite failure occurs not only due to the deviatoric component of the stress tensor, but also to the hydrostatic component,

which has an important contribution. Furthermore, for isotropic materials the failure criteria are written in terms of principal stresses and ultimate tensile, compressive and shear strengths, and thus the load carrying capacity can be predicted from the knowledge of these three strengths. However, in the case of orthotropic materials, the strengths and the elastic constants are direction-dependent, and an infinite number of strengths can be obtained, depending on the loading direction. Thus, the models for failure of isotropic materials, such as von-Mises and Tresca, could not be used. They had to be replaced by failure theories that are more appropriate for composites and non-isotropic materials. A large number of theories and alternatives exist. The most important of them and the most commonly used are presented in appendix B.

2.7 Applications of biocomposites

Natural fibre composites find applications in a vast number of products, in constant growth the last decade.

Lines, ropes, textiles, clothes, baskets and paper are some of the traditional applications [6; 12]. However bio-composites are also used in the design and manufacturing of sensing flanges, grinding disks, fan rotor and seats. The nova-institute reported also on their use in the packaging industry (packages for cosmetics and others), but also in speaker boxes, chairs and tableware [51]. Other examples include steam cleaners, toilet seats, ironing equipment and a range of other domestic applications. Natural fibre composites have made their appearance also in the sport equipment (e.g. golf). A catamaran boat (made of flax fibres) and a caravan coach are two more examples.

In the automotive, the list is endless. Door panels, seat backs, dashboards and package trays, head restraints and seatback linings, are just some of the examples of applications. Mercedes uses jute-based composites for the door panels of the E-class, banana-fibre reinforced composites for the A-class and different other bio-composites for the S-class [10]. BMW follows the same example, using a considerable amount of green materials and green composites in their vehicles. The brand reported the use of approximately 10,000 tonnes of natural fibres in 2004 [68].

Figure 2-13 illustrates the large number of C-class components, made of different natural-fibre composites, used in a Mercedes car, while Figure 2-14 depicts a Four Motors GmbH green racer, with the body-shell made of plant fibre reinforced composites.



Figure 2-13: Mercedes C-class components made of different natural-fibre composites
(www.dottal.org)



Figure 2-14: Four Motors GmbH green racer; the body-shell is made of plant fibre reinforced composites

Daimler-Chrysler is another example with up to 50 components made of natural-fibre composites in its European vehicles, some of which are the innovative abaca-fibre exterior under-floor protection for passenger cars and the front bumpers made of flax fibres. General Motors uses a mixture of kenaf and flax to produce package trays and door panel inserts for Saturn L300s and the European version of the Opel Vectra [68]. Audi's A2 car carries a door trim made of mixed flax and sisal fibres. Audi uses natural fibre composites also in other vehicles of its range (A3, A4, A6, A8, Roadster) for seat backs, side and back door panels, boot lining and others [6]. The 'Trabant' car has cotton fibre reinforced polyester. The Toyota Lexus HS250h hybrid vehicle is yet another car containing plant fibre reinforced composites. Others include Ford, Renault (Clio), Peugeot (406), Fiat (Punto, Brava, Marea and others), Saab, Seat, Volkswagen (Golf A4, Passat, Bora), Volvo (C70, V70). Lotus recently incorporated natural fibres composites in the Eco-Elise bodyworks, using hemp fibres, while its interior trimmings are made of sisal composites [10]. Goodyear produces corn-infused tires, which have lower rolling

resistance, providing lower fuel consumption. These tires are now used in several European vehicles. The same route is followed by many other Tiers 1 and Tiers 2 suppliers.



Figure 2-15: The Grasshopper



Figure 2-16: Fiat EcoBasic (www.fiat.co.uk)

The Araco Corporation in Japan presented in 2003 the Grasshopper, a fully electric vehicle (Figure 2-15). Its body is totally made out of plant-based composites, mainly kenaf [16]. The efforts of Fiat for a more environmentally friendly vehicle resulted in the Fiat Ecobasic prototype (Figure 2-16), which saves weight and has no need for painting, by using natural fibre composites on the external panels. Furthermore, the BioConcept Car project of Four Motors GmbH resulted in successfully building an endurance racing car made of natural fibre-reinforced plastics. In 2006, this racing car competed successfully for the first time a 6-hours race [69]. Rinspeed developed a new concept car presented in the 2011 Geneva Motor show. The Rinspeed Bamboo, as its name reveals, has major components of the interior made of bamboo fibre reinforced composites.

The European Union supports since a long time the use of natural fibre composites in the automotive industry. The ECOFINA project, part of the FP5 Growth Project, addressed the man-made fibers, presently used in the automotive parts, with polymeric

matrix composites based on annually renewable natural fibres [70]. The project included the standardization of a processing technology to produce natural-fibre products of constant quality. Several other EU projects encourage the production of natural fibres and their use in structural application.

2.8 Conclusions and scope for research in light of literature review

The automotive industry shows an increasing interest towards the use of biocomposites, which to date has been restricted to non-structural interior components due to their poor mechanical properties associated mainly to the thermal stability and the interactions between the fibres and the matrix. The extended use of bio-composites for the manufacturing of vehicle components would benefit largely the industry as these material gather very attractive properties such as their low density, the degradability and recyclability and their low production costs. EU regulations push towards more eco-friendly solutions making biocomposites a very attractive option.

Although studies report the properties and potential improvements of biocomposites, focusing individually on the constituents (fibres and matrix) but also in different combinations, the overall mechanical behaviour from a structural point of view is not completely understood and mechanical performance is below the target. Further the performance of these materials under different environments and their mechanical response under different loading conditions are still not understood well enough for adoption in mass products in the transport industry.

Specifically for flax fibres and PLA resins the scientific literature is being enriched at an increasing rate, targeting mainly the understanding of their chemical and physical structure, as well as the interfacial adhesion of the resulting composites and the possible solutions for its improvement. Mechanical properties such as the strength and stiffness have also been reported and studied extensively as well as the influencing parameters such as the fibre length, treatment, volume fraction and manufacturing properties.

A number of studies have also been focused on the impact performance on biocomposites, showing that their specific impact strength can be comparable to that of glass mat composites. The studies have mainly looked into the fracture energies principally concentrated on Charpy and Izod impact testing, and again the influencing parameters of associated with the manufacturing, fibre/matrix mixture, and different fibre treatments.

From this literature review the following key findings can be summarised:

- Natural fibre biocomposites have already found their way into the automotive industry for a wide range of components. Their use into structural applications or exterior vehicle components is still limited by relatively lower properties and several technical considerations.
- The chemical and structural composition of both natural fibres and bio-resins have been extensively studied and reported, whilst a wide number of studies exist on the modifications of natural fibres to improve the interfacial adhesion of the composite constituents, and therefore improve their mechanical performance.
- Currently there is lack of information on the thermo-mechanical performance of flax/PLA, stress-strain behavior under different loading condition and strain rate effects.
- Although impact and fracture energies have been studied in a material level, to date there is lack of information on the localised impact performance of biocomposites, the failure characteristics and the mechanisms of impact energy absorption and damage.
- Currently there are no results on the post impact strength of natural biocomposites and flax/PLA subjected to a localised impact of different energies and different environmental conditions.
- Very limited work on modelling of natural fibres has been reported focused primarily on the rule of mixture and different variations of it, to represent the specific characteristics of natural fibre and resins. To date and to the author's knowledge no FE work has been reported.

Chapter 3. Structural performance of flax/PLA natural fibre biocomposites

3.1 Introduction

The increased social awareness of the environmental problems posed by non-degradable or recyclable materials, combined with the established European regulations requiring 95% of each vehicle being recyclable or degradable by 2015, is now forcing a turn of the automotive industry towards natural eco-friendly materials. Additionally, industry attempts to lessen the dependence on petroleum-based fuels and products, and therefore replace the existing glass fibre and carbon fibre-reinforced materials [1].

Natural fibre composites are fast emerging as viable alternative to traditional materials and synthetic composites. Their low cost, lightweight, good mechanical performance and their environmentally friendly nature makes them an ideal choice for the automotive. The automotive industry has already embraced those composites for several years for the production of non-structural components, predicted to constantly increase.

Flax is considered to be one of the strongest and easily available plant fibres. Its strength varies between 350 and 1500 MPa while its modulus can be as high as 80 GPa [6; 8; 11; 14; 17; 18; 33]. These properties combined with its very low density, make flax fibres a very competitive contestant against glass. As a reinforcement flax was found to improve considerably the stiffness and strength of the matrix, whether

thermoset or thermoplastic [34-36], with the performance being affected by the fibre length, volume fraction within the composite and the interfacial adhesion between the fibres and the matrix [36; 37]. Many studies focused on the improvement of the incompatibility of the hydrophilic fibres and hydrophobic resins and proposed a number of modifications that significantly enhanced the material performance.

Although intensive research and developments have been carried out to optimize the properties of the fibres and the manufacturing of the composites to overcome the drawbacks and weaknesses associated, few have looked into potential of using bio-sourced polymers as a matrix for natural fibres, resulting in a 100% natural material.

One of the most promising bio-sourced polymers is poly(L-lactide) (PLA), product of polymerization of lactic acids derived from the fermentation in renewable resources, such as corn, wheat, barley, cassava, and sugar cane [41]. PLA-based polymers are completely degradable and after use can be recycled or disposed of by incineration or by land-filling. In order for PLA to be processed on large-scale production lines such as injection moulding, compression moulding and extrusion, the polymer must possess adequate thermal stability to prevent degradation and maintain molecular weight and properties. Poly(lactic acid) (and its polymers) has a glass-transition and melt temperature of about 50 °C and 150 °C respectively while it undergoes thermal degradation above 200 °C. Although PLA has been frequently used for packing, numerous tests have shown that PLA is also suitable in as matrix for the embedding of fibres in composites. Tokoro et al [43] mixed three types of bamboo fibres into a PLA matrix to improve its impact strength and heat resistance. Their studies resulted in good quality composite materials with the presence of the bamboo fibres increasing greatly the impact performance and thermal properties. Ochi [44] investigated kenaf/PLA composites with different fiber proportions. Tensile and bending strength as well as Young's modulus increased linearly up to a fibre content of 50%. He also concluded that unidirectional biodegradable composites fabricated using an emulsion-type PLA resin and kenaf fibers at a fiber content of 70% have high tensile and flexural strengths of 223 MPa and 254 MPa, respectively. Shibata et al. [45] in a comparison study prepared composites with lyocell fabric and PLA by compression moulding. The tensile modulus and strength of lyocell/PLA composites improved with increasing fibre content. Impact strength was considerably higher than that of pure PLA. Pan et al. [46]

also produced kenaf/PLA composites by injection moulding with fibre contents ranging between 0% and 30%. At 30% a tensile strength improvement of 30% was observed.

The extended use of bio-composites for the manufacturing of vehicle components would benefit largely the industry, but to date their low mechanical properties associated mainly to the thermal stability and the interactions between the fibres and the matrix, restrict their use. Although studies report the properties and potential improvements of biocomposites, the overall mechanical behaviour from a structural point of view is not yet understood. The properties of the material as a unit, its mechanical performance under different environments and the effect of different loading conditions are still unclear.

In this section of the work (Chapter 3), systematic studies have been conducted on flax/PLA biocomposites, with aim to determine the phenomena dominating their mechanical behavior and their potential use in structural automotive applications. The mechanical properties are evaluated through tensile testing in different environmental and loading conditions. To support and understand the outcomes thermal studies with dynamic mechanical thermal analysis (DMA) and differential scanning calorimetry (DSC) are conducted. Fracture surfaces and fibre/matrix interactions are investigated with scanning electron microscopy (SEM).

3.2 Materials and methods

3.2.1 Materials

A commingled/pre-impregnated Flax/PLA fabric (mixed flax and PLA fibres) was provided by Composites Evolution using a Poly(L-lactide) acid (PLA) based on lactides acquired from corn starch fermentation supplied by Natureworks. Typical density of the PLA used is between 1.23-1.25 g/cm³. The reinforcement used was a 2x2 twill flax weave with an approximate unconsolidated thickness of 0.8mm (once consolidated the thickness is around 0.3mm). All samples were prepared by NetComposites using a hot press moulding process with 12 layers of the fabric for the 3mm samples and 16 layers for the 4mm samples ending with 40% flax by volume composite. The parts were moulded at 180 °C and held there at maximum temperature for 5 mins before being cooled. The pressure used was about 15 bar. The resulting density was estimated between 1.35-1.4 g/cm³. For the cutting of the samples a band saw was used.

For comparative reasons, the more conventional and widely used and researched flax/epoxy samples have also been tested. All samples have been manufactured and prepared from MaHyTec. A 0/90° balanced woven fabric provided by LINEO (FlaxPly BL300) was combined with a bio-sourced epoxy resin based mainly on epoxidised pine oil waste from Amroy (Epobiox LV with hardener Ca23) with a 50% fibre volume fraction. The samples have been manufactured in plates with a compression -RTM- process and then cut out using a milling machine. A pressuring force of 10kN was used, with a sequential cycle of 2 hours in 800 °C and 3 hours with a temperature of 1250 °C. Basic measurement was used to assess the density of the material, estimated 1.274 g/cm³.

3.2.2 Characterisation

Scanning electron microscope

For the study of fracture surfaces emerged during mechanical testing of different samples and the morphology of the composite, a Scanning Field Emission Gun SEM (scanning electron microscope) was used; model XL30 from FEI, with an acceleration voltage of 15 kV. Before examination all samples were sputtered coated with gold/palladium for 2 minutes to avoid charging.

Dynamic Mechanical Analysis

To assess the temperature of decomposition and the rate of degradation of the materials DMA testing was performed. The DMA instrument used was a Q800 from TA Instruments equipped with a dual-cantilever bending fixture. The frequency was constant at 1Hz and the temperature was set at 25°C and then linearly increased by 1°C per minute until 150°C. The samples were cut into rectangles of 35 mm × 13 mm × 3 mm to accommodate the DMA. At least three samples per material were tested.

Differential Scanning Calorimetry

DSC was performed on a TA instruments Q200 with aluminium sample pans, to evaluate the degree of crystallinity of the PLA in the composite. The glass transition temperature (T_g), cold crystallization and melting temperatures (T_m) were also determined. PLA was

pulverized using a blade to scratch from composite panels' surface. The powdered samples, between 5-10 mg in weight, were packed into a stainless steel high volume DSC pan and sealed. Five samples were tested and heated between 25 °C and 200 °C with a rate of 1 °C/min in a nitrogen atmosphere. Two of the samples were also tested in cooling with the same rate for better understanding of the materials transitions.

3.2.3 Mechanical testing

All mechanical tests were carried in a 23 °C and constant humidity environment. The specimens had been conditioned in the same environment for at least 24 hours before testing. Their dimensions were measured with a caliper in at least three locations.

The tensile tests were performed according to the ASTM 3039 standard on an Instron 5500R electro-mechanical machine. Five samples were tested per material at a nominal strain rate (2mm/min cross-head velocity). The length and width of the samples were 250mm and 25mm respectively with a 3 mm thickness. Aluminium tabs were added to avoid stress concentrations and damage of the samples by the fixing jaws.

For the temperature studies a thermal chamber was attached on the Instron that allows temperature control from -40 to 150 °C with a step of 1 °C. The specimens were put into the chamber and tested after the temperature measured on the samples with a thermocouple was stabilized.

A high precision laser extensometer was used throughout the testing. This equipment uses a high speed laser scanner to measure the spacing between two parallel reflective tape strips positioned on the sample during the test. A visible laser light is simply aimed at the specimen, and reflected back from the tape strips set at the gage length desired. The extensometer displays the actual measured length between the strips or, if desired, the difference between the actual and initial distances.

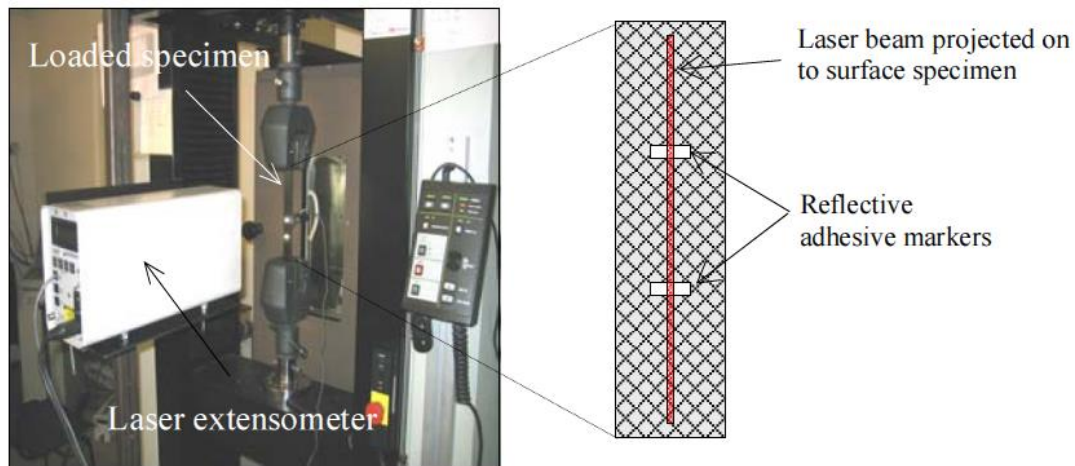


Figure 3-1: Laser extensometer method: experimental setup [58]

Advantages of the method include the non-contacting nature of the method which allows measurements without affecting the sample, and through chambers, the high resolution, and the fact that maximum strain or strain rates are not affecting the result. However, the positioning and alignment of the strips can often introduce an error and is a job that needs precision and time. Further, the resulting measurement is based on an average strain between the two strips.

3.3 Results and discussion

3.3.1 Microscopy

Figure 3.2 shows the SEM photographs of the fracture surface of the Flax/PLA composite after mechanical testing. Extensive fibre pull-outs together with corresponding holes were observed in all specimens, suggesting a poor interfacial adhesion between the PLA and the Flax fibres, besides the hydrophilic nature of the PLA. The clean surface of the pulled fibres strengthens this conclusion. The visible voids between fibres and the matrix puts forward the question whether those gaps are the result of debonding during the testing or existed already from the manufacturing. Either indicates poor adhesion resulting in insufficient transfer of the loads between the composite components, and hence reduced mechanical performance.

Observation of the fracture reveals the brittle characteristics of the PLA with the surface being clean and perpendicular to the loading. The fibre edges suggest that the fibres also fail in a rather brittle manner and without plastic deformation or necking.

Further, the SEM micrographs show that the flax fibres in the material are often very tightly collected into bundles with very little or no resin between them. This fact proves poor separation of the fibres prior to the weaving that could harm the overall properties. Finally, the fibre cross-section is random with often the lumen and kink bands along the fibre length visible. The dimensional instability of natural fibres and their random shape and form explained through the different extraction processes as well as environment, age and treatment of the plants, is among the main disadvantages of natural fibre composites affecting their quality and performance [40]. Better separation and dispersion through the composite could also be beneficial [71].

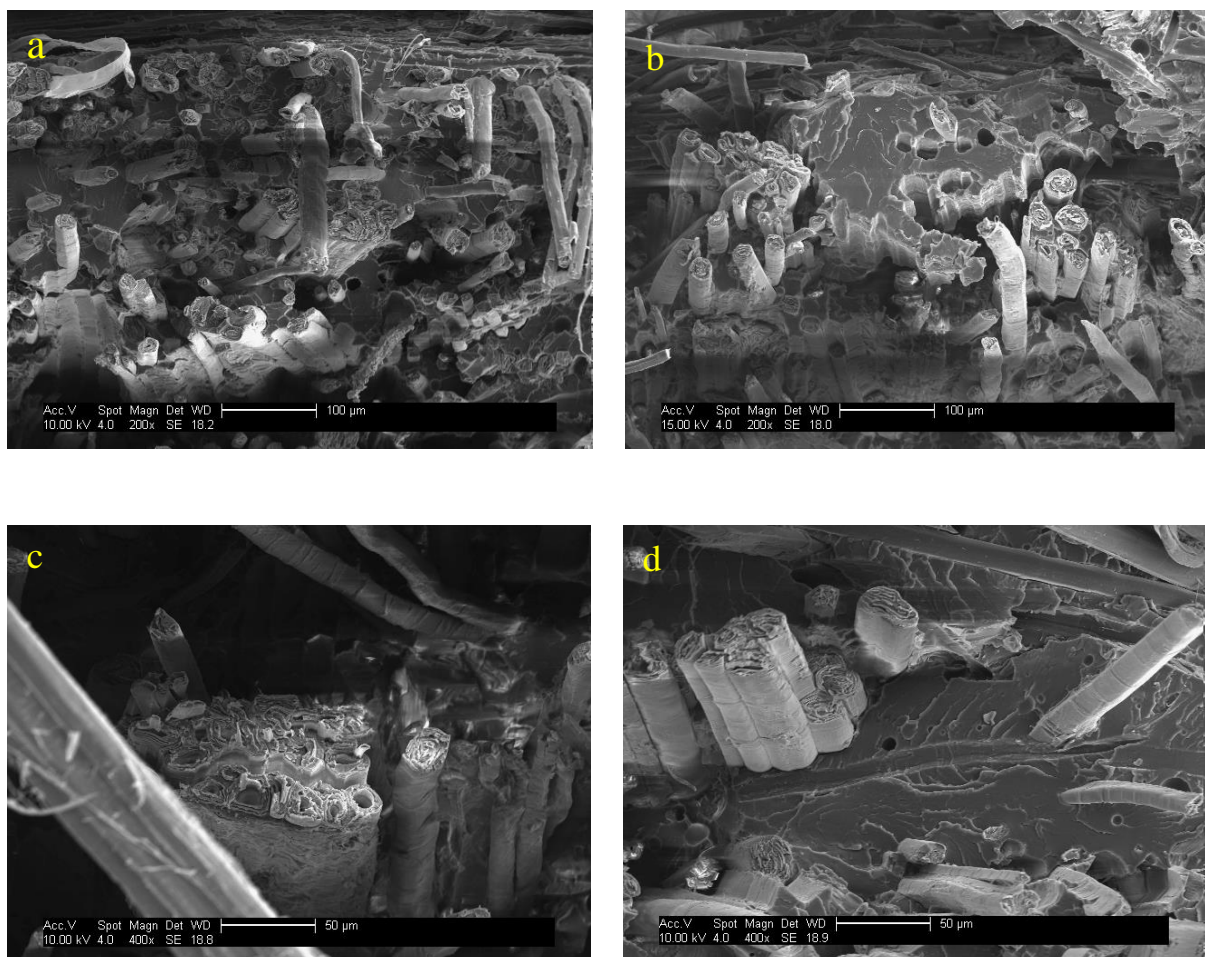


Figure 3-2: Overview of the fracture surfaces of flax/PLA tensile specimens

Previous studies on natural fibre/PLA composites had similar conclusions as per the difficulty of the fibres and the resin to show good adhesion. Bax et al. [72] worked with flax and cordena fibres mixed with PLA, and observed poor adhesion and extensive fibre pull-outs. In MAPP (maleic anhydride-grafted polypropylene) as a matrix for flax fibres showed improved performance and reduced pull-outs after testing. SEM photographs from bamboo/PLA composites studied by Tokoro et al. show the same weakness in the composite, with the two components being insufficiently attached [43]. However, treatment of the fibres to remove the surface lignin from the bamboo fibres had a considerable effect on the performance of the specimens.

3.3.2 DMA

Figures 3.3 and 3.4 show the results from the DMA and the variation of storage modulus and $\tan(\delta)$ for the Flax/PLA and Flax/epoxy composites with respect to the temperature. Storage modulus is the expression of the ratio of the in-phase stress to the applied strain, representing the energy stored in the material in every cycle of deformation [46]. The glass transition temperatures are between 63-65 °C and 74-76 °C for the Flax/PLA and Flax/Epoxy respectively, showing a disadvantage of the PLA composite in terms of thermal properties. Further, the properties for both materials start deteriorating after about 60-65 °C with the epoxy showing a more gradual loss compared to the PLA which loses more than 80% of its storage modulus before 70 °C. However the glass transition of pure PLA as found in the literature is within 50 and 60 °C with a $\tan(\delta)$ of more than 2 [46; 71], which signifies that the flax fibres had a positive effect on the properties of the PLA. A possible explanation for this is associated with the fact that the presence of fibres restricts the chain mobility of the neat PLA [46].

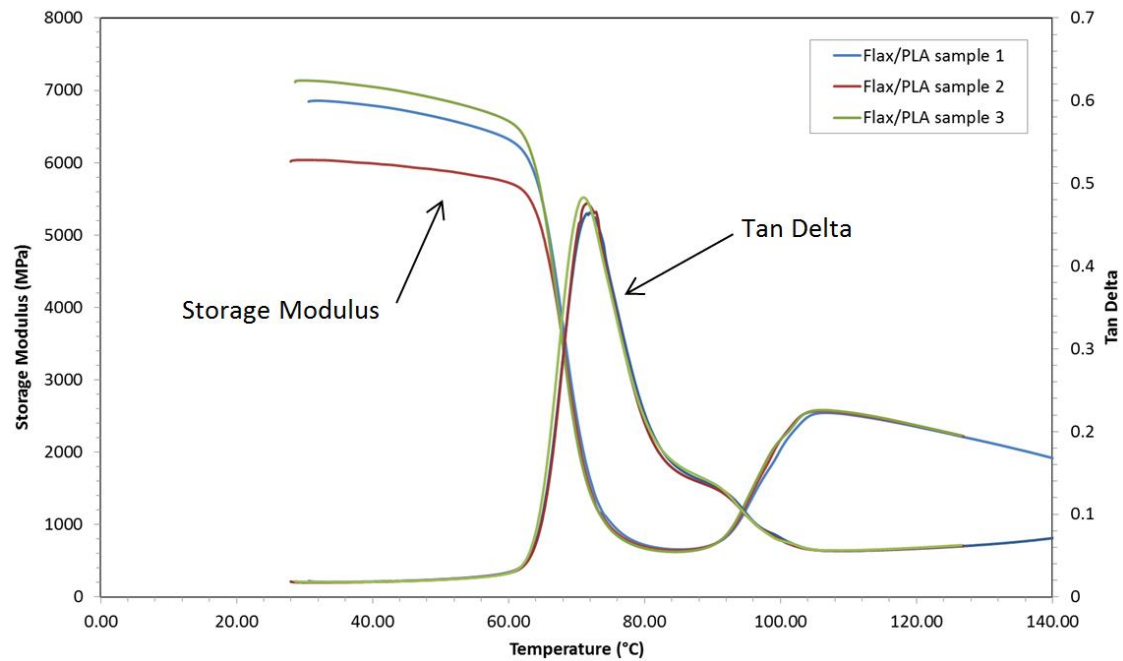


Figure 3-3: DMA runs for flax/PLA; Storage modulus and tan delta [tests performed at 1Hz frequency]

Close and above 80 °C the storage modulus of the PLA composites starts increasing again, an effect associated with the cold crystallization of the amorphous part of the thermoplastic PLA (as will be better described later with the DSC results). No such transition occurs to the epoxy. As the crystallized part of the matrix increases compared to the amorphous the properties after the crystallization are improving, with results from the literature confirming this effect Tokoro et al. experimented with bamboo/PLA composites and the effect of annealing on the properties of the composite. They proved that specimens with 100% crystallinity (annealing at 110 °C for 5h) had significantly improved thermal properties and heat resistance than non-annealed ones [43]. However, the effect of this process on the mechanical properties of the composite has not been discussed.

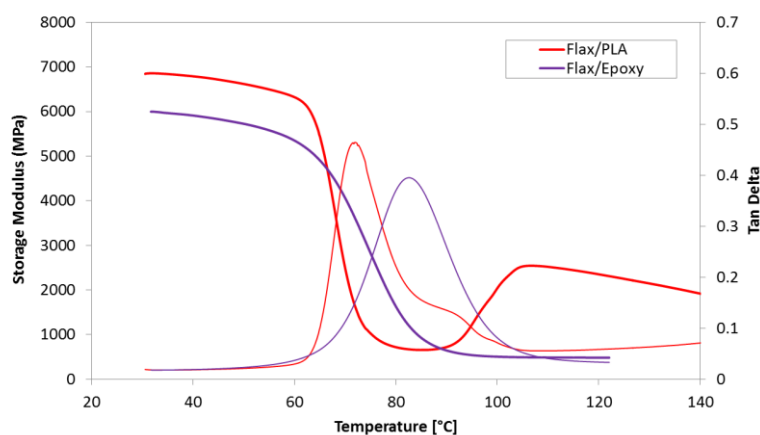


Figure 3-4: Comparison of storage modulus and tan delta from DMA runs of flax/PLA and flax/epoxy composites [tests performed at 1Hz frequency]

3.3.3 DSC

The percent of crystallinity is directly related to many of the key properties exhibited by a semi-crystalline polymer including brittleness, toughness, stiffness or modulus, optical clarity, etc. [73]. In order to calculate the percentage of crystallinity in the PLA and relate it later to the mechanical properties measured, DSC studies were carried out in a temperature range of 25-220 °C and a variable heating rate. The glass transition temperature (T_g), melt temperature (T_m), cold crystallization temperature (T_{cc}), as well as the heat of melting (H_m) and crystallization (H_c) are determined for all the samples. The degree of crystallinity is then calculated using the relationship

$$X_c (\% \text{ crystallinity}) = \frac{\Delta H_m - \Delta H_c}{\Delta H_{m\%}} \cdot 100 \quad (3.1)$$

Where ΔH_m and ΔH_c are obtained via integration of the corresponding endothermic and exothermic peak of the melting and crystallization process respectively, and $\Delta H_{m\%}$ is the melting enthalpy of a totally crystallized PLA sample. $\Delta H_{m\%}$ is reported in the literature equal to 93 J.g⁻¹ [73; 74]. This calculation works under the assumption that after the exothermic transition only a small and unknown part of the amorphous material gets crystallized.

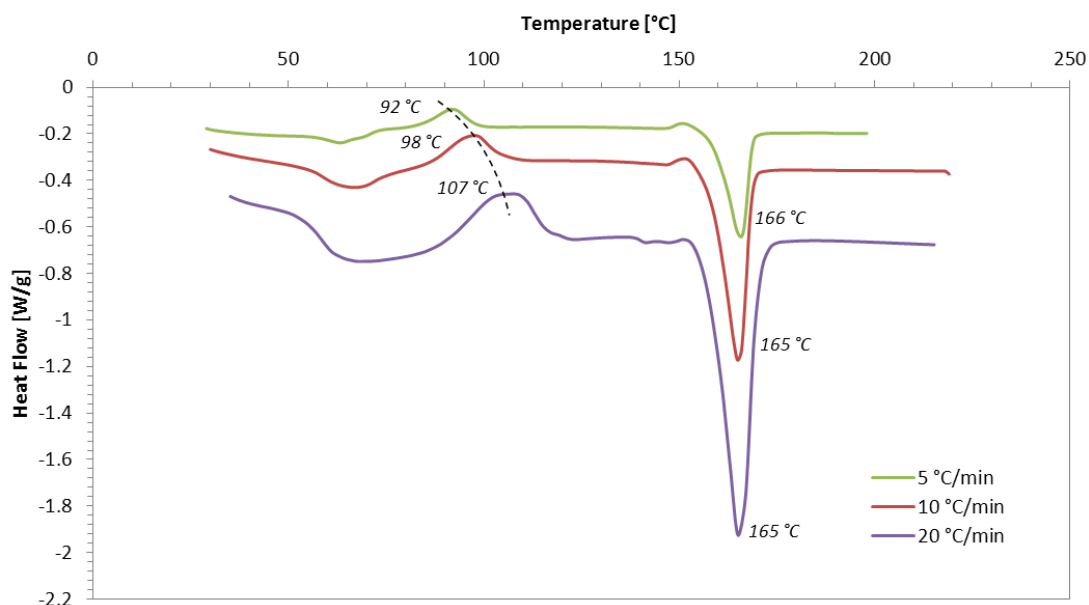


Figure 3-5: Effect of heating rate on DSC curves of flax/PLA

Figure 3.5 shows the DSC thermograms of the PLA as acquired from the composites as a function of the heating rate. The exothermic peak of cold crystallization is apparent in all three cases signifying the presence of an amorphous part into the polymer. The glass transition is also visible in about 60 °C in each case. However, its duration and temperature range are affected by the heating rate. The exothermic transformation of the cold crystallization is visible between 90-100 °C, after which the heat flow remains constant. It has been observed that the cold crystallization peak increased and shifted towards higher temperatures as the heating rate increased. Interestingly, another exothermic peak appears prior to the melting temperature at around 150 °C. This second exothermic reaction is apparent in previous studies with PLA in the literature but has never been discussed. The increased mobility of the chains close to the melting point, allows the crystallization of an amorphous component not able to transform during the cold crystallization [46; 73; 74]. As the PLA samples were obtained through the composites, this could be associated with the presence of fibre particles, and the fact that the mobility near the fibres is reduced. In higher heating rates this exothermic peak is eliminated. The melting process starts at around 155 °C and is completed before 170 °C, after which the heat flow remains again constant. The heating rate seems to have again an effect on the starting temperature of the melting process and the associated enthalpy. However the peak temperature of melting remains constant. The re-

crystallization of the material to a solid state after melting was observed between 90 and 100 °C for the faster to the slower cooling rates respectively, a typical observation for polymeric materials attributed to the dynamics of a nucleation-area. All temperatures and transitions observed with the DSC, fit nicely with the results acquired above from the dynamic mechanical analysis (DMA).

The degree of crystallinity was calculated between 26-28% from three different samples using equation (3.1), meaning that the manufacturing parameters do not promote high crystallization of the PLA, although studies have shown that natural fibres help the crystallization process as their surface topography and roughness assists the crystallization acting a nucleating agent [46]. In general, crystalline PLA has better mechanical properties in comparison with amorphous PLA, but the crystallization of PLA requires an annealing process after the moulding that could potentially delay the manufacturing time.

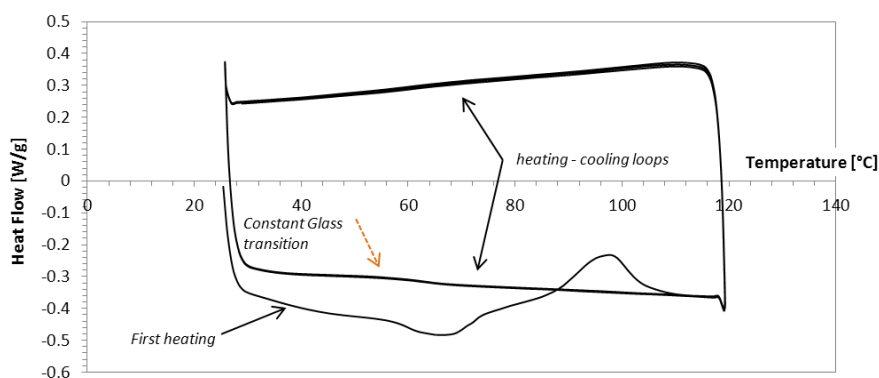


Figure 3-6: DSC thermograms with repetitive heating-cooling cycles

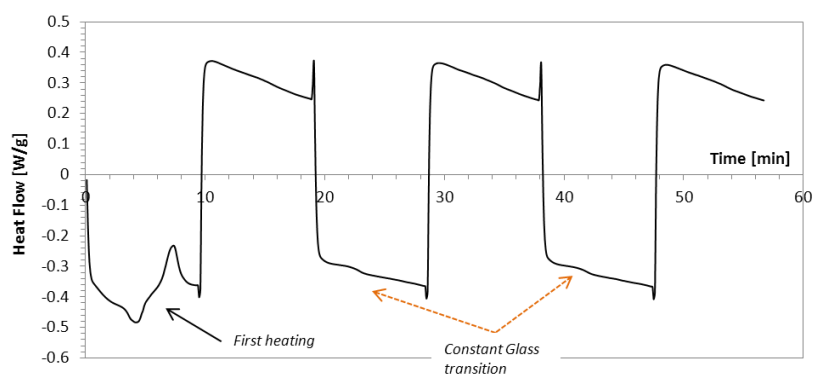


Figure 3-7: Heat flow as a function of time for repetitive heating-cooling cycles of flax/PLA

The fact that the enthalpy of melting is close to a third of that of 100% crystallized PLA ($\Delta H_{m\%}=96 \text{ J/g}$, $\Delta H_m \approx 30 \text{ J/g}$) reveals that only a small portion of the amorphous material changes state after during the exothermic transition. To understand this fact and investigate further the thermal properties of PLA and the process of the thermodynamic transitions a test with repetitive cycles between heat and cooling was conducted. The samples were heated from 25 °C past the exothermic transition (120 °C) and then cool down to the initial temperature to start another heating process. The temperature change rate was kept constant to 10 °C/min. The results are depicted in figures 3.6 and 3.7. In the first heating process the T_g and cold crystallization temperatures are clearly visible at the same temperature and with same characteristics as described above. However the material after these first transitions shows a very stable and repetitive behaviour. During cooling the heat flow remains constant (with an insignificant decrease in heating capacity in cooler temperatures most probably associated to thermal expansion/contraction of the material) while during the reheat a glass transition is repetitively appearing. Independent of the number of cycles no other exothermic transition is visible, or change in the thermal reaction of the PLA. This observation is opposed to the expected behaviour that every cycle would gradually increase the amount of crystallinity and decrease the ΔH_c to eventually reach zero [73].

3.3.4 Tensile tests

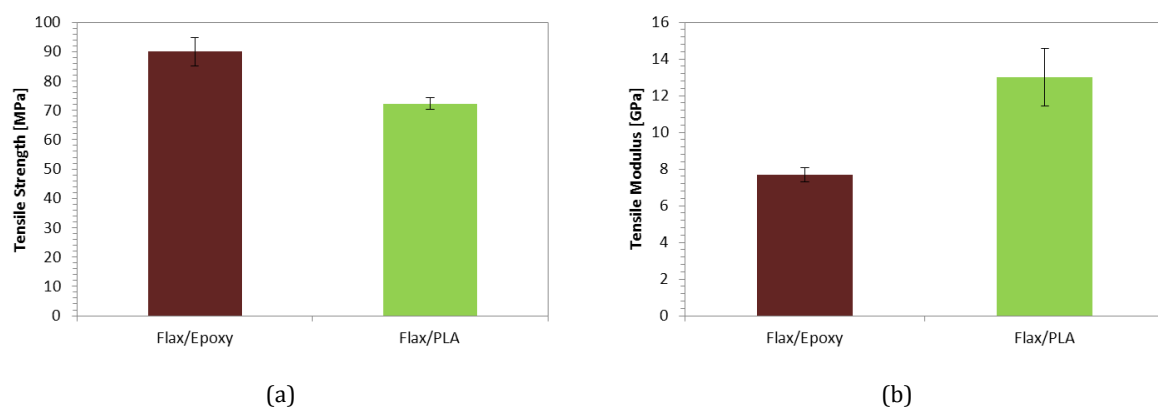


Figure 3-8: Tensile strength (a), and young modulus (b) for flax/PLA and flax epoxy composites

The mechanical properties of flax/PLA composites were compared to flax/epoxy. The measured mechanical properties for the both the PLA and epoxy composites are summarized in Table 3-1. The flax/epoxy has tensile strength of 90 MPa and a modulus

7.6 GPa, compared with 72.2 MPa and 13 GPa respectively of the flax/PLA. The elongation at break was measured 1.85% and 1.5% for the flax/epoxy and flax/PLA material respectively. The epoxy shows an advantage in terms of strength but its modulus is more than 40% lower than that of flax/PLA. The modulus and strength of the pure PLA are 3.3-3.6 GPa and 50-55 MPa respectively, while those for the bio-epoxy are 3 GPa and 63-66 MPa strength. The lower modulus of the flax/epoxy, is not only explained through the lower modulus of the epoxy, but also through the poor interfacial adhesion between the bio-sourced resin and the fibres, as well as potential manufacturing defects during processing. According to the above, the addition of flax will increase the modulus of elasticity of both materials, but will not significantly improve the tensile strength. This could be the result of the poor interfacial adhesion between the fibres and the matrix as observed in the SEM photographs, which results in failure of the composite when the stress reaches the matrix limits. The transfer of load to the fibres is insufficient. On the relevant literature on natural fibres it is widely reported that addition of natural fibres to a polymer matrix has no effect on the ultimate stress of the resulting composite, explained by the quality of fibres and adhesion with matrix [40; 45; 71; 75]. The fracture strain has been reduced with the addition of the flax fibres (both pure PLA and epoxy have an elongation at break of about 2%), possibly due to stress concentration in the fibre/matrix interface that promotes crack propagation.

Table 3-1: Tensile properties for flax/PLA composites; Comparison with flax/epoxy (standard deviation)

	Modulus [GPa]	Strength [MPa]	Elongation [%]
Flax/Epoxy	7.6 (0.4)	90 (4.8)	1.85 (0.2)
Flax/PLA	13 (0.9)	72.2 (2.0)	1.5 (0.08)

Oksman et al. [71; 75] have studied PLA with 40 wt.% flax composites, and reported a tensile modulus of 8.3 GPa modulus and a strength of 53 MPa. They also found that by increasing the percent of flax the mechanical properties were getting lower possibly due to manufacturing issues. These values are very low compared to the ones we measured, showing an improvement on the preparation methods as well as the composite components individually. Another possible explanation could also be the very low processing temperature used in this work (50 °C). Packett et al. [40] experimented with

jute/PLA composites of 40% by weight fibre content. They concluded increasing the process temperature has a positive effect on the strength and stiffness of the resulting composite due to the reduced viscosity of the PLA which led to better flow properties and hence better wetting of the fibres. Ochi et al. [44] reported very high properties with strength of more than 200 MPa and a modulus higher than 20 GPa on kenaf/PLA composites. The use of an emulsion type PLA and high kenaf fibre content allowed them to get properties comparable to glass fibre reinforced plastics.

Figure 3.9 shows the stress strain curves obtained from the tensile testing of the flax/PLA and flax/epoxy composites. A non-linear behavior can be observed for both the elastic and plastic region, with no clear yield point or transition area, typical in polymeric materials. The curves show a monotonic increasing behaviour up to a sudden failure point with brittle characteristics. The epoxy specimens have a less steep onset of the stresses due to the lower stiffness and keep rising steadily up to the ultimate strength, in comparison with the PLA specimens where the high stiffness is obvious followed by a faster constant reduction of the curve's derivative. Marklund et al., [143] observed and reported the same nonlinearity in their studies, using hemp/lignin biocomposites. It is also worth noting that although the behavior is non-linear the extraction of the modulus of elasticity was determined to allow comparisons as per the ASTM standard at the very initial stages of the test at strain between 0 and 0.05%.

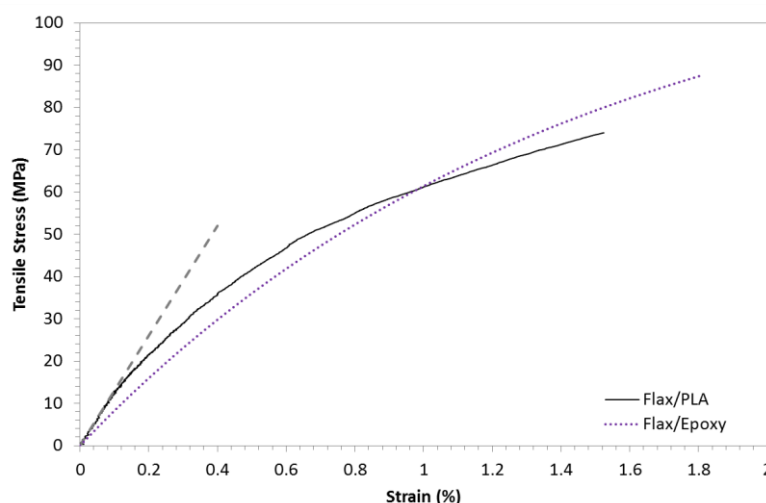


Figure 3-9: Stress-strain curve from tensile testing of flax/PLA and flax/epoxy

To investigate the transition point between elastic and plastic regions of the flax/PLA, and understand the nonlinearities of the stress strain curve of the material, cyclic tests

were conducted on tensile samples. The curve was divided into at least 5-6 points (areas) according to the strain. The specimens loaded up to specific strain and then unloaded to a zero stress condition, to be reloaded up to the next strain target. Five specimens were tested. Figure 3.10(a) shows the results of the cyclic test on the flax/PLA samples. The elasticity limit was found between 0.3 and 0.4% of the strain. The material before that point had a non-linear behaviour but unloading would bring the specimens back to the initial dimensions. The non-linearity continues in the plastic region. Observation of the modulus progress throughout the test leads to the conclusion that there is some damage accumulation during the loading possibly due to debonding between the matrix and fibres. Figure 3-10(b) shows the degradation of the tensile modulus as a function of the applied strain. Varna et al. [76] in the effort to create a material model for natural fibre biocomposites, used short flax fibres in a PLA matrix to investigate the nonlinearities of the stress-strain curves often related to these composites. They concluded that the non-linearity is a combination of micro-damage, viscoelasticity and viscoplasticity, with the damage however not having an important role before the higher stress of the curve, and therefore could be disregarded. Although the composites used in the study had a different behaviour compared to those in the present study because of the short fibres and the very small fibre content (10 wt.%), the findings show a similarity and could be extrapolated. Conclusions drawn on Hemp/PP composite studies by Gehring et al. [77], showed that the dissipating phenomena reducing the material stiffness throughout the testing were mainly due to damaging of the PP matrix.

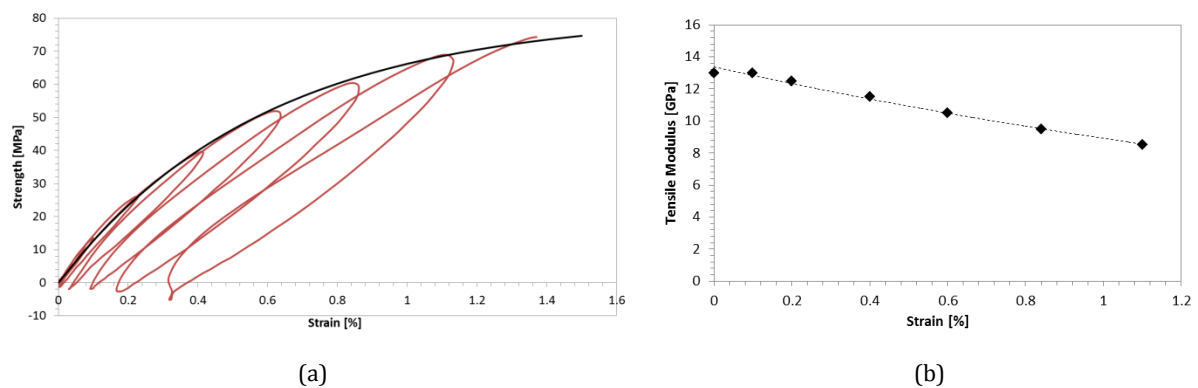


Figure 3-10: (a) Cyclic test for flax/PLA and (b) tensile modulus reduction as a function of strain due to damage accumulation during testing

3.3.5 Degree of crystallinity

The cold crystallization temperature of PLA matrix used was found to be between 90-110 °C (dependent on the heating rate) with a relatively low degree of crystallinity (X_c) between 26-28% with an average value of 27.2%. The effect of annealing to increase the degree of crystallinity and study the effect on the resulting mechanical parameters was therefore investigated. Tokoro et al. [43] results with bamboo/PLA composites proved that specimens with 100% crystallinity (annealing at 110 °C for 5h) had significantly improved thermal properties than non-annealed ones. However, the effect of this process on the mechanical properties of the composite has not been discussed.

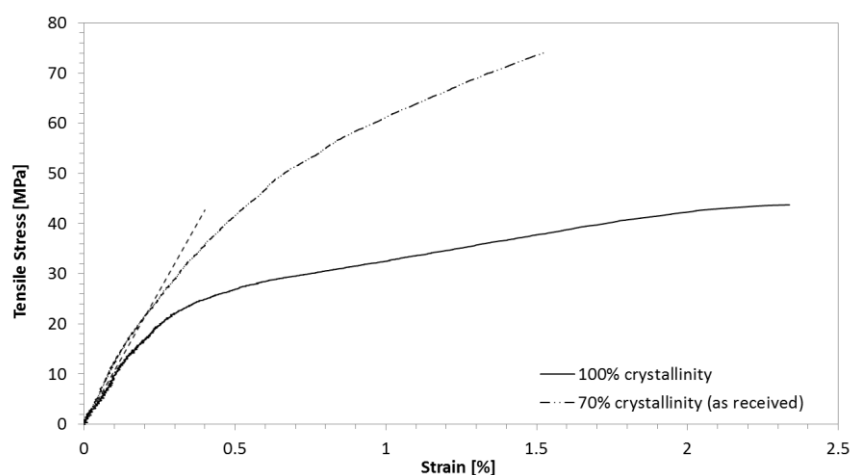


Figure 3-11: Stress strain curve of annealed flax/PLA samples compared to original samples (as a function of X_c)

Three tensile samples were heated at 110 °C for 1 h in a temperature control chamber then cooled back to room temperature and tested following the same standards as above. The degree of crystallinity was calculated using equation 3.1, and was found to be in average 30.3% for the annealed specimens compared to 27.2% of the untreated. Table 3.2 contains the obtained values compared to the properties of the original flax/PLA material. Figure 3.11 shows the characteristic stress-strain curve from these tests compared to that of the original composite. Despite the increase of X_c from the annealing process, a significant decrease of the tensile strength and modulus was observed. Observation of the surface with naked eye and the optical microscope shows

already a discoloration of the samples and different surface texture indicating a significant transformation of the material. SEM observations (figure 3.13) show that the deterioration of the properties is related to cracks formed on the matrix surface due to shrinkage of the PLA during heating.

Table 3-2: Tensile properties of annealed and non-annealed flax/PLA samples

	Modulus [GPa]	Strength [MPa]	Elongation [%]
Flax/PLA (27% crystalline)	13	72.2	1.5
Flax/PLA (30% crystalline)	10	40.2	2.2

An increased elongation was also observed, 2.2% compared to 1.5% of the baseline samples, as the reported deterioration of the matrix resulted in the failure being controlled by the untagling of the fibres bundles. During testing, the cracks are progressively grown to eventually intersect and create separated PLA micro-plates that either flow attached to the fibres or are detached from the specimen. SEM micrographs (figures 3.13) depict this phenomenon as observed close to the failure point of the tested samples. In the same micrographs the poor adhesion is again apparent as clean fibre surfaces can be observed.

An additional possible explanation, could be the water evaporation from the samples at the annealing temperature (110 °C), causing the reduction of the mechanical performance of the flax fabric. After testing a weight reduction was observed on the annealed samples, and further investigation showed that the weight reduction from exposing the specimens in 110 °C for 1 h, is as high as 1.4%. Figure 3.12 depicts the data gather in different time intervals from heating flax/PLA specimen at constant temperature of 50 °C and 110 °C.

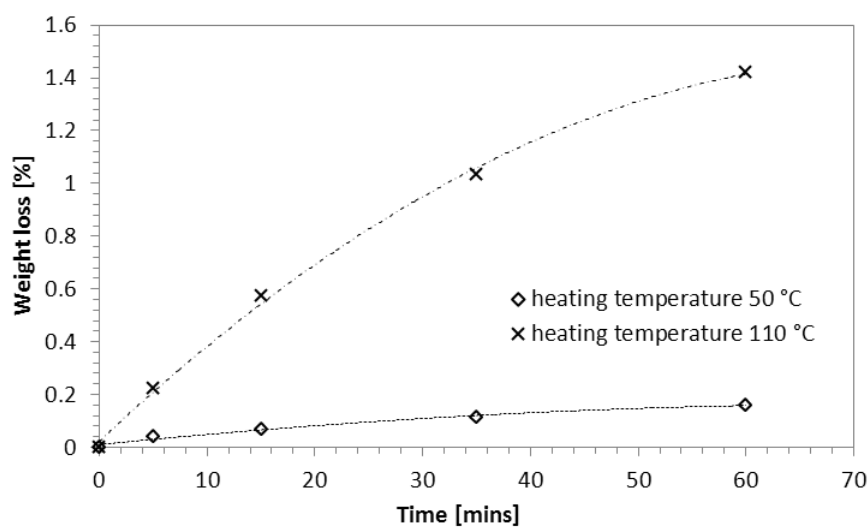


Figure 3-12: Weight loss of flax/PLA due to drying for 1h at 50 °C and 110 °C

Moisture content influences significantly the properties of flax fibres. Baley et al. [78] have shown that drying of flax fibres has negative influence on the mechanical properties of both the fibres alone and combined with epoxy resin in composite samples. They also conclude that a number of different phenomena are responsible for this loss of performance, ranging from the fibre microstructure to the fibre constituents, to stress concentration in the fibres/matrix interface due to geometrical changes of the fibres [78]. Van de Velde et al. [79] observed that exposure to different temperatures results in weight decrease and affects the mechanical properties of the fibres, with strain being more influenced than stress.

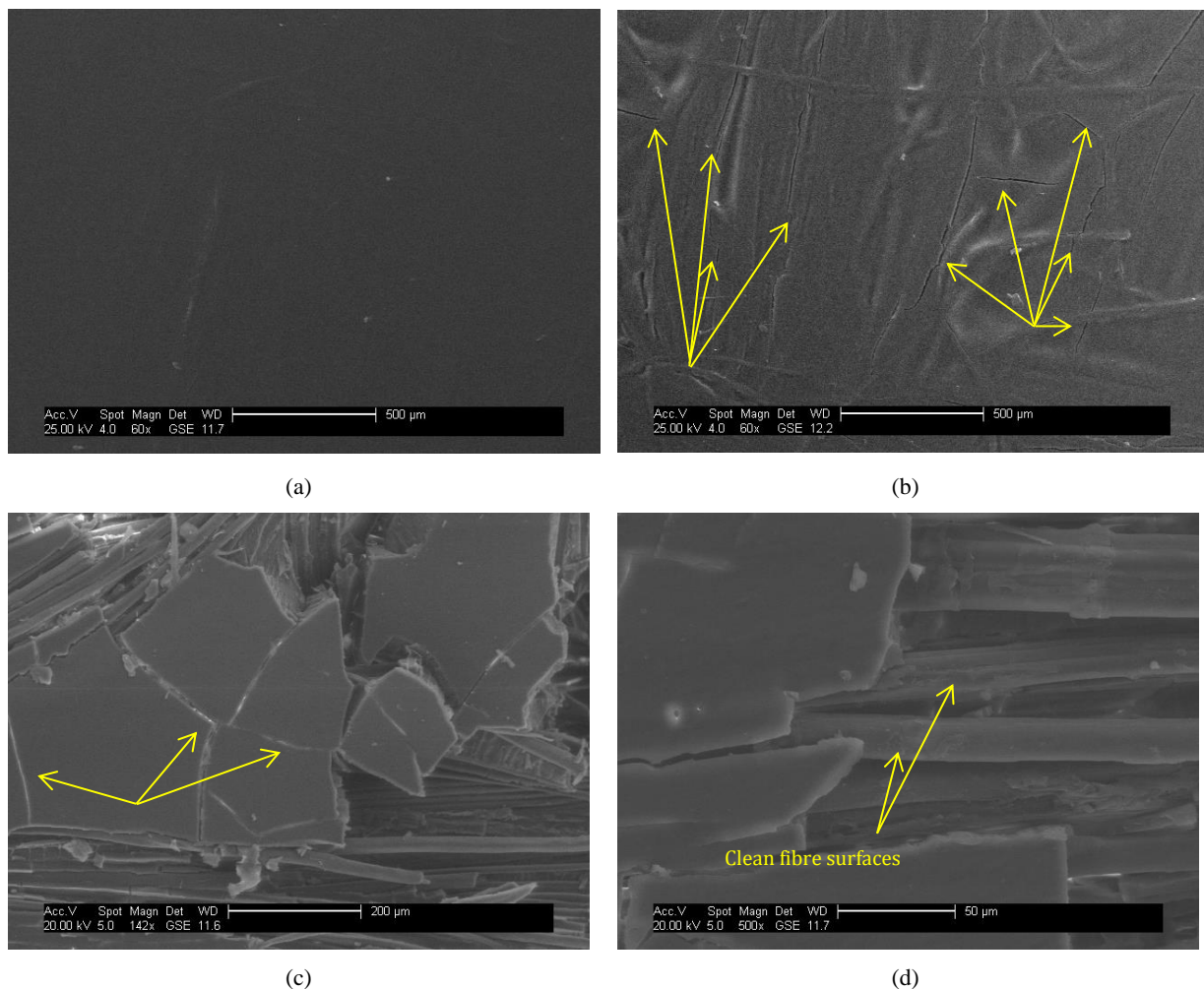


Figure 3-13: Detailed SEM photographs from (a) original flax/PLA samples compared to the surface of (b) annealed samples. The formation of cracks and the deterioration of the PLA's surface is visible. During testing, the crack growth results in breakage of the PLA (c). Poor interfacial adhesion was observed as the fibre surfaces were clean (d)

3.3.6 Influence of temperature

The properties of thermoplastics are temperature dependent. The increase of temperature reduces the Young's modulus and tensile strength but increases the failure strain leading to a material more ductile and less stiff [80]. With increasing temperature, thermal transitions occur which can impart dramatic step-changes in material behaviour. As observed and discussed in the results above, PLA is semi-crystalline and exhibits a complex combination of thermal transitions occurring in the crystalline as well as in the amorphous phase, in relatively short range of temperatures. Furthermore, the mechanical properties of a composite and hence the effect of temperature alterations, depend on both the polymer matrix characteristic and the

reinforcing fibres. Additional energy dissipation mechanisms can be activated thanks to the addition of fibres [81], and very little is known on how temperature will affect the properties of the flax reinforcement.

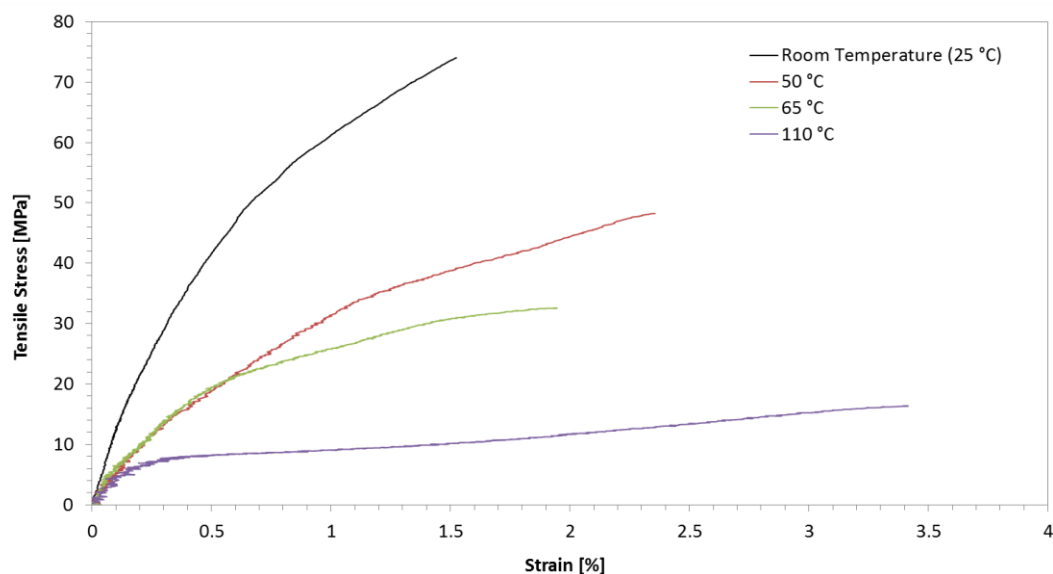


Figure 3-14: Stress-strain curves of flax/PLA tested in room temperature (25 °C), 50 °C, 65 °C and 110 °C and nominal strain rate

Although a number of studies have been conducted at room temperature, little is known on the effect of temperature on flax/PLA reinforced composites properties such as tensile strength and modulus. In order to evaluate this effect, studies were undertaken and the resulting stress–strain curves were plotted over a temperature range of 25 to 110°C. Figure 3.14 reveals a strong dependence of the material properties on temperature, as of the deformational behaviour changes from brittle to more ductile-like characteristics. The material deforms up to higher strains with both the modulus and strength reduced significantly. Already around 50°C, prior to the T_g point, the stiffness is reduced by half. This result combined with the results from the thermal studies of the PLA signifies the deterioration of the PLA during the constant heating. On the DMA graphs this high deterioration is not visible, as the storage modulus reduces at 50 °C but not more than 10%. This could be related to the fact that the heating rate during the DMA test was set to 1 °C/min while for the tensile testing the samples were

first left to reach the desirable temperature for a period of 30 minutes. The above observation denotes a thermal inertia and is evidence of a strong viscous behaviour of flax/PLA. The prolonged exposure to temperature deteriorates further the mechanical properties resulting in a very weak material. Table 3.3 summarizes all the values acquired from the testing of the material under different temperatures.

Table 3-3: Tensile properties of flax/PLA for all four temperatures tested (standard deviation)

	Modulus [GPa]	Strength [MPa]	Elongation [%]
Flax/PLA - 25 °C	13 (0.9)	72.2 (2.0)	1.5 (0.08)
Flax/PLA - 50 °C	6.2 (1.0)	53.2 (3.2)	2.4 (0.14)
Flax/PLA - 65 °C	7 (1.5)	35.7 (2.8)	2.04 (0.19)
Flax/PLA - 110 °C	5 (0.3)	15.5 (1.6)	3.2 (0.4)

The effect of temperature on the properties of flax/PLA composites is more explicitly shown in Figures 3.15-3.16 where it can be seen that the tensile stiffness and strength decrease with an increasing temperature following a non-linear relationship, while the elongation has an opposite but similar increase with increasing temperature. Interestingly, at a temperature of 65 °C (glass transition point, T_g) an increase of the modulus together with a decrease of the elongation at break were measured compared to the same values for 50 °C. The material becomes stiffer with a modulus of 7 GPa and elongation of around 2%. An explanation for this unexpected behaviour can be the higher mobility of the chains together with the increased ductility of the PLA matrix past the T_g that results in less debonding between the resin and the fibres, thus better transfer of loads between the composite constituents. Further, the temperature effect on the mechanical properties of composites derives partly from the internal stresses introduced by the differential thermal coefficients of composite components. Such internal stresses change magnitude with temperature, and can control the matrix cracking. The strength however, related mainly to the decreased load limits of the matrix, is reduced to more than 50% of that in room temperature, with a characteristic higher reduction gradient than between 25-50 °C and 65-110 °C.

The mechanical performance of flax/PLA in around 110 °C is relatively low, with the modulus decreasing another 30% from the 65 °C case, but with the strength remaining being only 15.5 MPa in comparison with 72 MPa at ambient temperature. It is also worth noticing that the stress-strain law also changes from a 2nd order non-linear curve, to an approximately bilinear response. After the elastic linear region at around 2.3-2.5% strain, the material yields at a constant stress, with a visible hardening after 1-1.5% strain. The elongation at break at this temperature is on average 3.2%, more than double of that in room temperature.

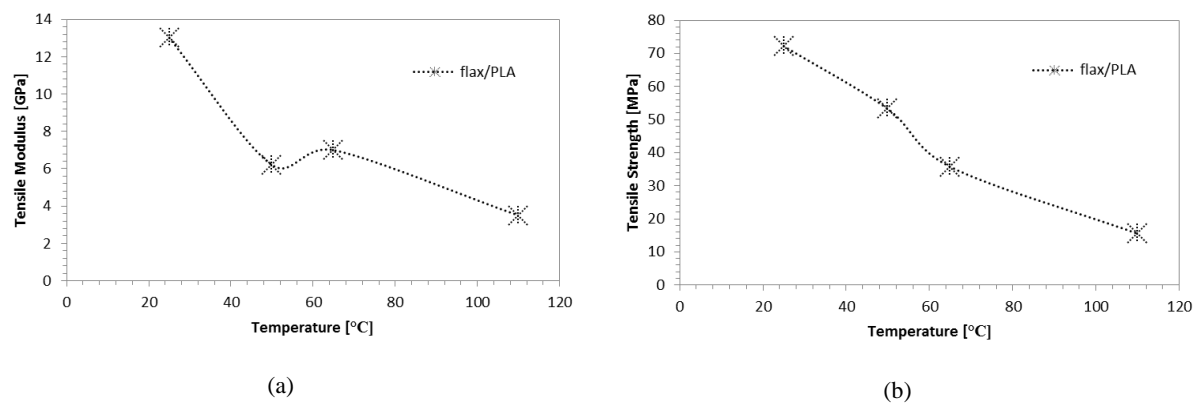


Figure 3-15: Tensile modulus and ultimate strength of flax/PLA specimens as a function of temperature

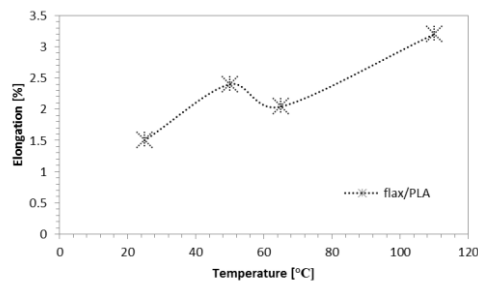


Figure 3-16: Elongation at break as a function of temperature

Although the mechanical curves depict a shift from a brittle to a ductile material, the characteristic modes of failure do not show the same. The failure remains brittle up to 65 °C, with the matrix snapping in a 90° angle to the loading direction, no formation of neck or any material yield. At 100 °C, due to the high deterioration of the matrix (PLA), the material debonds and reacts as if no resin is present. This result can be explained through the SEM observation and conclusions drawn above from testing of the annealed samples. The loading appears to be only carried through the fibres at this temperature, which after a load limit, and as they consist of fibre bundles, start slipping apart and

unwrapping (figure 3.17). Further, the temperature and heating time had also an effect on the fibres through reduction of the moisture content [82-84].

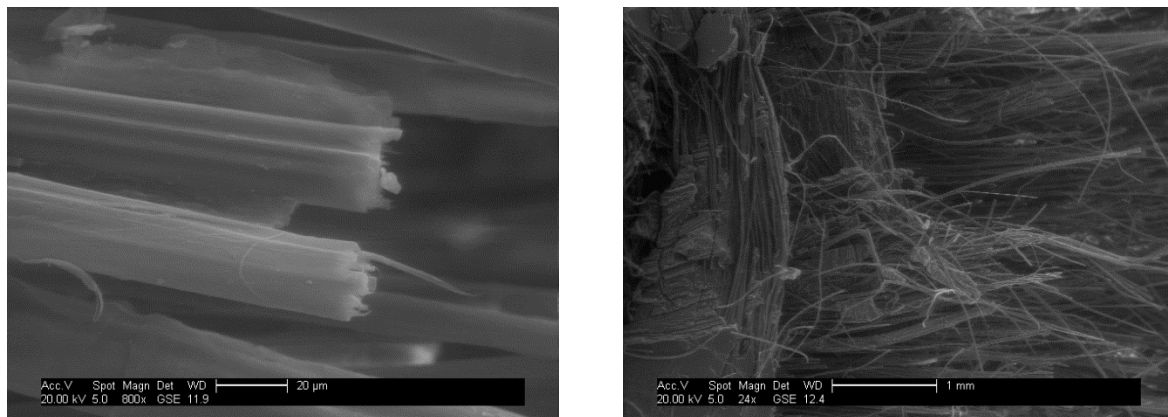


Figure 3-17: Detailed SEM micrograph of flax fibres after testing of flax/PLA samples at 110 °C

3.3.7 Strain rate effect

Some polymers exhibit significant rate dependency while others do not. At lower strain rates a polymer usually exhibits a more ductile behaviour while at increased deformation rates the response of the material becomes brittle-like, with a significant increase of the ultimate strength and yield points. This increase in stress can be directly related to the secondary relaxation processes ($T < T_g$), or/and the decreased molecular mobility of the polymer chains at high rates of deformation [85]. The stress dependency on strain rate is often expressed as a power-law relationship that can be represented as:

$$\sigma = B \cdot \dot{\epsilon}^m \quad (2)$$

where B is a constant and m is the strain-rate sensitivity coefficient, which is always greater than or equal to zero. For materials with negligible strain-rate sensitivity, m is near zero, making σ constant as a function of strain rate ($\dot{\epsilon}$). Materials with greater strain-rate sensitivity have greater values of m .

Table 3-4: Tensile properties of flax/PLA as a function of the crosshead displacement tested at room temperature (standard deviation)

Crosshead velocity	Modulus [GPa]	Strength [MPa]	Elongation [%]
nominal strain rate	13 (0.9)	72.2 (2.0)	1.5 (0.08)
0.5 m/sec	14 (0.7)	87.1 (3.8)	1.5 (0.09)
4.2 m/sec	22 (2.2)	95.7 (6.2)	1.3 (0.15)

This feature of the mechanical behaviour is particularly relevant for applications with polymeric components required to resist impacts. In the automotive, impact resistance of exterior panels and components exposed to road debris is critical. Up to date very little is reported on the effects of strain rate on the mechanical characteristics of natural biocomposites. Omar et al. [86] investigated the dynamic mechanical properties of jute and kenaf fibres combined with a polyester resin. They reported that the modulus and strength of both materials were highly dependent on the strain rate, and showed a significant amount of rate sensitivity dependant on the deformational speed. Gehring et al. also observed an increase of the maximum stress supported by hemp/PP composites at an increased strain rate, and concluded that the mechanical responses of the material show a high sensitivity to the strain rate up to failure [77].

Monotonic tensile tests at different cross-head velocities were conducted to investigate the effect of strain rate on the mechanical performance of flax/PLA. Three speeds were used, 2mm/min (quasi-static), 0.5 m/sec and 4.2 m/sec, limited by the capabilities of the equipment used. For each velocity at least three samples were tested. The results for the modulus, strength and elongation at break are summarized in table 3.4.

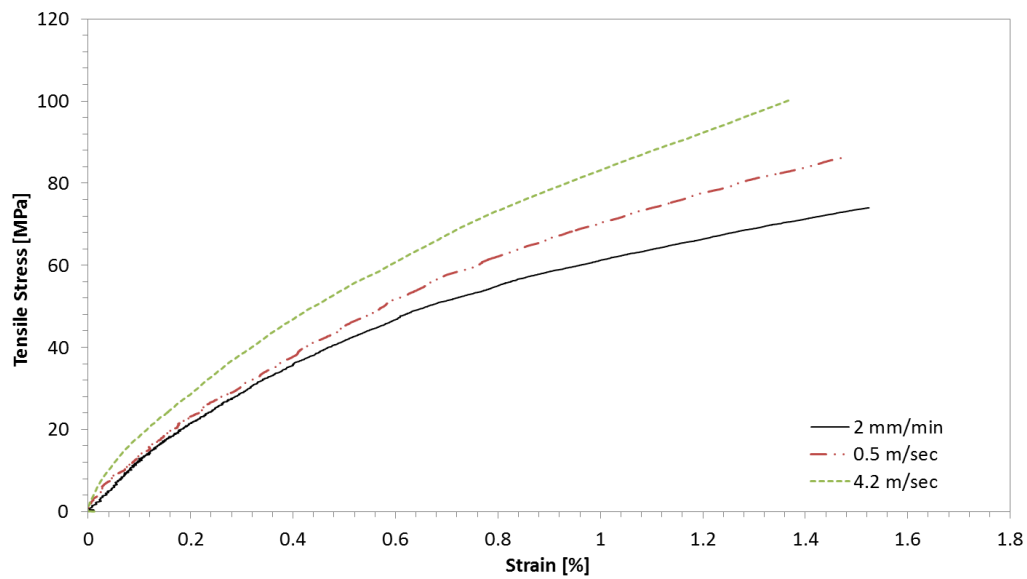


Figure 3-18: Stress-strain curve of flax/PLA tensile specimens, tested in three different crosshead velocities.

Figure 3.18, depicts the stress-strain curves obtained in different testing speeds. The material mechanical properties are strongly affected by the strain rate. Already in 0.5 m/sec cross-head velocity, the ultimate strength of the material is increased by 20% compared to the quasi-static velocity, with an increase of the modulus from 13 to 14 GPa. Further increasing the strain rate, results in 22 GPa tensile modulus (70% increase), with a strength as high as 95.7 MPa, representing a 32% increase. As observed the above results illustrate a change of both the strength and modulus of the flax/PLA as a function of the rate of deformation. The material at higher strain rates becomes stiffer and stronger, while its elongation at failure decreases. In all cases the failure mode has brittle characteristics, with failure occurring without necking or signs of plasticity. Studies with higher strain rates with the use of a Hopkinson bar are needed for the investigation of the strain rate sensitivity, and would be reported in follow up studies.

3.4 Conclusions

Aim of this work was the study of the thermo-mechanical performance of flax/PLA biocomposites, going beyond the typical investigation of the properties to an understanding of the mechanical behaviour of such composites from a structural point of view, for the potential use in load bearing application in the automotive sector. Focus

was given into the interlink between the thermal and mechanical properties, and the material response under different loading conditions and environments.

The strength and stiffness of flax/PLA samples – 72 MPa and 13GPa respectively – indicate a very promising material to replace traditional choices in load bearing application. However, SEM micrographs show that the interfacial adhesion of the constituents is still poor and modifications need to be applied on the fibre's surface in order to improve it. The poor adhesion is confirmed through tensile testing and the comparison of the mechanical properties of pure PLA with those obtained from the flax/PLA specimens. The need for better fibre separation prior to the manufacturing process is also underlined. The PLA matrix shows brittle characteristics, with an average failure strain of 1.5%. The stress-strain law is non-linear with the non-linearity introduced due to viscous behaviour of the material combined with a certain level of damage accumulation throughout the testing.

DMA results show deterioration of the composite properties with a tan delta peak at around 74-76 °C. An increase of the storage modulus is however visible after 80 °C, explained due to the cold crystallization transition of the amorphous part of the PLA. The flax fibres have a positive effect on the thermal response delaying the loss of stiffness to higher temperatures compared to that of pure PLA. The crystallinity of PLA was measured to be approximately 27%. Annealing above 100 °C for an hour brings that value to 30%, but analysis of tensile results of annealed specimens reveals a significant reduction of both the tensile strength and modulus. This reduction is associated with micro-cracking that occurred on the surface of PLA during the heating as well as deterioration of the flax properties due to drying.

Temperature affects enormously the properties of flax/PLA. At 50 °C the stiffness is reduced by half, and the ultimate strength is reduced significantly. 110 °C bring the modulus further down to about 5GPa with a remaining strength of 15.5 MPa. With increasing temperature the elongation at break increases. The failure characteristics remain brittle for the temperatures up to 65 °C, while at 110 °C high degradation of PLA is observed and the load seems to be carried through the fibres which progressively slip apart.

Strain rate has an effect on the material and its viscous behaviour. Strength and modulus increase with increasing strain rates, while elongation at break reduces respectively. A modulus of 22 GPa was recorded in 4.2 m/sec crosshead velocity. Studies with a Hopkinson bar would be required for the calculation of the material's strain rate sensitivity.

The mechanical properties of flax/PLA were compared with a more commonly used a studied flax/epoxy material. Although flax/epoxy has some advantages in terms of strength and thermal stability, flax/PLA has significantly higher modulus. Improvement of the interfacial bonding and the temperature characteristics, combined with the thermoplastic nature of PLA, will make flax/PLA composites ideal for use in structural automotive applications.

Chapter 4. Low velocity impact properties and strength after impact performance of flax/PLA biocomposites

4.1 Introduction

Natural fibre biocomposites have already found their way into the automotive industry for a wide range of components such as door panels, seat backs, dashboards and package trays and head restraints.[9; 14; 68; 87]. Their wide use into structural applications or exterior vehicle components is still limited by relatively lower properties and several technical considerations. In particular, the study of their mechanical properties in respect to their loading capacity, the deformation behaviour and their response under different loading conditions is crucial [88]. As the use of natural composites in the automotive industry increases, the need to determine their impact responses (high strain rates) to ensure safety and stability of designed structures is important. The testing setup should be designed to simulate realistic loading conditions to which the composite component is subjected in operational service, and then reproduce the failure modes and mechanisms likely to occur.

It is well acknowledged that, during an impact condition, composites can fail in a wide variety of modes and contain visible or barely visible impact damage, which severely reduces the structural integrity of the components. Most thermoset composites are brittle, for instance, and so can only absorb energy in elastic deformation and through damage mechanisms, and not through plastic deformation. Furthermore, the prediction of the post-impact load-bearing capability of a damaged composite structure is

relatively difficult since the damage zone is generally complex in nature and consequently very difficult to characterize [89]. Understanding the failure process and damage accumulation is vital for the design of reliable structural components that will replace their traditional and less eco-friendly metallic or synthetic-composite equivalents.

In the literature, most efforts in understanding the impact performance and failure mechanisms of reinforced thermoplastics were principally concentrated on Charpy and Izod impact testing, and to a lesser extent, drop weight tower impact testing [90-93]. These tests yield information on the processes of energy absorption and dissipation within composites [89]. A number of studies have already reported on the impact properties and the effect on those properties from different manufacturing and environmental conditions. Studies using the above two testing techniques can also be found on the energy absorption properties of flax, PLA and their combined composites [71; 72; 94]. Bax et al. [72] conducted Charpy impact test on Flax/PLA and Cordenka/PLA samples, and reported for them significantly poor properties, affected however by the fibre content up to 31 vol.% flax. Similar results were observed on Flax/PLA by Oksman et al. [71]. For the samples tested they reported that triacetin plasticizer does not have any influence on the energy absorption (11 kJ/m²). Izod impact tests were conducted by Alimuzzaman et al. [94], on notched flax fibre reinforced polylactic acid (PLA) samples. The samples were fabricated using a new compression moulding technique for nonwoven natural fibre reinforcements. Based on the observed increasing impact strength with increasing fibre content, they achieved 28.3 kJ/m² impact strength. They also studied the link between the manufacturing properties and the impact performance of their samples, and reported a drop in performance directly proportional to the moulding duration and temperatures increase [94].

Charpy and Izod impact tests, however, are usually destructive and therefore induce failure modes that are not necessarily observed under real conditions on operational structures such as a running vehicle. They force the specimen to fail at a predetermined area rather than along the weakest plane. The results can be skewed because of the highly anisotropic nature of reinforced thermoplastics. Consequently, these tests are only suitable for comparing impact resistance of composite materials.

A more representative test to simulate the effect of flying stones impact would be to conduct low velocity impacts (<50m/s) [95; 96] with a blunt tip impactor or projectile. This can be achieved with a gas gun or to a certain extent with a low velocity drop weight tower [89; 91; 97]. A low velocity gas gun impact test gives a more representative test of a stone impact scenario and can be used to test large structures in different angles. It is a single stage high performance projector using compressed air to propel projectiles with various profiles and masses [37]. These tests are not necessarily destructive, but can often result in large-scale damage. Until recently, the technique suffered from the limited information that could be obtained from the test itself. Instrumented gas guns have now been developed, enabling force/displacement histories to be measured and the impact event to be analyzed in more details. One point to note is that the impact energy is controlled by the pressure in the barrel and pressure and friction losses of the projectile can often result in different velocities of the impactor and thus of the energy. Systematic calibration and detailed post-processing of the data is needed prior to testing.

In this chapter, the performance of flax/PLA composites subject to an impact with a flying projectile using a gas-gun is studied. Such a study has not been made before for natural fibre reinforced composites. The purpose of this study is to provide an insight on the possibility of using these composites in exterior automotive applications and components often subjected to impacts with road debris. Focus of the studies was the assessment of the damage and the mechanisms by which it occurs, failure thresholds, as well as the remaining strength in the material after such impact.

4.2 Materials and methods

4.2.1 Materials

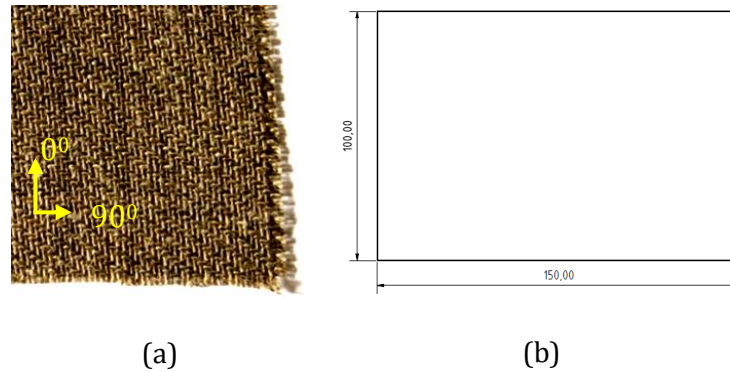


Figure 4-1: (a) The 0/90⁰ woven flax fabric and (b) impact sample dimensions

A commingled/pre-impregnated Flax/PLA fabric (mixed flax and PLA fibres) was provided by Composites Evolution Ltd (UK) and it contained a poly(L-lactide) acid (PLA) based on lactides acquired from corn starch fermentation supplied by Natureworks. Typical density of the PLA used is between 1.23-1.25 g/cm³. The reinforcement used was a 2x2 twill flax weave with an approximate unconsolidated thickness of 0.8mm (after consolidation, the thickness was around 0.3mm). All samples were prepared using a hot press moulding process with 12 layers of the fabric for the 3mm samples and 16 layers for the 4mm samples, ending with 40% flax by volume composite. The parts were moulded at 180°C and held at this temperature for 5 mins before being cooled. The pressure used was about 15 bar. The resulting density was estimated between 1.35-1.4 g/cm³. For the cutting of the samples, a CNC milling machine was used with the speeds and feeds carefully selected to give a good edge finish and make sure that no sample was destroyed during the process. After manufacturing, all samples were C-scanned for any damage during the process. Several similar samples were tested under different conditions and the results are presented below.

Immediately after manufacturing all samples were sealed in polyethylene bags to keep them dry and avoid any exposure or contamination from the environment.

4.2.2 Impact testing

Gas gun impact tests are conducted with a low velocity gas gun manufactured by Sabre Ballistics Ltd with up to 8 bars of effective low pressure. The tests performed propel a 22 g projectile with a 10 mm hemi-spherical profile to the centre of the plate. The desired projectile velocity is obtained by adjusting the pressure of the gas before firing. It obtains velocity by using a solenoid valve which releases a set volume of gas into a chamber within the gun. The gun is positioned thanks to a laser beam. The distance of firing is set to 400 mm and kept constant. This distance has been chosen to be not too close to the target, in order to avoid rebound damage on the barrel, and not too far, in order to minimize the loss of velocity of the projectile due to gravity and air friction. The projectile velocity was recorded at the muzzle of the barrel via two fibre optic sensors. The impact energy was ranged from 1 to 7J, corresponding to an impact velocity range from 10 to 23 m/s. The impactor and projectile used, illustrated in Figure 4-2, correspond to an average 10 mm dart profile road stone. Few tests were conducted at higher energy levels, however the corresponding very high pressures (>8 bar) required the use of an additional highly pressurized gas bottle, and the accuracy and repeatability of the tests were poor. These tests were only used to measure an approximate penetration energy level.

Test samples for the gas gun tests are rectangular plates of 150x100 mm in length and 4 mm in thickness. In both situations, a clamping frame constrains the edges of the plate, leaving an exposed surface to impact of 140 by 90 mm. The dimensions of the samples were specifically selected to reduce geometrical effects, such as corner stress concentrations due to the clamping, and to comply with the necessary dimensions needed for other testing standards, such as the compression after impact (ASTM D7137). A testing fixture (Figure 4-3) was specifically designed for the purposes of this study to accurately measure and record force/displacement and time-histories throughout the tests. In order to exclude frequency response and inertial effects a stiff and lightweight aluminum clamping plate was designed and supported on an aluminium frame through four piezoelectric load cells, one on each corner of the plate. To assure good vibration response and consequently accurate and high resolution results, the stiffness of the load cell was specifically selected. A signal amplifier and conditioner were used, and all measurements were recorded by a National Instruments

digital to analogue converter (DAC), combined with a specifically designed LabVIEW interface. A minimum of 5 tests per energy per material were performed at 90° to the surface.

Figure 4-2 shows an image of the road stone, and impactor (right) used and the corresponding size scale.



Figure 4-2: Road stone, projectile and impactor [80]

The damage assessment after an impact test is made by visual inspection on the external surfaces of the impacted sample. However, sometimes it was difficult to determine whether or not the sample has failed. This is specifically the case when the intensity of the impact is near the failure capacity that the structure can withstand. For this reason, the recourse of a non-destructive testing is needed to inspect and eventually determine the extent of the damage. Ultrasonic C-Scan technique was used to detect any damage by the attenuation or reflection of ultrasonic waves across the impacted sample. Figure 4-3 shows the test fixture used for the impact assessment of the samples, while Figure 4-4 shows the low velocity gas gun setup used.

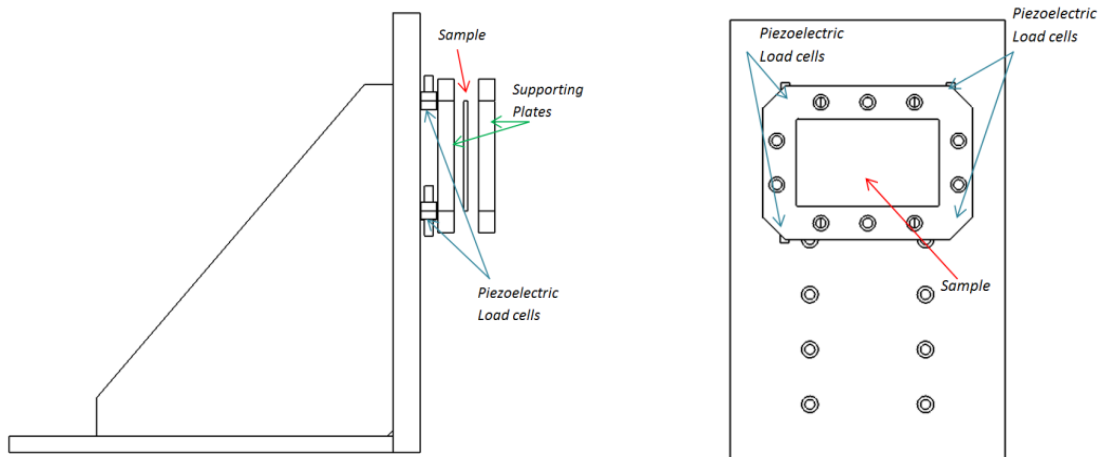


Figure 4-3: Test fixture used for the impact assessment of the material

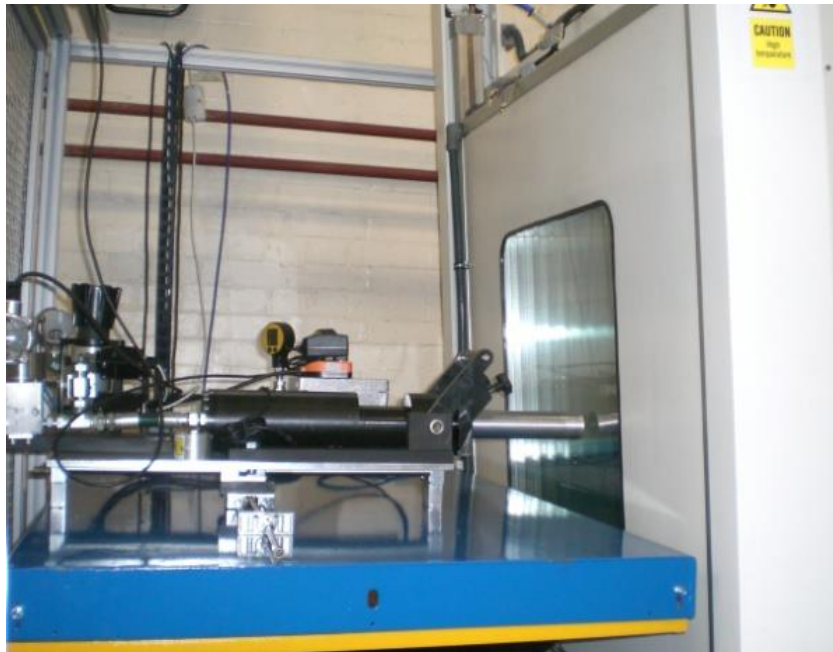


Figure 4-4: Low velocity gas gun setup

4.2.3 Compression after Impact (CAI)

The impacted samples were mounted into the compression fixture and subjected to compression loading according to ASTM D 7137. An Instron 5500R electro-mechanical universal testing machine was used for subsequent CAI testing, along with a fixture

assembly that meets the relevant specifications. A constant crosshead displacement rate of 1 mm/min was applied until failure or until the load experienced a 30% drop off from its maximum. Applied force and crosshead displacement were recorded during loading. Since strain gauges were not attached to the specimen, residual compressive strength is the only property that resulted from this test.

The compressive test fixture is designed with adjustable vertical knife-edge supports to inhibit buckling without restraining local out-of-plane rotations of the specimen. If gaps occur between the specimen and side supports, errors may arise from sample bending or concentrated loading conditions at the top and bottom specimen surfaces. The fixture must also be carefully centred with the loading axis to ensure uniaxial displacement of the fixture/specimen assembly. The compressive residual strength support fixture is illustrated on Figure 4-5.

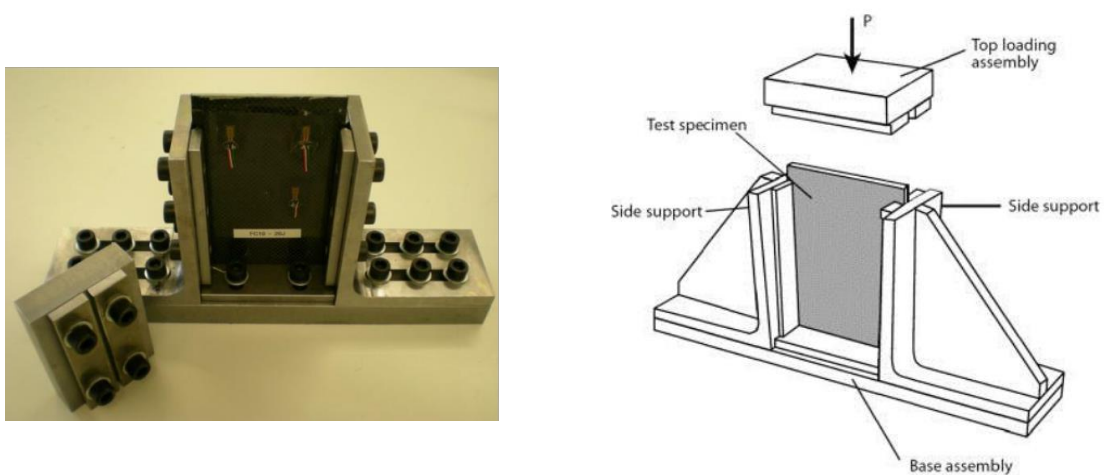


Figure 4-5: Compressive residual strength support fixture (ASTM D 7137)

4.3 Results and discussion

4.3.1 Impact properties

The gas gun impact tests show that the plates fail at barrel pressures higher than 3.3 bar, corresponding to a velocity of approximately 20 m/s and energy of 4.4J. For impact velocities up to 9.7 m/s only very local front surface marks were created in the specimens due to the pressure created by the impactor tip during the test. No visible cracking or back surface splitting occurred. At energies higher than 4.4J, e.g., 4.5 or 6 J, in addition to the front surface damage, some back surface splitting was also observed,

differing on the scale of the failure (Figure 4-6). The length of the front surface crack increased with increasing impact velocity. The plates tended to fail with a cross-shaped crack and the scale of the damage increased with the energy. The cross-shaped failure was expected and explained through the fibre directions being at 0/90°.

Table 4-1: Average impact loads recorded at specific impact energies and their corresponding velocities
(standard deviation)

Gas gun pressure	Impact velocity [m/sec] (average value)	Impact energy [J]	Load [kN]
1.8 bar	10 (1.1)	1	3.6 (0.41)
3.3 bar	20 (0.94)	4.4	6.2 (0.45)
4.0 bar	23 (0.91)	5.8	6.9 (0.47)
≈8.0 bar	≈40 (-)	≈16	-

Table 4-1 depicts the average impact loads recorded at the specific impact energies and their corresponding velocities to which the sample plates were subjected by the air gun impact tester under dry as moulded conditions at room temperature. Table 4-2 provides the assessment of their post-impact damage, characterized by the shape and the size of the failure. Figure 4-6 shows fractographs of the samples subjected to gas gun impact testing at 4.5 J (left) and 5.8J (right). The upper images show the front face of the samples, while the lower images the back face. We see that cracking is further expanded at higher loads.

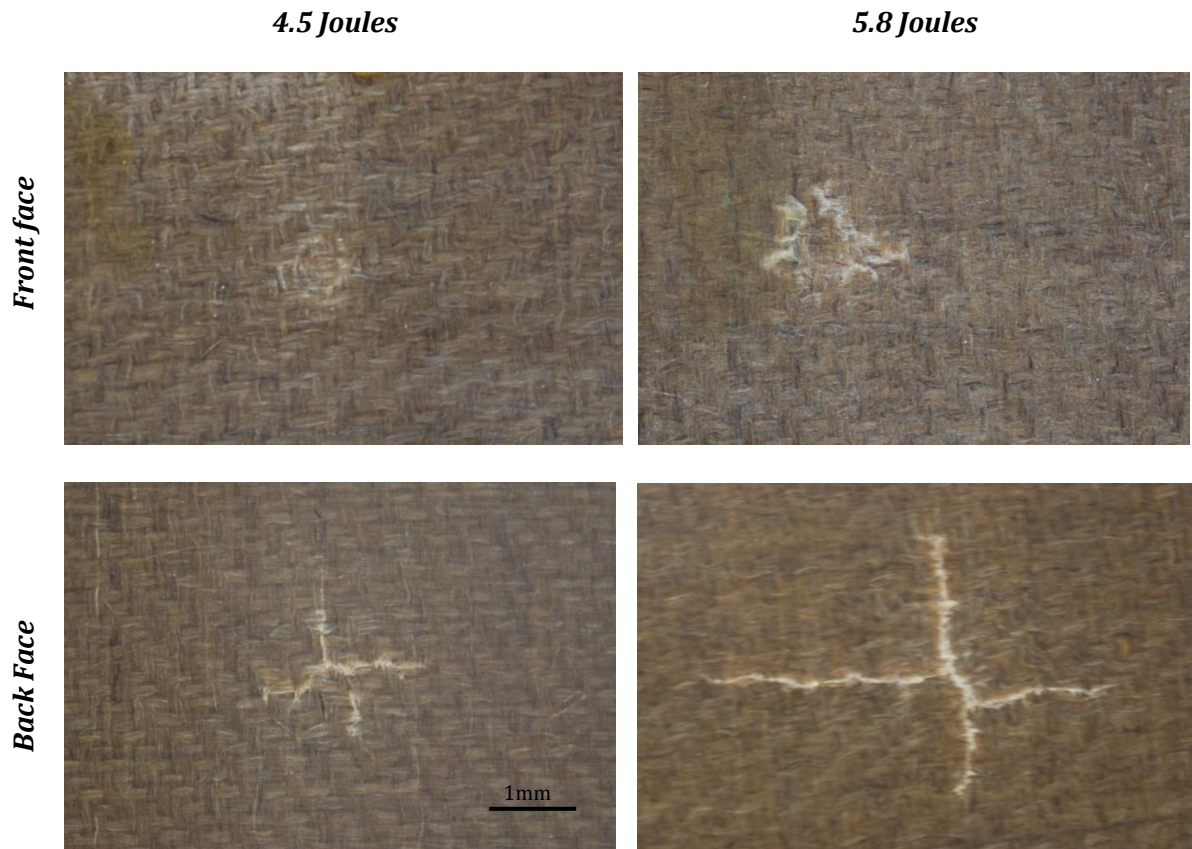


Figure 4-6: Fractographs of the samples subjected to gas gun impact testing at 4.5 J (left) and 5.8J (right). The upper images show the front face of the samples, while the lower images the back face.

As mentioned before, an NI data acquisition system was developed to measure the force/time history during every impact, while the velocity of the impactor (initial impact velocity) was recorded at the barrel exit through a combination of optic sensor beams. The remaining parameters, such as absorbed energy, velocity of impactor and deflection, were calculated using the equations of motion.

Figure 4-7 shows high speed optical camera images of the impact sequence for the 23m/sec test of flax/PLA samples.



Figure 4-7: Impact sequence for the 23m/sec test of flax/PLA samples (high speed camera imaging)

At 1.8 bar pressures (velocity ≈ 9.7 m/sec), the force–time histories of the samples (Figure 4-8) showed an almost linear increase of the impact for the first msec, followed by a smooth decrease of the tangent (acceleration rate) up to the maximum impact load. After the maximum load the force decreased more rapidly down to zero, as if there was no contact between the impactor and the specimen. For the higher impact energies however (Figure 4-8), a different force/time shape was observed. Prior to reaching the maximum load and after about 0.05-0.07 msec, a slope decrease was observed, reaching a slight plateau, followed by an increase up to the full specimen impact capacity. Further studies and testing are necessary to confirm this behaviour and the theory that relates the observed force response to the creation of the cracks. The entire impact event was again at about 0.17-0.2 msec and the maximum force occurred at around 0.1 msec. The above results are summarised in Table 4-2, which shows the damage assessment of the tested samples after gas gun impact at different conditions.

Table 4-2: Damage assessment of the tested samples after gas gun impact at different conditions

Impact Velocity	Gas Gun pressure	Size WxH [cm]	Shape
10 [m/sec]	1.8 bar	No damage	No damage
20 [m/sec]	3.3 bar	2.1 x 2.1	+
23 [m/sec]	4.0 bar	4.6 x 2.75	+
≈ 40 [m/sec]	≈ 8 bar	Penetration	

Evaluation of the force–time histories and observation of the optical pictures of the impacted composites led to the conclusion that this sudden flattening of the force–time histories of the higher energy impact tests was due to back surface splitting exhibited by the samples. We have seen that the force–time histories of the tests which produced no or very little back surface splitting did not show the same behavior. At low pressure, the force generated due to the contact of impactor-composite was linear with the applied pressure since the impactor was pushing the specimen without causing any damage. As soon as some damage was produced, the force–time history rate showed a sharp decrease. This damage appeared to be in the form of delamination, front surface cracks or front surface indentation. The back surface-splitting observed in the specimens tested at 3.3 and 4 bar pressures, reduced the resistance of the composite, resulting in the flattening of the graph. The remaining resistance of the composite, however, pushed back the impactor and rebound occurred. Instances with the projectile impacting a second time the samples after the rebound were observed, and these tests were discarded and repeated.

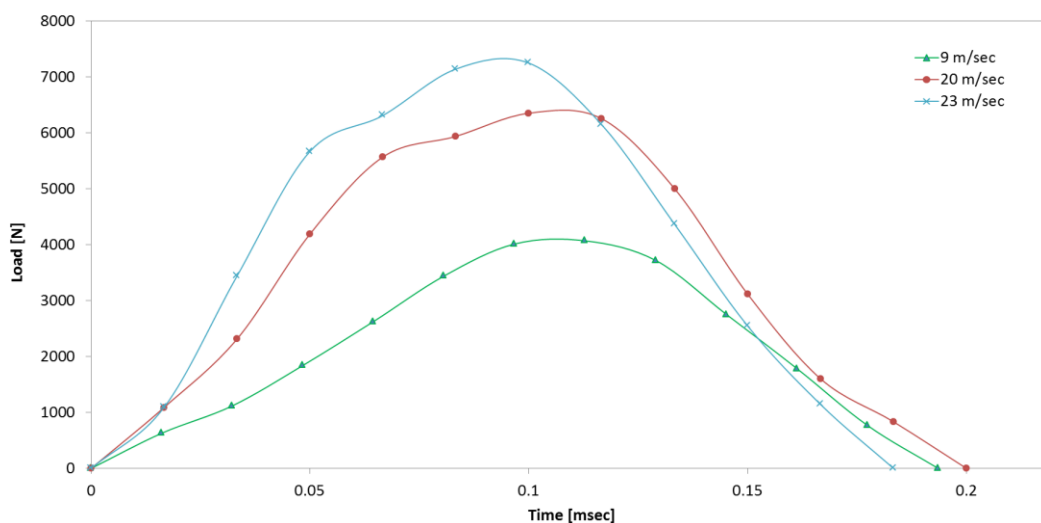


Figure 4-8: Time histories of the contact forces of the composite specimens conducted at three different impact velocities

Figure 4-8 shows time histories of the contact forces of the composite specimens conducted at three different impact velocities. The average impact loads recorded for each impact energy were 3.6, 6.2 and 6.9 kN for the 1, 4.4 and 5.8J impact energies

respectively. Previous studies on flax/PLA natural composites [88] showed that their mechanical properties are strongly affected by the strain rate. Already at 0.5 m/sec cross-head velocity, the ultimate strength of the material was increased by 20% compared to the quasi-static velocity, Further increase of the strain rate results in 22 GPa tensile modulus (70% increase compared to the nominal strain rate), with a strength as high as 95.7 MPa, representing a 32% increase. These results illustrate a change of both the strength and modulus of the flax/PLA as a function of the rate of deformation, with the material at higher strain rates becoming stiffer and stronger (Table 4-3). To conclusively assess the effect of the strain rate on the mechanical properties (resistance) of the material, strain measurements of the samples throughout testing are required, using for example the setup of an optical strain-measurement method [98]. Strain gauging can be affected not only by the material properties, but also by the fact that the velocities of the impact and the vibrational behaviour of the samples during testing can potentially affect the readings.

The stresses on a flat plate (dimension $a \times b$) with straight boundaries and constant thickness (t) subjected to a uniform load over a small concentric circle (W), can be calculated using the following equation [99-101]:

$$\sigma_b = \frac{3W}{2\pi t^2} \left[\frac{(1 + \nu) \ln 2b}{\pi r'_o} + \beta_1 \right] \quad (4.1)$$

By using the above formula for our samples with a value $\nu=0.3$ [100] the obtained values of the maximum stress in the middle of the plate (where the impact occurs) were 91, 160 and 190 MPa for the impacts at 10, 20 and 23 m/sec respectively. These values, combined with the values measured in quasi-static tensile tests performed previously [88], explain the failure and cracking of the samples for speeds above 20 m/sec. By using the following equation (equation 4.2) the values for the modulus can also be estimated.

$$E = \frac{\alpha W b^2}{y_{\max} t^3} \quad (4.2)$$

Using the calculated displacements (0.6, 1.3 and 1.5 for the three different impact velocities), the modulus was estimated at approximately 60 GPa (10% coefficient of variation (CV)) for all three conditions. The above values support our claim that the strain rate has a significant effect on the mechanical properties of the material. However, it is clear from the above results that the modulus and strength of the studied materials do not follow a linear increase with the loading rate, but saturation is reached after a certain value of the load.

Table 4-3: Tensile properties of flax/PLA as a function of the crosshead displacement [88]

Crosshead velocity	Modulus [GPa]	Strength [MPa]	Elongation [%]
2 mm/min	13 (0.9)	72.2 (2.0)	1.5 (0.08)
0.5 m/sec	14 (0.7)	87.1 (3.8)	1.5 (0.09)
4.2 m/sec	22 (2.2)	95.7 (6.2)	1.3 (0.15)

Very few studies exist in the literature reporting gas gun or drop weight impact results for natural fibre composites. Among those, Petrucci et al. [102] studied the impact performance of hybrid composite laminates based on combined glass, flax and hemp fibres. They observed very similar failure characteristics, with a cross-shaped crack being formed on the back of the samples at 6J impact energies. When combined with glass fibres, the damaged areas were considerably restricted and the impact loads recorded were as small as half the ones recorded for hemp. Santulli et al. [103] studied flax/epoxy laminates with 31% fibre content (in weight) subjected to drop weight impacts. Although the energies used were considerably higher than the ones used in this study (approximately 50J), the maximum penetration energies were in the range 16-

18], depending on the flax fibre thread diameter. On the contrast Sevkat et al. [104] on their studies with glass-graphite reinforced epoxy composites, they observed an opposite fracture behavior. Drop weight impacts on both the pure glass and the combined glass-carbon composites, showed a cross-shaped fracture on the front face of the plates, without back face splitting. This opposite behavior can be associated to lower compressive properties of the glass-graphite reinforcement, which resulted in cracking and failure on the compressive side. At 3.9 and 4.4 m/sec impact velocities (47 and 60J), the average maximum load was approximately 12 and 16 kN respectively. Glass reinforced polyamide (PA66-GF) composites have been studied by Mouti [80]. The resulting composites showed high potential for use in automotive application to replace metallic components. Performing gas gun impact studies, Mouti observed crack formation at energy levels above 4J and the respective velocities of approximately 20 m/sec. Although the crack shape was not consistent and varied from test to test, Mouti [80] reported cracks between 20 and 30 mm (4mm thickness samples).

Figure 4-9 shows a comparison of the obtained maximum impact load during testing of the flax/PLA natural composite samples subjected to different impact velocities.

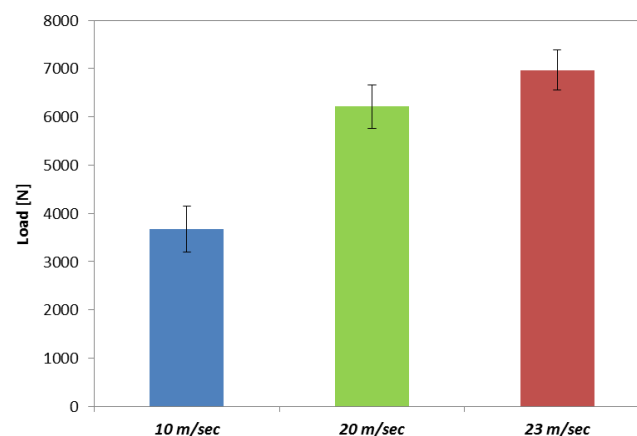


Figure 4-9: Comparison of the maximum impact load observed during testing of the Flax/PLA samples subjected to different impact velocities

Depending on the level of energy, impact tests usually result in three distinct interaction modes between the composite panel and the impactor [104]. It follows that when the energy absorbed by the composite is very low, the impactor bounces back and vice versa when most of the energy of impactor is absorbed by the composite through

various modes of damage, no rebound occurred. Finally, in the case of high energy level, perforation can be observed. A typical energy absorbing curve has an increasing phase up to a maximum level, which is the point where the impactor has stopped due to the interaction with the sample. This point coincides with the zero velocity of the impactor and the maximum deflection/deformation of the specimen. Close to that point the tangent of the energy curve smoothly drops to zero, before the rebound phase where the specimen releases the energy back to the impactor, accelerating it in the opposite direction. The energy from there drops up to a certain level different for each case. The final value of energy gives an indication of the absorbed energy stored in the sample in the form of plastic deformation, or in the case of composites damage, delamination, and failure. The difference between the maximum energy and the absorbed one shows the level of rebound energy that was temporarily stored in the form of elastic deformation.

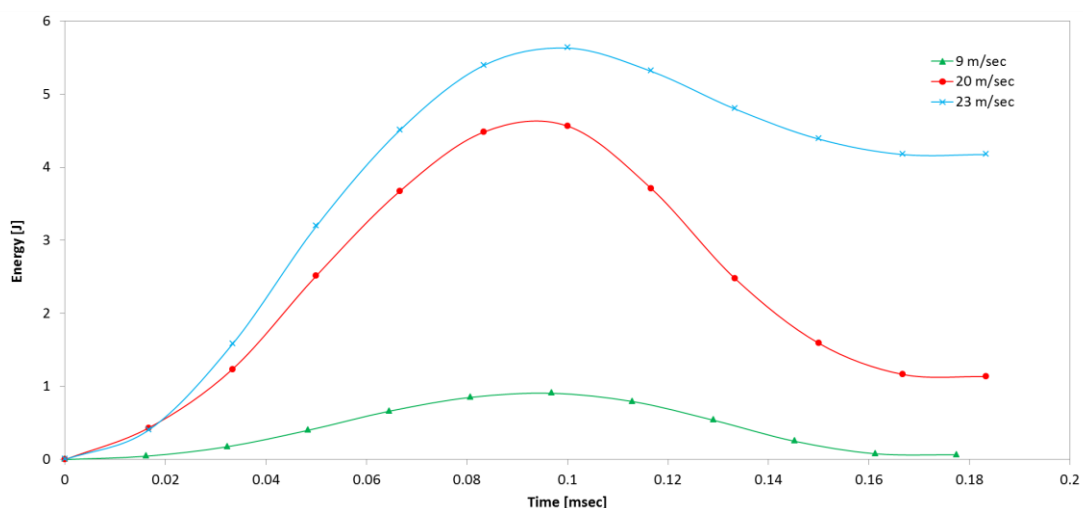


Figure 4-10: Energy time histories for the drop-weight impact tests of the composite specimens conducted at different impact velocities

Figure 4-10 depicts the energy curves as calculated for the performed test for each impact velocity. The energy was calculated using equation (4.3) using the energy at the beginning of the impact and the velocity of the impactor throughout the impact sequence. The curves for each energy level were very similar, however differed in the absorbed energy level. During the impact tests at 10 m/s impact velocities very little energy was stored in the specimens with approximately 80% being returned. For the 20

m/sec and 23 m/sec tests the absorbed energy levels were approximately 52% and 68% respectively (Figure 4-11). These high levels of absorbed energy indicate extensive damage of the composite, and can be explained by the material cracking, fibre and matrix failure visible through the visual inspection.

$$E = E_{init} - \frac{1}{2}m_{impactor} \cdot v_{impactor} \quad (4.3)$$

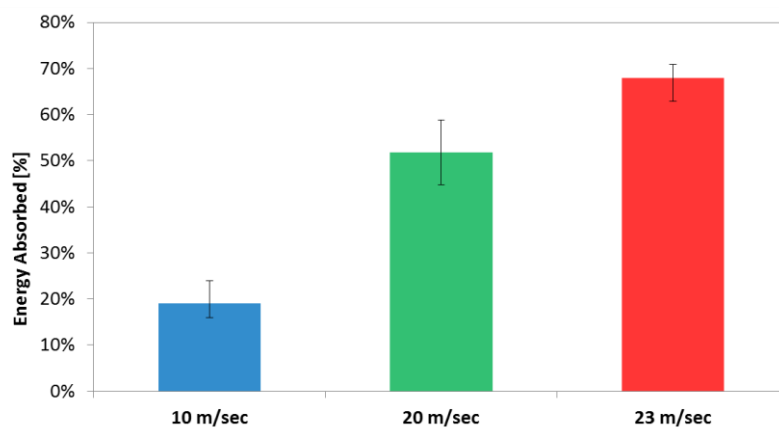


Figure 4-11: Comparison of the absorbed energy during testing of the Flax/PLA samples subjected to different impact velocities

Echo images from ultrasonic inspections (C-Scans) did not reveal any delamination or voids around the crack for any of the tested velocities. The reflection on the back surface was weakened around the crack area visible in both the A and S-scan images. However the C-scans do not show any significant problematic area, which indicates that the failure does not occur in an in-plane level but vertically to the surface.

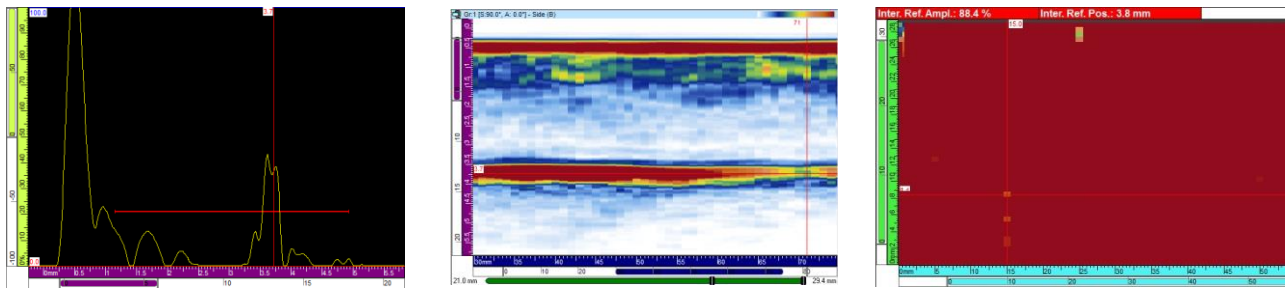


Figure 4-12: Typical C-scan images for the Flax/PLA samples subjected to gas gun impacts at 20 m/s

4.3.2 Strength after Impact

Only data for samples with acceptable failure modes were recorded. These modes may pass through or initiate away from the damage site, especially when the extent of damage is small. Unacceptable failure modes are those related to load introduction by the support fixture, local edge support conditions, and specimen instability. The support fixture was also employed to test undamaged specimens, although such tests demonstrated a relatively high incidence of undesirable failure modes such as end crushing. The values of the properly failed samples were verified using a standard compression test (ASTM 3410).

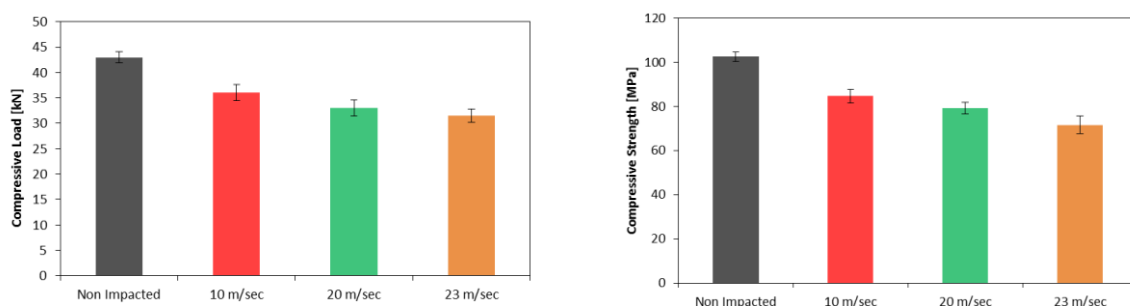


Figure 4-13: CAI average load and strengths of the composite specimen subjected to different impact velocities

Failure of damaged laminates under uniaxial compression load is caused by local buckling of the sublaminates originated in the impact [105]. Delamination propagates mainly perpendicularly to the loading direction (90°), being smaller in 0° direction. The damage of the sublaminates results in local buckling, and failure occurs under a lower load than in an un-impacted plate. The mean value of the residual strength was determined in all the specimens of each tested laminate under the same impact energy.

Dispersion, measured using the coefficient of variation (CV), was between 10% and 15%, even in the undamaged specimens, after the extreme values were removed as they were assumed to be the result of global buckling, misalignments, and high stress concentration factors at each end. These values of dispersion were not easy to assess as no data is available in the literature from previous testing of such materials, however similar values were found in other investigations [105; 106].

Figure 4-14 shows the average compression strength of the test specimens as a function of the impact energy, including those of unimpacted specimens. From this figure, the effect of the impact energy on the residual strength was evaluated in the laminates tested. As can be seen, with increasing impact energy the compressive strength decreases. From the un-impacted specimens to the samples tested at 10 m/sec the residual strength drops by approximately 18%, while for the tests at the higher impact velocity (23 m/sec) this drop was around 28%.

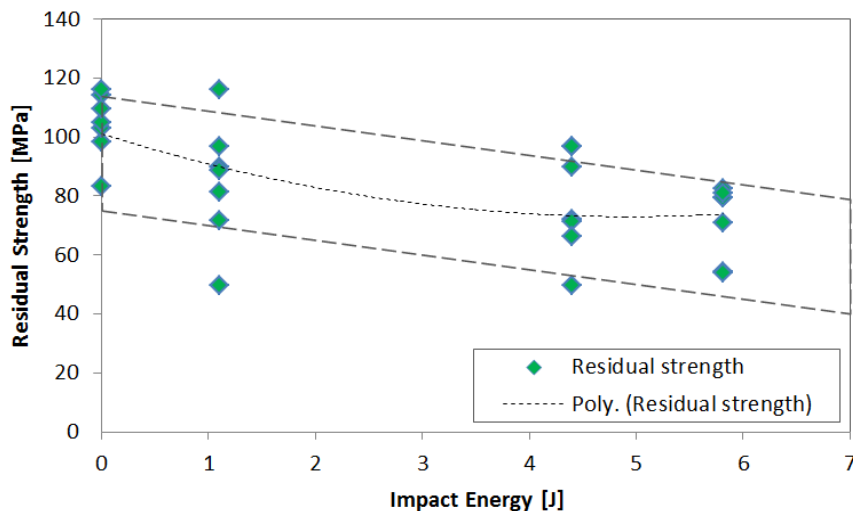


Figure 4-14: Residual strength of the Flax/PLA samples as a function of the impact energy

Throughout the tests, the compressive modulus was measured. An average of 20 GPa was recorded. The compressive modulus was observed to remain constant for all samples tested, and it was concluded that the impact energy did not affect the compressive modulus. The localized nature of the damage did not affect the overall performance of the composite, as the load path was running through the unaffected areas. The drop of strength is a linear function to the crack length, with a 21% section reduction in section due to the crack (21mm of 100mm in width) resulting in a 21%

reduction of the compressive strength for the tests performed at 20 m/sec, while for impacts at 23 m/sec the equivalent reduction was 28%.

4.4 Conclusions

Aim of the work in this section was to assess the properties and understand the behavior of flax/PLA natural composites subject to a localized low velocity impact with a flying projectile, as well as the remaining strength in the material after such impact. As exterior automotive components are often subjected to impacts with road debris, knowledge of the behavior and limits of the material under such loading conditions is crucial.

Flax/PLA samples were subjected to gas gun testing using a 20g projectile, at impact energies of 1, 4.5 and 6 J. The samples impacted at 1J did not show any visible damage or cracking, while in samples tested above 4.5J a cross-shaped crack was visible in the back face (tensile face) of the sample with a visible indentation on the front face. This result comes in contrast with glass and carbon fibre composites reported in the literature to form a crack in the front face without visible splitting on the back [104]. The average energy resulting in sample penetration was measured at 16J.

The initiation of the cracking of the samples at the higher impact energies was visible in the load-time histories as a drop of the acceleration derivative, hence a localized flattening of the force. The average maximum load recorded from the impacts was 3.6, 6.2 and 6.9 kN for each energy level respectively.

During the impact tests at 10 m/s impact velocities very little energy was stored in the specimens with approximately 80% being returned. For the 20 m/sec and 23 m/sec tests the absorbed energy levels were approximately 52% and 68% respectively, indicating damage of the composite explained by the material cracking, fibre and matrix failure visible through the visual inspection. Ultrasonic C-scanning shows no delamination through the samples tested as the material failure is vertical to the plate surface.

The impact energy has no effect on the compressive modulus of the samples which remained constant at 20GPa. This was explained as the damage was localized and did not affect the in-plane properties, thus the loading was transferred through the

unaffected areas. This resulted in progressive loss of strength as the impact energy was increasing.

Chapter 5. Influence of temperature and moisture on the impact performance of flax/PLA biocomposites

5.1 Introduction

All polymers and composites absorb moisture in humid atmosphere and/or when immersed in water. Natural fibers absorb more moisture compared to synthetic fibers [4; 107; 108]. The interfacial bonds between the hydrophilic natural fibers and the relatively hydrophobic polymer matrices are generally weakened with high water uptake. The weakened interface causes the reduction of the mechanical properties of the composites. Therefore, the effect of the moisture on the mechanical properties is vital for the applications of natural fiber reinforced composites in exterior structural or non-structural vehicle applications. Recent studies [109; 110] have reported that the effect of water uptake in bio-composites limits their outdoor applications

In general, moisture diffusion in a composite depends on factors such as fraction of fibers, void volume, additives, humidity and temperature [111]. The main mechanisms of moisture penetration into composites consists of water diffused directly into the matrix (2) through interphase matrix/reinforcements and (3) by imperfections, like pores and cracks formed during the manufacturing process [108; 111; 112]. Significant

progress has been made in understanding the phenomena of water absorption in synthetic fiber composites. Some results exist for short-term water absorption of natural fibers and their composites.

In this chapter, room temperature long term water absorption in flax/PLA composites has been studied, with the specific objective to characterize the effect of moisture absorption in the low velocity impact performance and post impact strength of these composites, and study the mechanisms of those effects.

Furthermore, the properties of natural fibre composites were found to be temperature dependent, with the increase of temperature reducing the Young's modulus and tensile strength, while increasing the failure strain, thus leading to a material more ductile and less stiff [80]. With the increase of temperature thermal transitions occur, which can impart dramatic step-changes in material behavior. The semi-crystalline nature of PLA results in a complex combination of thermal transitions occurring in the crystalline as well as in the amorphous phase in relatively short temperatures ranges. Additional energy dissipation mechanisms can be activated due to the addition of fibres [81] and very little is known on how temperature affects the properties of the flax reinforcement.

As concluded in previous studies (refer to Chapter 3) [113], temperature significantly affects the properties of flax/PLA. At 50°C the stiffness is reduced by half compared to that at room temperature, and the ultimate strength is reduced significantly. The failure characteristics remain brittle for the temperatures up to 65°C, while at 110°C high degradation of PLA is observed and the load seems to be carried through the fibres, which progressively slip apart. Interestingly however, at a temperature of 65°C (glass transition point, T_g), an increase of the modulus was observed compared to its value at 50°C, explained through the higher mobility of the chains, combined with the increased ductility of the PLA matrix above the T_g that results in less debonding between the resin and the fibres, thus better transfer of loads between the composite constituents Figure 5-1.

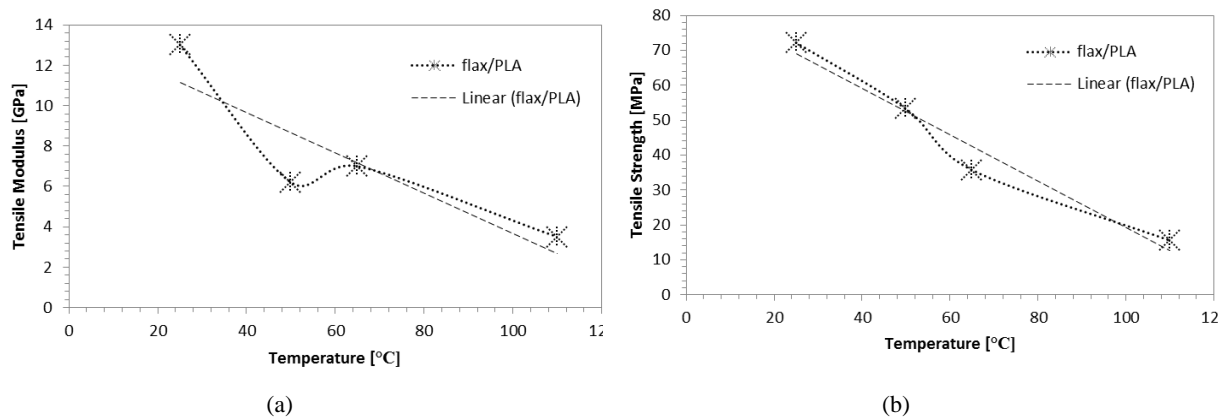


Figure 5-1: Tensile modulus and ultimate strength of flax/PLA specimens as a function of temperature [113]

Exterior automotive components are exposed and susceptible to a wide variety of environmental exposures [80]. Very little is known on how flax/PLA composites behave to impact when subjected to these environmental conditions. The work in this section therefore focuses on the effect of temperature and water exposure on the mechanical and impact properties of flax/PLA.

5.2 Materials and methods

5.2.1 Materials

All flax/PLA samples were prepared as outlined in previous chapter, refer to section 4.2.1.

5.2.2 Water absorption test

Water absorption test were carried out according to ASTM 5229. Specimens with dimensions of (150, 100, 4 mm) were used and their weight was measured to a precision of 0.0001g using a four digit balance. Prior to the test and the immersion of samples into water, all samples were dried at a 40°C for 5 hours, to condition the samples and eliminate the water content of the samples as received. Further, to eliminate moisture absorption through the edges, the specimens' ends were sealed with silicone. They were then placed into tubs containing water at 25°C (room temperature). For measurement, specimens were removed from the water, the surface water was wiped off using a soft dry cloth, and the specimens were weighted. After weighting, the

samples were immersed again in water. The samples were daily weighted and the process was continued until the saturation period was reached and no further mass gain was observed. The values of the water absorption were calculated using the following formula,

$$M\% = \frac{W_i - W_o}{W_o} \times 100, \quad (5.1)$$

where W_o and W_i denote the dry weight and weight after time t , respectively

After the moisture absorption characteristics of the samples were determined, another set of samples was conditioned through the same process. At selected water immersion time intervals (5% and 15% weight gain), specimens were taken out from the water bath and their impact properties were measured. For each test 5 samples were used.

5.2.3 Impact testing

Mechanical testing used in this study were already outlined in previous chapter, refer to section 4.2.2.

For the elevated temperature impact studies, the samples were mounted inside an environmental chamber capable of conditioning the samples from -40 to 200°C. The chamber is positioned in front of the gas gun apparatus and features a hydraulic slide door, which opens only for the few seconds of each impact in order to reduce heat losses. In order to determine the exact temperature of the samples, a laser infrared thermometer was used and the set temperature of the chamber was adjusted.

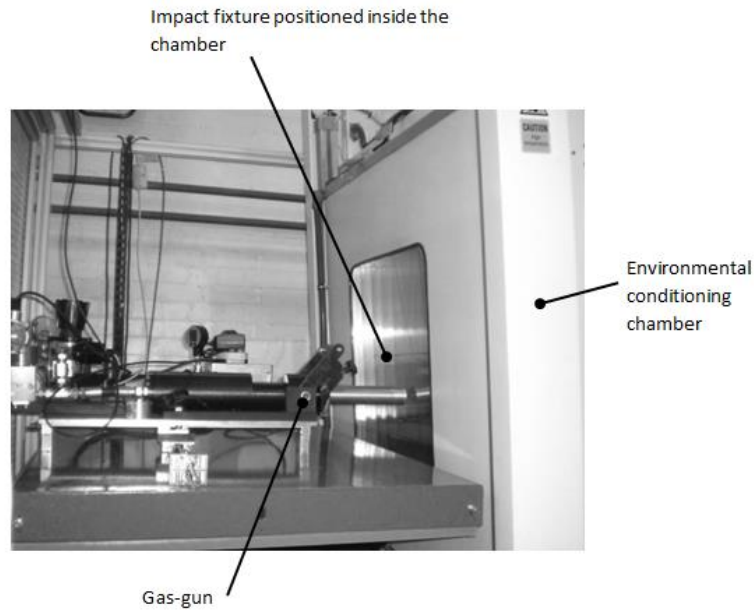


Figure 5-2: Low velocity gas gun setup with environmental chamber

5.3 Results and discussion

5.3.1 Absorption behaviour

The weight gain as a function of the square root of immersion time \sqrt{t} for the flax/PLA composites is shown in Figure 5-3. It can be seen that for all the samples, weight initially increases monotonically with \sqrt{t} before reaching a maximum, following a Fickian diffusion process. The samples absorbed water very rapidly during the first stages and reached saturation at a certain value, the saturation point. After this point no more water was absorbed and the content of water in the composites remained the same. This is in accord with most moisture absorption studies on natural fibre composites [107].

The percentage of water absorption in the composites was calculated by weight difference between the samples immersed in water and the dry samples, using equation 5.2. The average percentage weight gain (saturation) for the immersed samples (room temperature) was 15%. The water absorption for neat PLA as found in the literature is about 0.4-0.9% [110; 114; 115], indicating a very high influence of the fibres in the water intake. Natural fibers are highly hydrophilic in nature. Therefore, incorporation of natural fibers into polymeric matrices will generally increase the water sorption ability of the product. Alimuzzaman et al. [116] observed similar values of weight gain in their studies with flax/PLA composites. At 40% flax content the saturation percentage was 19%, increasing with increased fibre content, explained through the increased number

of pores in the resulting composite. The weight gain and moisture absorption characteristics of natural fibre bio-composites have been widely studied and similar values ranging from 10-20% saturation weight gain have been reported [110; 114; 117-119].

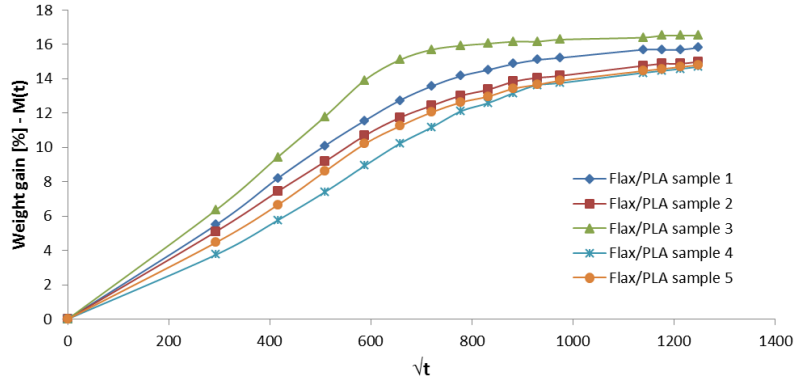


Figure 5-3: Water absorption curves for the Flax/PLA samples (\sqrt{t} [sec])

Different models have been developed in order to describe the moisture absorption behaviour of composite materials. For a plane sheet of thickness h with uniform initial distribution of the diffusing substance and equal initial surface concentration, (assuming that each sample is exposed on both sides to the same environment), within the hypothesis of a Fickian mechanism (one dimensional approach), the moisture content in the material for a given moisture exposure level is given by (ASTM 5229):

$$M = M_0 + G(T, t) \cdot (M_m - M_0) \quad (5.2)$$

where M_0 is the initial weight of the moisture in the material and M_m is the weight moisture in the material when the material is fully saturated, in equilibrium with its environment. G is the moisture absorption function and is given by:

$$G(T, t) = 1 - \frac{8}{\pi^2} \sum_{j=0}^{\infty} \frac{\exp\left[-(2j+1)^2 \pi^2 \left(\frac{D_z(T)t}{h^2}\right)\right]}{(2j+1)^2} \quad (5.3)$$

The above can be simplified as:

$$G(T, t) = 1 - \frac{8}{\pi^2} \exp\left(-\frac{D_z(T)t}{h^2} \pi^2\right), \text{ for } \frac{D_z(T)t}{h^2} > 0.05 \text{ and,} \quad (5.4)$$

$$G(T, t) = \frac{4}{\pi} \sqrt{\frac{D_z(T)t}{h^2}}, \text{ for } \frac{D_z(T)t}{h^2} < 0.05 \quad (5.5)$$

The diffusion coefficient D_z is an important parameter in Fick's law, obtained through the following equation:

$$D_z = \pi \left(\frac{h}{4M_m}\right)^2 \left(\frac{M_2 - M_1}{\sqrt{t_2} - \sqrt{t_1}}\right)^2 \quad (5.6)$$

For the tested flax/PLA (40 vol%) at room temperature, the diffusion coefficient was calculated as $D_z=4.8e-06$ mm²/sec. The values obtained for diffusion coefficients are in agreement with the range of values reported, in the order of 10E-6 mm²/sec [110; 120]. The above described model using the calculated values for the diffusion coefficient was found to nicely match the experimental curves for both the linear and non-linear parts (Figure 5-4). Equation 5.3 can be used for the prediction of the moisture absorption in the whole range from the initial stages to saturation.

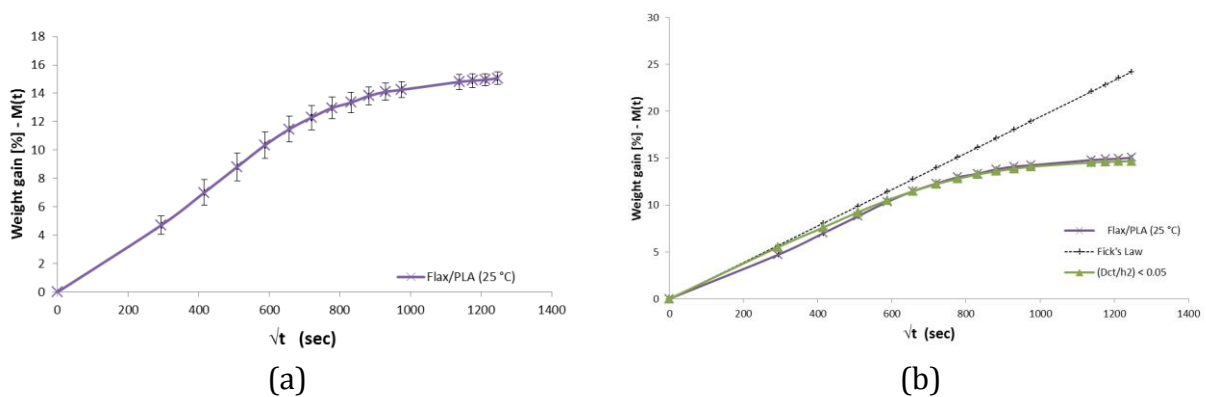


Figure 5-4: (a) Average flax/PLA water absorption curve and (b) Fick's law describes matches nicely experimental results

5.3.2 Impact testing

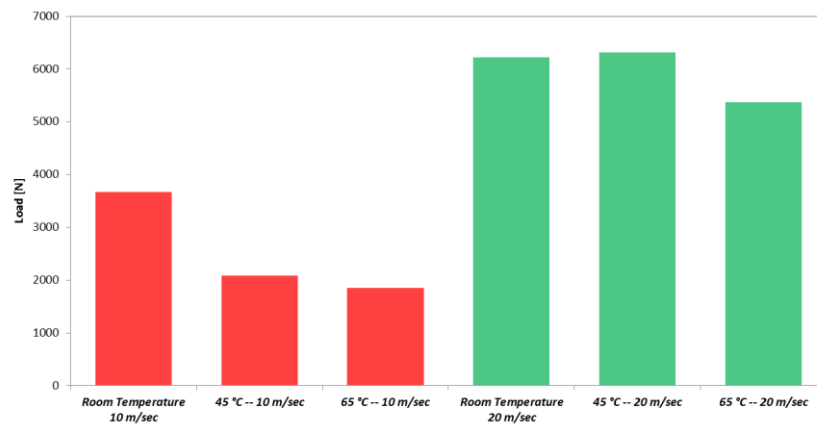


Figure 5-5: Average impact load recorded for different temperatures and impact velocities

Samples have been tested at temperatures of 45 and 65°C and impact velocities of 10 and 20 m/sec, corresponding to 1 and 4.4 joules impact energies respectively. The results have been compared to those from impact testing of samples at room temperature from previous studies (refer to Chapter 4) [113]. Figure 5-5 compares the average maximum loads recorded during the testing. At impacts at 10m/sec, a visible drop of the load can be observed for both the samples at 45°C and 65°C. The average maximum load for 45 and 65°C was 2,1 and 1,8 kN respectively, which represents approximately a 43 and 50% drop compared to the samples at room temperature. The above results are in good agreement with the thermo-mechanical results for flax/PLA studied previously [88], which reported 45-50% drop of stiffness and strength at temperatures between 45 and 50°C. This trend though did not remain linear after 60°C (glass transition temperature), exhibiting a slight increase of modulus, drop of the strength, elongation and break, explained through higher mobility of the chains and the increased ductility of the PLA matrix. The above results in less debonding between the resin and the fibres and thus better transfer of loads between the composite constituents [88]. This non-linearity is reflected in the present results, with the relative drop of load between the samples tested at 45°C and 65°C being approximately 10%.

A different picture can be observed at 20 m/sec. The average maximum recorded load at 45°C was similar to the load recorded at room temperature. It was observed that at higher velocities (higher impact energies) the dominant factor restricting the load is the

failure mechanism rather than the stiffness. The loss of strength and higher flexibility of the PLA matrix, resulting in higher elongation, maintained the load at 45°C similar to that at room temperature. A significant 13% drop was recorded for impacts performed at 65°C.



Figure 5-6: Fractographs of the samples subjected to gas gun impact testing at 20m/sec

Previous results in the previous chapter (Chapter 4) (room temperature) showed very local front surface marks in the specimens with back surface cross-shaped cracking also observed at impact velocities equal to 20m/sec and higher (Figure 5-6) [113]. The length of the front surface crack increased with increasing impact velocity. In contrast, observation of the damage on the specimens tested at higher temperature does not reveal any cross-shaped cracking on the front or back surface. However a significant damaged circular-shaped area is apparent in the impact position, forming locally a dent and visible discoloration of the samples (see Figure 5-7). Closer observation reveals micro-cracking and a change of the surface (discoloration and feel) due to matrix degradation. For both the 45 and 65°C samples the approximate diameter of the damage was between 10-15mm.



45 °C



65 °C

Figure 5-7: Fractographs of the samples subjected to gas gun impact testing at different temperatures

Ultrasonic inspection (C and A-Scans) of the samples clearly revealed internal damage. The lack of macro-cracking and the C-scan imaging give evidence of in-plane damage

Samples with different moisture content, namely 5 and 15% (saturated samples relative to the dried state), have also been impact tested at 20m/sec, to assess the effect of moisture on the flax/PLA properties and the ability of the material to withstand damage from stone impacts. Figure 5-9 compares the average maximum loads recorded during the testing with the result of dry samples. A linear drop of the load can be observed, with the 5% water samples performing approximately 13% lower than the dry samples (5.4kN), and the 15% water samples recording a maximum load about 45% lower (3.5kN). The increasing reduction on the load with increasing moisture contents signifies progressive loss of stiffness of the samples, also visible through the recorded force histories (Figure 5-10).

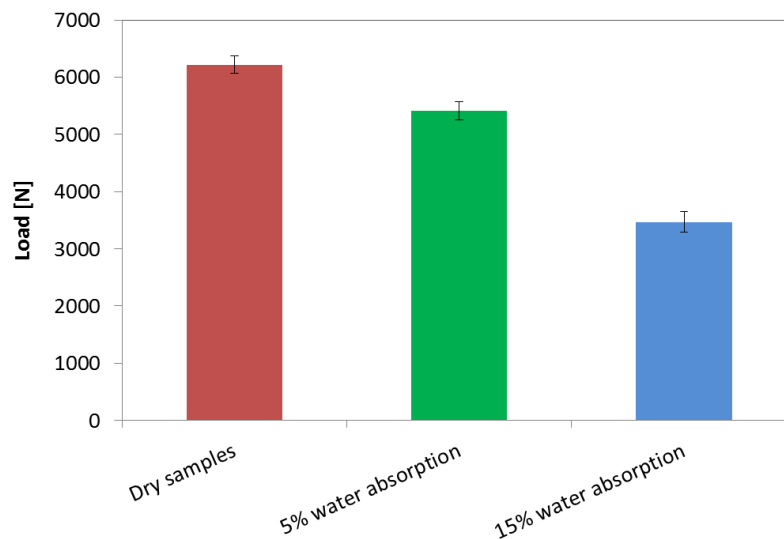


Figure 5-9: Average impact load recorded for the samples with different moisture contents

Although the shape of the curves appears similar to that of the dry samples, as well as to that of the samples tested at higher temperatures, the impact sequence appears significantly longer for the samples with higher moisture contents. The contact duration of the impacts at 5% and 15% moisture content was recorded 0.33 and 0.37 msec respectively, compared to 0.21 msec for the dry samples, suggesting higher deflection and elongation of the samples. Furthermore, lack of visible cracks from both the front and rear of the samples, indicates a significant shift of the impact properties of the material and the energy absorbing mechanism to water content as low as 5%.

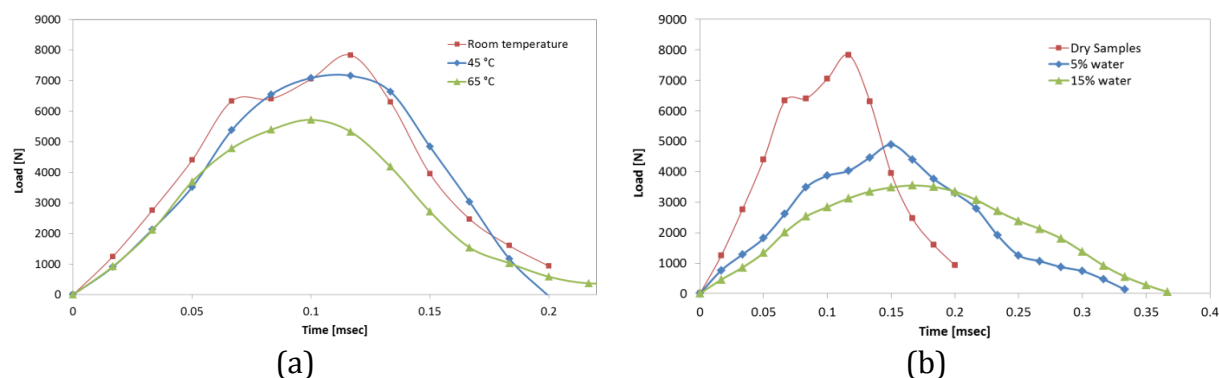


Figure 5-10: Force-time histories for the samples tested at (a) different temperatures and (b) with different moisture content

Ultrasonic inspection of the water samples was not possible due to high damping of the waves and lack of back wall reflection. The swelling of the fibres, the retention of water through the thickness, and the degradation of the PLA surface roughness due to the absorbed water, did not allow for the non-destructive testing to be performed.

Depending on the level of energy, impact tests usually result in three distinct interaction modes between the composite panel and the impactor [104]. It follows that when the energy absorbed by the composite is very low the impactor bounces back, while when most of the energy of impactor is absorbed by the composite through various modes of damage, no rebound occurred. Finally, in the case of high energy level, perforation can be observed. A typical energy absorbing curve has an increasing phase up to a maximum level, which is the point where the impactor has stopped due to the interaction with the sample. This point coincides with the zero velocity of the impactor and the maximum deflection/deformation of the specimen. Close to that point the tangent of the energy curve smoothly drops to zero before the rebound phase where the specimen releases the energy back to the impactor, accelerating it in the opposite direction. After that point, the energy decreases down to a certain level different for each case. The final value of energy gives an indication of the absorbed energy stored in the sample in the form of plastic deformation, or in the case of composites damage, delamination and failure. The difference between the maximum energy and the absorbed one shows the level of rebound energy that was temporarily stored in the form of elastic deformation.

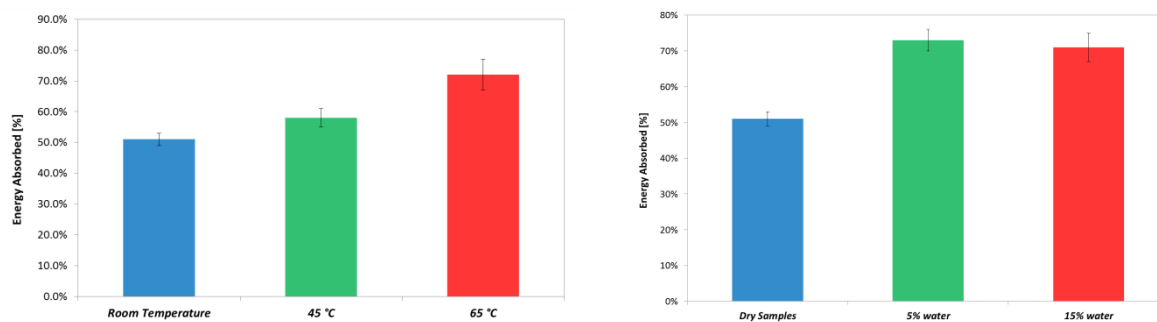


Figure 5-11: Average energy absorption for the tested samples at different environmental conditions

Figure 5-11 depicts the absorbed energy values calculated for the performed tests at 20 m/sec. For the dry samples tested at room temperature, 51% of the initial energy was absorbed, with approximately the same amount being returned. With increasing temperature and moisture content, the amount of energy stored in the samples was higher, however surprisingly samples with 5% and 15% moisture content absorbed on average the same amount of energy.

Table 5-1: summarizes the loads and energy for all samples tested at 20 m/sec (4.4J) at different conditions.

Table 5-1: Summary of the average recorded load and energy absorption for the tested samples and conditions

Sample	Load [kN]	Energy absorbed [%]
Dry Samples – Room temperature	6.2	51%
5% water	5.4	73%
15% water	3.5	71%
45 °C (dry)	6.3	58%
65 °C (dry)	5.3	72%

5.3.3 Strength after impact

Only data for samples with acceptable failure modes were recorded. These modes may pass through or initiate away from the damage site, especially when the extent of damage is small. Unacceptable failure modes are those related to load introduction by the support fixture, local edge support conditions, and specimen instability. The support fixture was also employed to test undamaged specimens, although such tests

demonstrated a relatively high incidence of undesirable failure modes such as end crushing. The values of the properly failed samples were verified using a standard compression test (ASTM 3410).

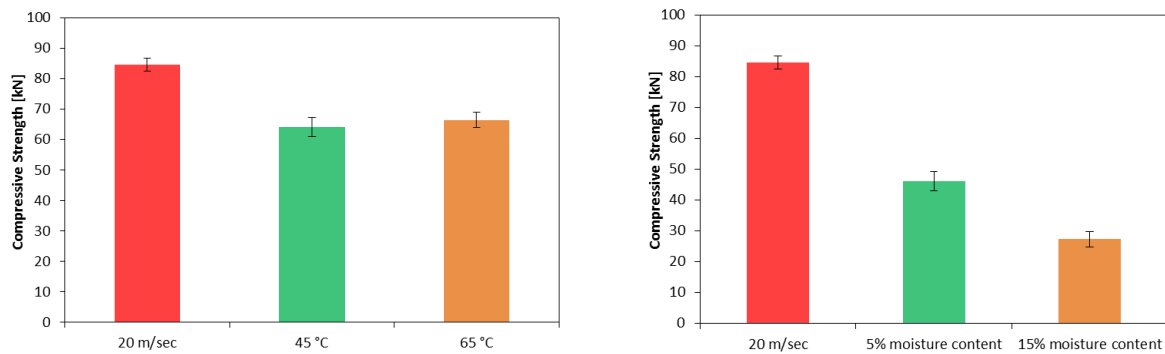


Figure 5-12: CAI average strengths of the composite specimen subjected to different temperatures and moisture content

Failure of damaged laminates under uniaxial compression load is caused by local buckling of the sublaminates originated in the impact [105]. Delamination propagates mainly perpendicularly to the loading direction (90°), being smaller in the 0° direction. The damage of the sublaminates results in local buckling and failure occurs under a lower load than in an unimpacted plate. The mean value of the residual strength was determined in all the specimens of each tested laminate impacted at 20 m/sec. For the dry samples at room temperature the dispersion measured using the coefficient of variation (CV) was between 10 and 15%, after the extreme values were removed, as they were assumed to be the result of global buckling, misalignments, and high stress concentration factors at each end. For the samples tested at 45 and 65°C, similar dispersion values were calculated, in the range of 10%. However for the water submerged samples, a decrease of this value down to 8% and 5% respectively was observed for the 5% and 15% moisture content samples. These values of dispersion were not easy to assess because no data are available in the literature from previous testing of the same materials. However similar values were found for other similar composite material testing [105; 106].

Figure 5-12: shows the average compression strength values of the test specimens at different conditions and compares them to the equivalent values for the dry samples tested at room temperature. From this figure, the effect of the impact energy on the residual strength was evaluated in the laminates tested. As depicted, with increasing temperature the compressive strength decreases. From the reference dry specimens measured at room temperature to the samples tested at 45°C the residual strength drops by approximately 20%, whilst interestingly no further drop was observed for the tests at 65°C. For the samples containing 5% water the compressive strength was measured on average at 46 MPa, a significant reduction of 45% compared to the 84 MPa of the dry samples. The samples with higher moisture content showed a further loss of strength of approximately 66% compared to the reference tests.

Throughout the tests, the compressive modulus was measured. Previous studies recorded an average of 20 GPa for all samples tested, a valued that remained constant for different impact velocities. In the current studies the compressive modulus was also found to remain constant for different temperatures, and it was concluded that for impacts occurred at higher temperatures the modulus was unaffected. The localized nature of the damage did not compromise the stiffness of the composite, as the load path was running through the undamaged areas. However, for the water conditioned samples a loss of stiffness was now observed, increasing with increasing moisture content. The average recorded values were at 14 GPa and 10 GPa respectively for the 5 and 15% samples. This loss of stiffness ties well with the impact results described above, where the material showed significant degradation of properties and softening.

5.4 Conclusions

For the material flax/PLA (40 vol%) tested at room temperature, the diffusion coefficient was calculated at $Dz=4.8e-06$ mm²/sec. Good agreement with fick's material models was found to be followed. The average percentage weight gain (saturation) for the immersed samples (room temperature) was 15%.

As exterior automotive components are often subjected to impacts with road debris, knowledge of the behavior and limits of the material under such loading conditions is crucial. Aim of this chapter was to complete the results from Chapter 4 and assess the

properties and behavior of flax/PLA natural composites subject to a localized low velocity impact with a flying projectile under different environmental conditions.

Flax/PLA samples were subjected to gas gun testing using a 20g projectile, at 4.5 J impact energy, different temperatures and moisture content. Although the reference samples showed a cross-shaped crack in the back face (tensile face) of the samples with a visible indentation on the front face, the samples tested at higher temperatures did not show any visible macro-cracking, but only micro-cracking and discoloration in both samples' surfaces. Ultrasonic inspection revealed significant internal damage of the samples tested at 45 and 65°C. Cracks did not form in samples initially submerged into water, but a significant deformation of the whole sample could be observed. The average maximum load recorded from the dry samples impacted at room temperature was 6.2 kN, whilst both temperature and moisture brought this number down to 6.3 and 5.3 kN for the 45 and 65°C respectively, and 5.4 and 3.5 kN for the moisture samples.

The impact energy absorbed during the impact increased with increasing testing temperature from 51% to 72% at 65°C. Higher moisture content also affected the energy absorbed to 73% for the samples with 5% water content; however this number did not increase further at higher moisture contents.

The testing temperature has no effect on the compressive modulus of the material which remained constant at 20GPa. This was explained by the fact that as the damage was localized and did not affect the in-plane properties, the loading was transferred through the unaffected areas. In contrast, the higher the moisture content was, the lower was the remaining material modulus. At 15% moisture content the compressive modulus was measured at 10 GPa, being approximately 50% lower than reference value.

Chapter 6. Flax/PLA biocomposites application for superlight city car - a case study on side impact analysis to meet EuroNCAP Regulation

6.1 Introduction

The environmental problems posed by the high CO₂ emissions, the extended use of petroleum-based products and the high consumption rates of non-recyclable goods, demand a shift of the industry in every level of product design and production [1; 2; 4; 121; 122]. The automotive industry is no exception. The automakers are now focusing their interest on the electric-moving vehicles but also on the use of alternative materials and production methods that will, in the same cost, provide same mechanical properties while being environmentally friendly and easily reusable or recyclable. The development of optimal structural solutions for superlight electric vehicles based on new materials and novel designs is quite challenging. Traditionally this category of urban vehicles (usually driven without specific driver license) has been relatively expensive and of lower safety measures, thus less attractive for popular use. However, in terms of CO₂ emissions efficiency and life cycle based cost of use, it proves to be the one with the most potential in particular for European, urban, densely populated areas. Two major drawbacks should be addressed, production cost and safety, whilst at the same time improving the associated environmental advantages through the application of innovative biodegradable materials for both the chassis and body of the vehicle.

Concerning materials, it is desirable to achieve a full bio-composite made of natural fibres and high performance natural resin matrices, resulting in the use of totally natural, environment friendly composites, with enhanced strength and biodegradability characteristics designed for electric vehicles. In this respect, design and manufacture key lightweight components for automotive load bearing applications in a compact class car should be developed.

According to the EU regulations released in 2000, by 2015 [5] vehicles must be constructed of 95% recyclable materials, with 85% recoverable through reuse or mechanical recycling and 10% through energy recovery or thermal recycling. Asian countries introduced regulations as well, with the example of Japan requiring 95% of a vehicle to be recovered by 2015 [87].

Key in the design and development of such a vehicle and all the necessary structural components is the use of modelling techniques and FE analysis. So far very little numerical work is found in the literature on the mechanical performance of bio-composites and very little work is related to modeling, based mainly on generic assumptions and models initially created for man-made composites (glass, carbon, aramid etc.).

ECOSHELL (Development of new light high-performance environmentally benign composites made of bio-materials and bio-resins for electric car application) is the name of a European project among the *Fp7*, concerned with the development of optimal structural solutions for superlight electric vehicles. Research projects such as ECOSHELL [123] proposes to achieve full bio-composite car, made of natural fibres and high performance natural resin matrices.

Traditionally, superlight electric urban vehicles (usually driven without specific driver license) have been relatively expensive and of lower safety measures, thus less attractive for popular use. However, in terms of CO₂ emissions efficiency and life cycle based cost of use, it proves to be the one with the most potential in particular for European, urban, densely populated areas. This project aims at solving the two major draw backs (production cost and safety) whilst at the same time improving the associated environmental advantages through the application of innovative biodegradable materials for both the chassis and body of the vehicle.



Figure 6-1: The Citi-Zen Concept. Vehicle proposed by the Ecoshell project

ECOSHELL project proposes to achieve a full bio-composite made of natural fibres and high performance natural resin matrices, resulting in the use of totally natural, environment friendly composites, with enhanced strength and bio-degradability characteristics designed for electric vehicles. It aims to develop, design and manufacture key lightweight components for automotive load bearing applications in a compact class car.

The project is fully in line with the European (E.U.) regulations released in 2000. The end-of-vehicle life directive states that by 2015, vehicles must be constructed of 95% recyclable materials, with 85% recoverable through reuse or mechanical recycling and 10% through energy recovery or thermal recycling. Asian countries introduced regulations as well, with the example of Japan requiring 95% of a vehicle to be recovered by 2015 [87].

Purpose of this study is to initially assess different modelling methods and the capability of existing material models to predict the response of natural composites. A case study is then performed using these models to understand, develop and improve the side crash performance of a superlight city car prototype. The side remains the most vulnerable area of a modern car. The management of the loads, the dissipation of the energy and ensure the occupants remain intact is a hard challenge that needs good understanding, careful design and powerful simulation tools.

6.2 Modeling Natural fibre composites - an overview

Depending on the application, the manufacturing process, the type of fibres and finally the required degree of approximation, a number of theoretical models have been presented, mainly predicting the stiffness and strength of natural fibre composites. Based on laws such as the rule of mixture (ROM) or the laminate approach, models representing short and long fibres have been presented and validated through different experimental tests [53]. Most of them are general models concerning mathematical approaches and analytical prediction of the response of composites under mild conditions, with a modification factor to correct for the complexity of natural fibres.

Garkhail et al. [36] used the Cox-Krenchel model [124] to predict the stiffness of flax fibre thermoplastic materials. Their results showed good agreement with a series of experimental tests. Oever et al. [125] used the same model for the prediction of flax reinforced polypropylene with again satisfying results. The work of Cox [124], completed later by Krenchel, is often referred to as “shear-lag theory”. This simple model used to predict properties of short fibre composites, is a modification of the rule of mixture for short fibre reinforced composites which incorporates an orientation factor (η_{oE}) and a fibre length efficiency factor (η_{ol}), and is described by the following equation.

$$E = \eta_{oE}\eta_{ol}E_f v_f + (1 - v_f)E_m \quad (6.1)$$

However this approach together with the rule of mixture, do not include many of the characteristic drawbacks of natural fibres, and many other researcher proposed different modifications in respect to a specific property [126]. Madison et al. [127-129] conducted several studies on hemp/polyethylene and polypropylene composites and observed a high impact of porosity on the material properties. They proposed a porosity correction factor $(1-V_p)^n$ to modify the rule of mixture into:

$$E = (\eta_{oE}\eta_{ol}E_f v_f + (1 - v_f)E_m) \cdot (1 - v_p)^n \quad (6.2)$$

where V_p is the porosity volume fraction and n is a porosity coefficient. Lamy and Baley [130] proposed another modification of the rule of mixture to include the influence of the fibre diameter dispersion in natural fibre composites. In their model, the measurement of the diameter of a number of fibre samples is needed and classified into a number of classes. The final equation takes into account this dispersion to calculate the global stiffness.

$$E = v_f \sum_{i=1}^n \frac{n_i d_i^2}{\sum_{i=1}^n n_i d_i^2} E_i + v_m E_m \quad (6.3)$$

In the Lamy-Baley equation above, n is the number of classes and E_i the modulus of the fibres in the specific class. Summerscales et al. [126] proposed an improvement of the above model by including the diameter effect with a single coefficient (η_d) ranging from 0-1.

Another very commonly used model for the prediction of composite stiffness and applied in natural fibre composites is the Halpin-Tsai model [53; 131]. This model initially developed for continuous fibre composites, accounts for the geometry of the reinforcement (ζ parameter) and can be expressed with the help of the following equations, where P_f and P_m are the corresponding fibre modulus and matrix modulus respectively.

$$\frac{P_f}{P_m} = \frac{1 + \zeta \eta v_f}{1 - \eta v_f} \quad (6.4)$$

with,

$$\eta = \frac{\left(\frac{P_f}{P_m} \right)^{-1}}{\left(\frac{P_f}{P_m} \right)^{+\zeta}} \quad (6.5)$$

To predict the strength of natural fibre composites, many authors [36; 125; 132] proposed the use of the Kelly and Tyson equation 6.6 [133], which is an extension of the rule of mixture. In equation 6.6, σ_c represents the composite strength, σ_f the fibre tensile strength and $(\sigma_m)_{\varepsilon_f}$ is the matrix stress at the strain equal to the fibre failure strain. For low fibre volume fraction, equation 6.6 is no longer correct, and the composite strength is estimated through equation 6.7, where $\sigma_{m_{max}}$ is the maximum matrix tensile strength.

$$\sigma_c = \sigma_f V_f + (\sigma_m)_{\varepsilon_f} (1 - V_f) \quad (6.6)$$

$$\sigma_c < (\sigma_m)_{max} (1 - V_f) \quad (6.7)$$

Facca et al. [134] proposed another micromechanical model, again as an empirical modification of the rule of mixture. Their model includes a clustering parameter to correct the fact that the available fibre stress area decreases with increasing fibre loading.

$$\sigma_c = \alpha \tau_i V_f \frac{l}{d} + \sigma_{c_{max}} (1 - V_f) \quad (6.8)$$

For cylindrical fibre composites, Facca et al. equation has the form above (equation 6.8) where α is the clustering parameter, τ_i the interfacial shear strength, $\sigma_{c_{max}}$ the estimated maximum stress in the composite strength, l is the fibre length and d the fibre diameter.

However, initially created again for man-made fibres, most of the models presented fail to include the specific character of natural fibres. Modifications as above are thus needed for more accurate prediction. In an effort to improve the prediction models,

several statistical methods to assess and classify the properties of natural fibres have been studied and reported. Peponi et al. [135] based on their studies on flax, jute, abaca and sisal, proposed a neural network algorithm based on the Weibull distribution. Their results showed a very accurate prediction of the dimensional and physical properties of natural fibres. Virk et al. [132] made use of Weibull distribution both for estimating the cross sectional area, length and diameter of jute fibres for the prediction of the mechanical properties of jute/epoxy composites. Sparnins [53] in his studies of flax fibre composites used a modified Weibull distribution to estimate the mechanical properties of the final composites and achieved very close agreement with experimental data. Another stochastic method for the prediction of flax fibre strength, in relation with the fibre defects distribution, was proposed by Anderson et al. [136].

Most of the models presented above include a number of approximations, the most important of which being the following [53]:

- The fibres and matrix are linearly elastic
- The matrix is isotropic and the fibres isotropic or transversely isotropic
- The fibres are axi-symmetric and identical in shape
- The fibres and matrix are well bonded at their interface and remain as such during deformation

However, none of the above seems to perfectly describe natural fibre composites properties. Facca et al. [137], running a series of experiments with hemp/polyethylene composites, conducted comparative studies between different existing models (ROM, shear-lag theory, Halpin-Tsai, etc.) to assess their success and potential for use with natural fibre composites. They concluded that the existing models cannot always predict the properties of natural fibre composites. Thus, in order to get close results, a number of correcting factors must be used to account for the increased cell wall density, the moisture, the non-perfect adhesion, and other factors. In another comparative study, Ku et al. [19] reached the same conclusions. They reported that although in overall Halpin-Tsai gave the closest predictions to the experimental results; all models underestimated the composites' strength, proving a clear weakness and a gap in the prediction of properties for natural plant and animal fibres.

As it stands, the modeling of natural fibre composites is yet in its infancy. Further, all existing work concerns analytical models for the prediction of the strength or elastic modulus of the final composite when the properties of the constituents are known. To the authors' knowledge, however, numerical modeling of natural fibre composites has not been reported. Today, a large number of numerical tools and methods exist for the accurate simulation of traditional composites, and a lot of work is still being done to improve their results and include all the parameters affecting their behavior and response. None of these tools has, however, been used for the reproduction of the response of natural fibres and their composites. Neither finite element results nor the use of models including plasticity, damage, failure criteria or delamination effects have been reported. This may be attributed to the fact that natural fibres have not been used in structural applications so far. As this fact currently changes, tools giving an accurate prediction of the structural behavior under different load cases and environmental conditions are required for the further development of the "green" composites. The ability to simulate the response of both the fibres and the matrix, including also the interactions between them, is of great importance. The consistent static and dynamic modeling of natural fibre composites can save time and money from long experimental campaigns and will give to the automotive industry a spark and a tool for the development of low carbon emission - "green" - cars.

6.3 Experiments

Finite element models replicating (a) tensile and (b) gas gun localized impact testing have been built and used to calibrate and validate the material law and modeling techniques respectively.

6.3.1 Materials and samples preparation

All flax/PLA samples were prepared as outlined in previous chapter, refer to section 4.2.1.

6.3.2 Tensile and impact testing

Gas-gun and tensile test were performed as outlined in previous chapter, refer to section 4.2.2.

Uniaxial compression test was performed for open-cell rigid PVC foam with densities 45, 65, 100 and 200 kg/m³. Mechanical properties were evaluated as a function of foam

density using a conventional mechanical test frame. Tests were conducted at an initial quasi-static rate of 2 mm/sec and at room temperature. Deformation and acting force was measured by position sensor and compression load cell. For each density specimen were cut at dimensions 50x50x50 mm. Table 6-1 shows the measured properties for the foams tested.

Table 6-1: Material properties of the different PVC foams tested

	<i>Density</i> [kg/m ³]	<i>Compression</i> <i>Modulus [MPa]</i>	<i>Specific Modulus</i> [MPa]	<i>Plateau force</i> [N]	<i>Plateau stress</i> [MPa]
H100	106.4	66.12	0.62	5000	2
H45	46.4	24.18	0.52	1500	0.65
H200	214.4	78.36	0.36	10000	4
MX119	65.6	17.11	0.26	1800	0.72

6.4 Modelling

LS-DYNA was used for the static and dynamic modeling, using mainly a macroscopic approach with the composite material modelled with a single shell with through the thickness integration points for each layer.

The FE (Finite Element) code LS-DYNA is designed to solve large deformation structural dynamics. The main solution methodology is based on explicit time integration, while an implicit solver is currently available. LS-DYNA has a library of over 200 material models including metals, plastics, foams, honeycombs and fluids, a large variety of elements including beams, shells and solids, and a large number of contact algorithms to simulate impact interactions (sliding with friction, gaps, etc.) [138]. It nicely fits the automotive industry needs because of its specialist modelling features like the airbags, spot welds, seatbelts and numerous material failure methods that enable detailed crashworthy analysis. For these reasons, added to the offered possibility to perform both explicit and implicit analysis, LS-DYNA is among the best options for non-linear dynamic simulations, hence its use in this work.

A wide range of material models for composite materials are available in LS-DYNA, each of them with a number of differences and approximations. All LSDYNA models are

based on the macro-scale approach with the possibility to include failure modes and damage from the meso-scale. MAT 22 and MAT 54 provide Chang-Chang fiber and matrix failure modes [138-140]. Material MAT 54 describes anisotropic, linear elastic behavior followed by nonlinearities introduced from various damage criteria. Failure due to out of plane shear and normal stresses is neglected. MAT 58 is based on the Hashin criteria and continuum damage mechanics. It is implemented only for shell elements and does not consider strain rate effects. However, this material model can be used in the initial design stage due to rather small amount of material properties and input information needed. MAT 59 is the only elasto-plastic material model, but it doesn't support strain rate effects or damage [140]. MAT 161 is a composite lamina model based on 3D stresses field, that can be used to effectively simulate fiber failure, matrix damage and delamination behavior. In order to account for the experimentally observed nonlinear and rate dependent behavior, a general rate dependent progressive failure model has been developed. Disadvantages of this material model are the fact that it applies only for solid elements and needs as input a quite large number of material properties, not easily accessed by standard material testing. MAT 161 needs also the purchase of a special license to be available with LSDYNA.

6.5 Models set up

As pre-processor, ANSA14.1 was used. ANSA is a powerful pre-processing tool that provides all the necessary functionalities for full-model build up, from computer-aided design (CAD) data to ready-to-run solver input file, in a single integrated environment. It provides a variety of data import options to facilitate the treatment of models built with different software, as well as several input cards, organized in different template options to realize models for a wide range of solvers (NASTRAN, LS-DYNA, Abaqus and others).

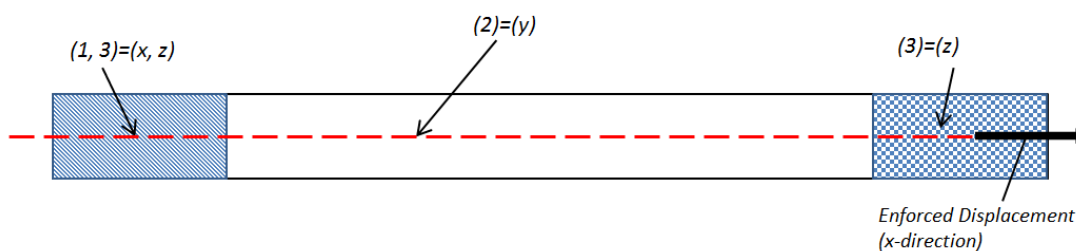
6.5.1 Tensile and gas gun impact modelling

In these models a macro modelling approach was used with a single shell representing the laminate. Laminate theory correction was used for the interlaminar properties. The tests were modelled by shell elements with Belytschko– Leviathan formulation. A multi-

layered shell was used with as many through the thickness integration points as the material layer and different ply directions. Material law 24 (piecewise linear plasticity) and 58 (laminated composite) were both tried. The different composite materials were modelled using material types 24 and 58. Material 24 is an elastic-plastic material model, and a tensile stress-strain curve was used as the input. The simplicity of the model was useful for the initial modelling stages and the understanding of the models, parameters and setup selected. Material 58, as described above, is a damage composite model with the stress-strain non-linearity being induced by the progressive material damage through the test. Data resulting from the mechanical characterization with statistical variability ranges were used as input parameters.

For the tensile tests the specimens were fixed with constraints as depicted in Figure 6-2 and pulled with a prescribed velocity in the x-direction on the right boundary. To investigate the mesh sensitivity a number of simulations were run. Finally 1mm four-node shell elements were selected for the mesh and mesh size that proved not only to be robust in terms of stresses and strain through the specimen, but also computationally efficient.

For the impact tests 3-DOFs (x, y, z) were used at the perimeter of the samples and for a 10mm width as per the tests. Fine meshes around the center and course meshes away from center were used to capture the increased stresses and failure around the area, starting with 1mm four-node shell elements on the outside perimeter and resulting to 0.5mm on center. The impactor was modelled as a sphere section with same dimension as the gas gun impactor and with LS-DYNA rigid material MAT 20, and was given an initial velocity of 9 and 20 m/sec. Shell elements of 0.3mm size were used. An automatic surface to surface contact definition was used in-between the impactor and the plates.



(a)

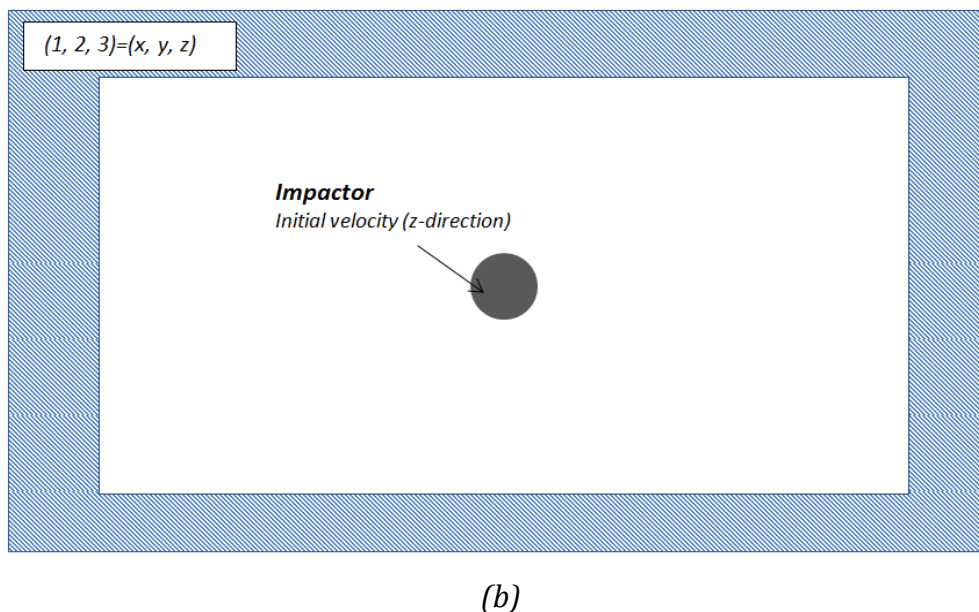


Figure 6-2: Schematic of the (a) the tensile test model and (b) the impact plate model with constraints and boundary conditions.

6.5.2 Side impact car model

A whole vehicle model (superlight city car) was developed by the ECOSHELL consortium and was used in this work for both front and side impact studies. The overall length, width and height of the car/model were 2960, 1600 and 1590mm respectively, while the overall weight of the vehicle was between 400-450kg as per the project's target values.

The full model consisted of 3 million elements for 223 parts including, besides the chassis, the electric motors, batteries, suspension members, seats, etc. The mesh size varied from 5 to 20mm size depending on the complexity and dimension of each part. The composites were modelled again with mainly four-node shell elements with three-node elements unavoidably used in the geometrically complicated regions. Different thicknesses were used between 2 to 5mm shells with different number of integration points for each thickness to represent the number of plies. For the representation of all structural parts using flax/PLA composite, material law 58 (laminated composite fabric) was used as described and with parameters optimized from the above validation studies. A Belytschko-Leviathan formulation was selected [139; 140], as it has been proven to give accurate results for laminated composites in different loading conditions

and crash analysis. Figure 6-3 shows all the different structural components designed as flax/PLA composite and composite/foam sandwich structures.

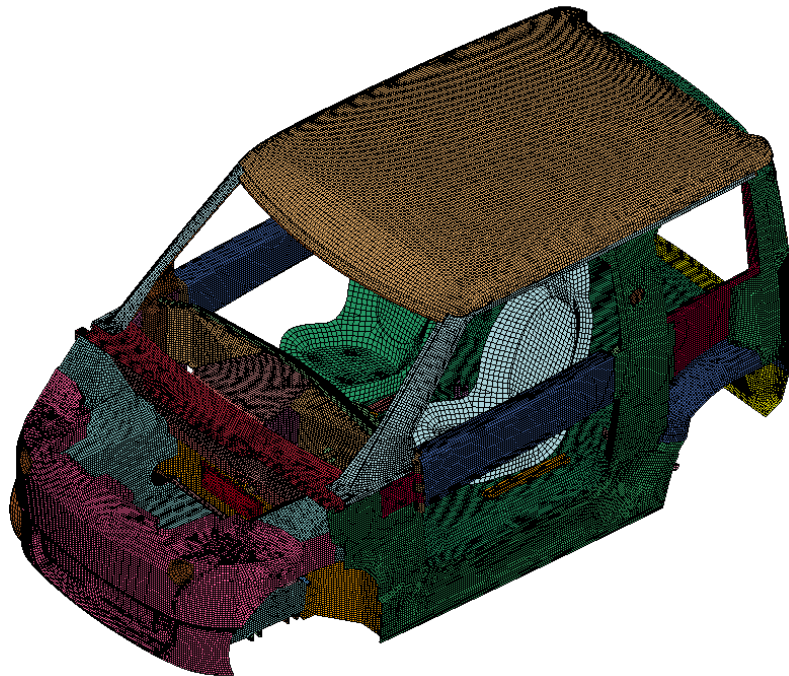


Figure 6-3: Meshed model showing all the different components designed flax/PLA and foam sandwich structures

Foam materials were also used to form sandwich structures in order to increase the stiffness of different components. Values for the properties of the foam were taken from the tested material described above. PVC foam with density 45 kg/m^3 was selected, with a $24,5 \text{ MPa}$ of modulus. All foams were modelled with constant stress solid elements and using mat 63 (crushable foam) as a material representation, which allows input of a user-defined curve representing the yield stress versus volumetric strain, optional damping and cut-off tensile stress. Figure 6-4 depicts the data used as input for the material specification.

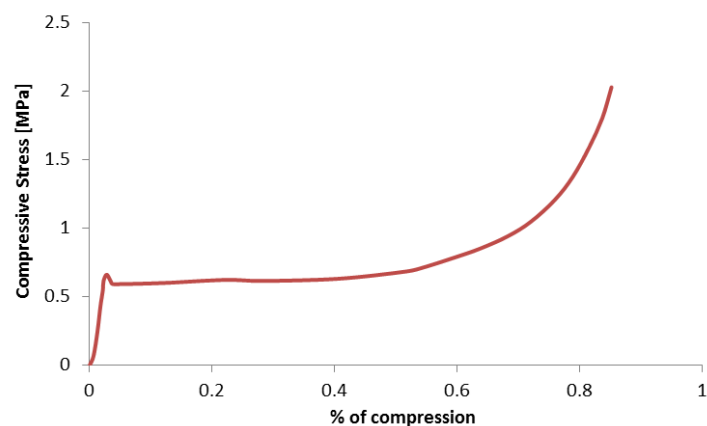


Figure 6-4: Stress versus volumetric strain of the PVC foam used (45 kg/m^3)

Metallic components such as suspension member, were modelled with mat 24 (piecewise linear plasticity) using elastic-plastic properties. A numbers of other material models (elastic, Johnson Cook, etc.) were used for the representation of the different vehicle components, as well as a number of elements including rigids, spring elements, beams and others.

This present study focuses on the side impact of the CITI car (ECOSHELL) following the EuroNCAP regulation [141]. The European union has adopted in 1996-1997 the European side impact regulation specified in the directive 96/27/EC, according to which a side impact test must be done to certify every mass production. The test consists of a moveable deformable barrier (MDB) driven at a speed 50 km/h hitting the side of a stationery car. To pass the test a number of criteria should be satisfied. A full barrier model, developed and provided by LSTC (Livermore Software Technology Corporation) [138], was used for the purposes of this study. The LSTC model was previously used successfully for side impact studies on World Rally racing cars and proved to be a very useful tool, easy to incorporate in the assembly model [142]. The barrier model uses a physical realistic representation of the honeycomb structure using shells, and an automatic surface to surface contact was used between the barrier and the vehicle model.

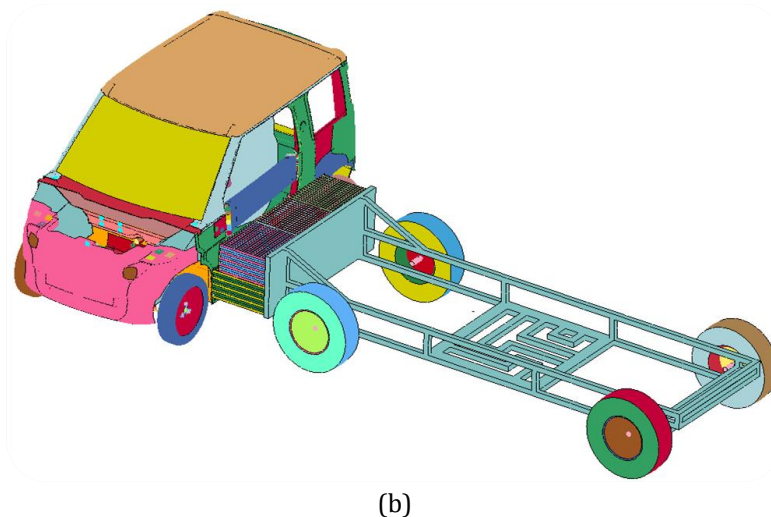


Figure 6-5: side impact models prepared for the Ecoshell Citi car

6.6 Results and discussions

6.6.1 Model Calibration results

Table 6-2: Tensile properties of flax/PLA [88]

FLAX/PLA	Modulus [GPa]	Strength [MPa]	Elongation [%]
	13 (0.9)	72.2 (2.0)	1.5 (0.08)

The measured mechanical properties for flax/PLA composites from our previous studies presented in the chapters above are summarized in Table 6-2. It was measured that flax/PLA material composite has a tensile strength and modulus of 72.2 MPa and 13 GPa respectively, with an elongation at break of 1.5%. A non-linear behaviour was observed from the stress-strain, with no clear yield point or transition area, and a monotonically increasing up to a sudden failure point with brittle characteristics. The non-linearity was explained through a viscous behaviour of the material combined with a certain level of damage accumulation throughout the testing. SEM micrographs [88] showed poor interfacial adhesion of the constituents, confirmed through tensile testing and the comparison of the mechanical properties of pure PLA with those obtained from the flax/PLA specimens.

The above measured properties through the tests conducted were used as input parameters for the material modelling. For the representation of material model 24, the whole stress-strain curve was used as input as the model offers this possibility. For the composite material model 58, the parameters were set as shown in Table 6-3. The strength and modulus were set as per the experimental results, whilst all the other specific non-physical composite parameters determining the damage initiation and accumulation have been fitted to give the requested non-linearity and result.

Table 6-3: Values of the input parameters for Mat58, T=testing, F=fitted, L=literature

Parameters		Mat58	Source
ρ [kg.m³]	Density	1490	T
E_a, E_b [MPa]	Modulus	13000	T
ν_{ab}	Poisson	0.3	T
τ_1 [MPa]	stress limit of the first slightly nonlinear part of the of the shear stress	45	F
γ_1	strain limit of the first slightly nonlinear part of the of the shear stress	0.096	F
G_{ab}, G_{bc}, G_{ca} [MPa]	Shear Modulus	2000	L [88]
ERODS	Maximum effective strain for element layer failure	0.08	F
SLIMIT,C,S	Factors to determine the minimum stress limits after failure	0	F
E_{11c}, E_{22c}	Strains at compressive strength	0.036	F
E_{11T}, E_{22T}	Strains at tensile strength	0.0135	F
GMS	Strain at shear strength	0.096	F
X_c, Y_c [MPa]	Compressive strengths	104	L [88]
Y_c, Y_t [MPa]	Tensile strengths	72.3	T

The result of the tensile test simulations are presented in Figure 6-6. Both simulations are in good agreement with the actual test results. The results from the analyses coincide reasonably well with the results from the material testing of the composites and the non-linear behaviour is captured well in the analyses. Failure and deletion of the elements occurs at 72.5 MPa on the gauge section of the samples, as also observed in the actual test.

To further validate the models, the impact force–time histories from localized impact testing were used and compared. The resulted curves (Figure 6-7) exhibit very good agreement between the FE model and experimental results for different impact velocities.

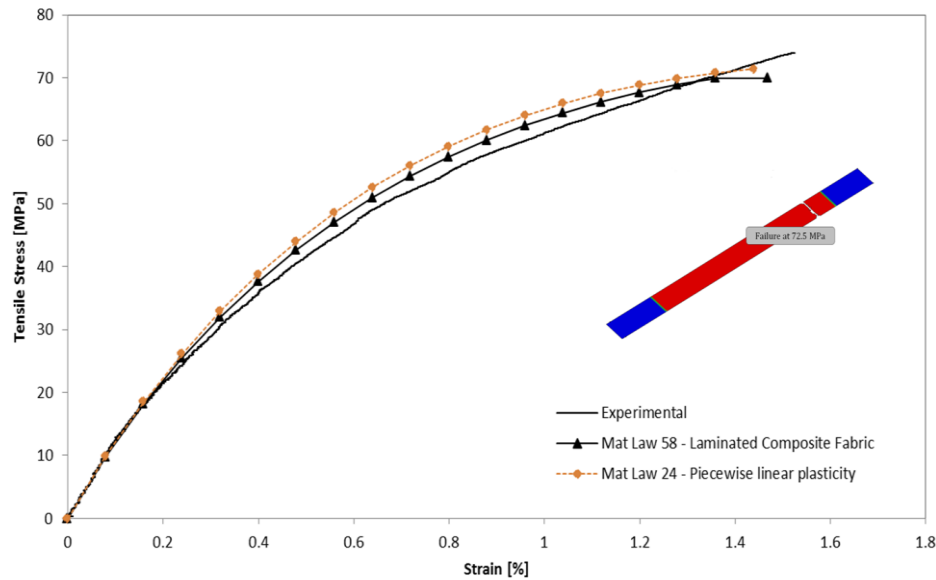


Figure 6-6: Comparison of experimental and simulated stress-strain curves

For the 9m/sec impacts, the FE maximum force–time curves recorded are slightly lower than the experimental ones due to a drop in the initial stages of the impact possibly due to the numerical contact interface or/and the damping properties of the material, not represented in the model. The above difference was calculated to be between 5-8% and considered acceptable. In the higher velocity impacts the maximum force was very closely predicted with the above difference being less than 2%, however the time-histories showed slight mismatch by apparent sudden drop in the period following maximum load, explained by the deletion of failed elements, which affected the contact between the plate and the impactor. For all impact velocities, FE calculations produced a little longer contact duration for all velocities.

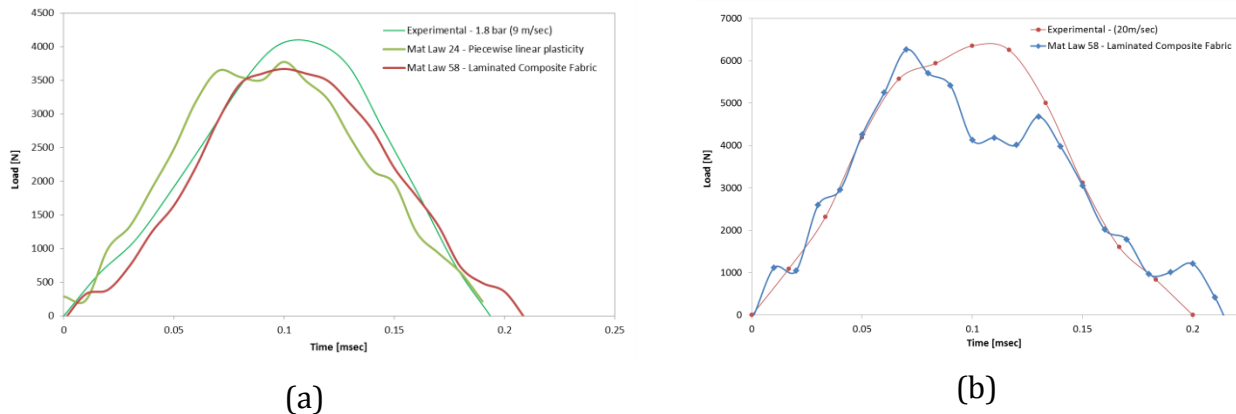


Figure 6-7: Experimental and simulated load time histories for (a) 9 m/sec and (b) 20 m/sec impact velocities

During the impact tests conducted on the flax/PLA composites, rebound was observed at all impact velocities, with evident vertical cracking at velocities 20m/sec and higher. The FE simulations predicted accurately these behaviors, as depicted in Figure 6-8. It should be noted that due to the erosion option used in FE calculations, cracking was apparent in the form of eroded elements removed from further calculations once failure criterion was met. Although failed elements were deleted only in the horizontal direction, closer investigation of the model showed nodal failure forming a cross-shaped crack as per the tested samples. Since the instrumented gas-gun system can only measure directly force vs. time history and the initial impact velocity just prior to impact, the experimentally-obtained contact force–time histories were the most reliable data for the validation of the proposed FE models. However energies, both internal and kinetic of the impactor, have also been compared and match within 5% error margin. Also, results for the maximum displacement draw similar conclusions to the maximum force.

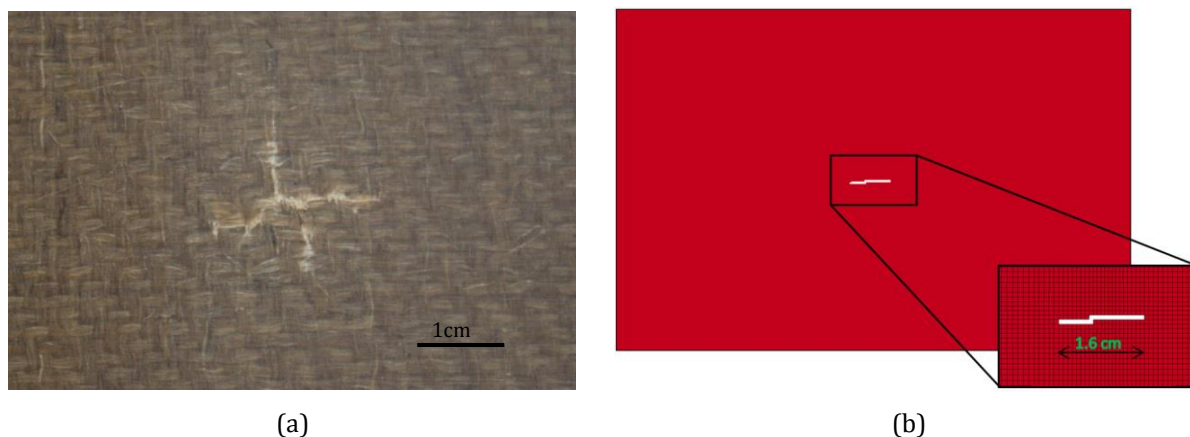


Figure 6-8: (a) Crack on sample tested at 20 m/sec and (b) Deleted elements representing crack formation on the simulated impact sample at 20 m/sec

6.7 Car side impact performance

Throughout the project, a number of models were made, from the first preliminary designs to the latest vehicle model. The first model as well as the last improved design are presented hereafter.

<i>Model Name</i>	<i>Description</i>
<i>Design 1</i>	Initial design
<i>Design 2</i>	Latest improved vehicle design

Figure 6-9 shows the resulted vehicle damage of the first vehicle models (design 1). The results show clearly the weaknesses of this first design with advanced penetration of the barrier into the occupants' space. Through an 80msec crash sequence (Figure 6-10) the barrier intrudes about 460 mm, with extensive damage shown among others on the floor, b-pillar and car seat. The contact of the barrier with the seat was one of the main areas of concern, as it directly suggests driver injury. The b-pillar also failed, with cracks and composite failure at the initial stages of the crash resulting in the pillar being detached and travelling towards the vehicle interior. Further, failure of the floor (composite/foam sandwich structure) together with the failure of the reinforcing tunnel and other attached parts (in contact with the barrier or not), suggested a significant contribution of the lower vehicle part to the energy absorption, as well as a weakness of the initial design.

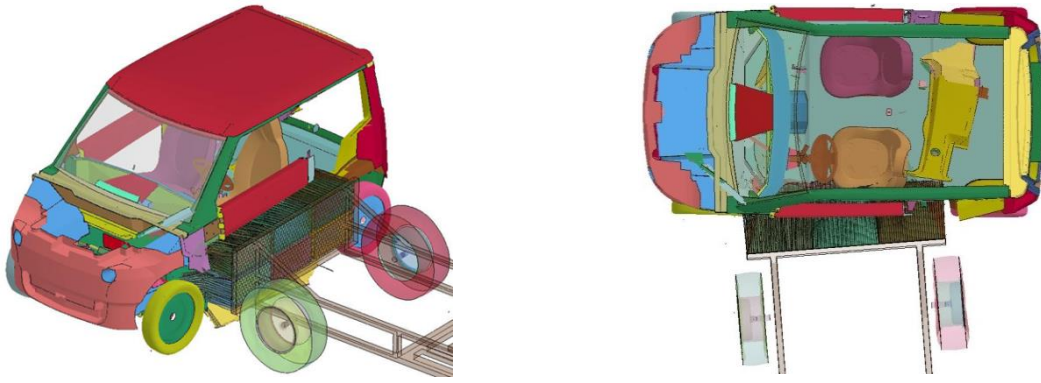


Figure 6-9: Predicted resulted damage from the side impact runs of design 1

The crash sequence as depicted in Figure 6-10 reveals a rotation of the barrier in the z-direction, suggesting a stronger load path through the A-pillar. Closer investigation of the model results showed contact between the barrier and the metallic door hinge mechanism which strengthened the front of the car in the area. Peak decelerations due to this contact and possible unpredictable behaviour of the barrier and A-pillar structure were undesirable and needed to be avoided.

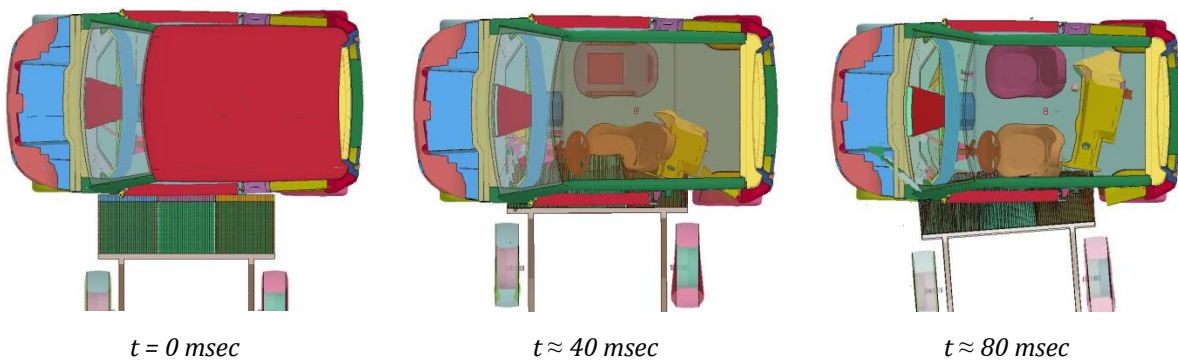


Figure 6-10: Impact sequence from the side impact runs of design 1

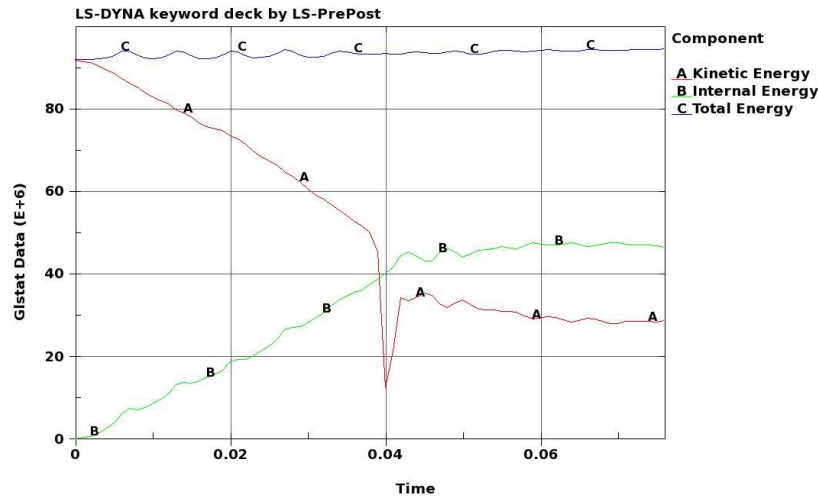


Figure 6-11: Energy time histories through the side impact of the initial design (design 1) of the Ecoshell Citi Car

Figure 6-11 depicts the kinetic and internal energy curves, as well as the overall energy balance extracted from the simulation results. The kinetic energy of the barrier starts to progressively reduce, and transformed into internal energy of the structure. The reduction appears linear in the first stages, with a very abrupt drop of energy after about 40 msec. Observation of the model and the crash sequence revealed that this drop was due to contact of the barrier's metallic frame with the very stiff door hinge of the car, due to the extensive penetration. Observation of the force-time history curves shows again this specific peak of force at around 300 kN, whilst up to then the force showed a plateau between 100 and 120 kN.

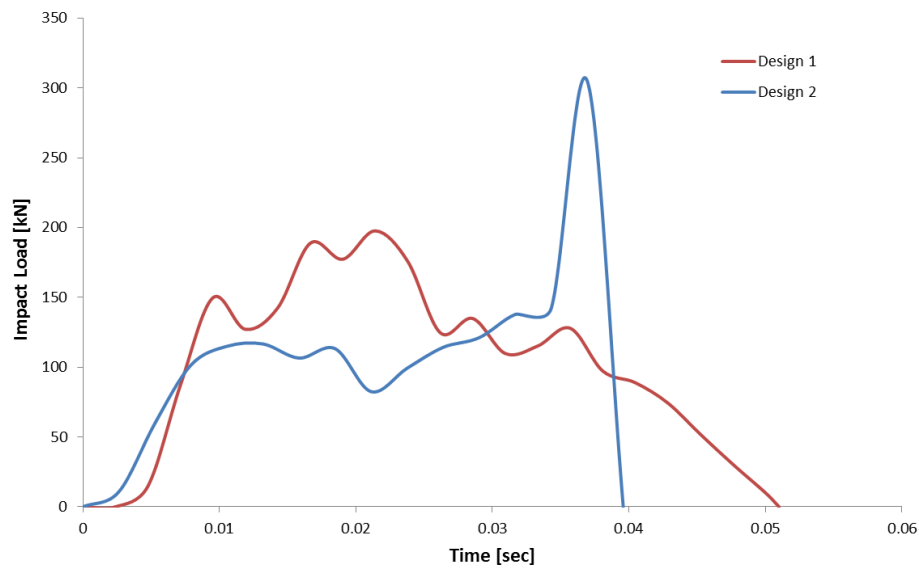


Figure 6-12: Comparison of the force-time histories for the initial and final design

Figure 6-13 shows the resulted damage and deformations of the simulated side crash of the optimized last vehicle design (design 2), following results and suggestion from the previous runs. The extensive damage of the floor reveals the fact that the main energy absorbing mechanism runs through the lower section of the car. The height of the vehicle, together with the lack of side door structure, contributes to that, whilst the positioning of the door band misses the intruding barrier to avoid injury of the occupants because of failed components pushed inside the driving space. The flax/PLA composite skin worked well in efficiently transferring the loading and compressing the foam in the area to absorb the impact energy. The lower part of the B-pillar is again failing, however optimization of the components strength and interactions resulted in only a localized failure, whilst the B-Pillar was withheld by the structure of the side panel. Contact occurred again between the barrier and the seat, which however resulted in a significantly smaller failure, localized at the lower part. Further studies using a dummy are required to assess the importance of this failure.

Observation of the barrier reveals a uniform compression in the middle section (where contact with the floor occurs), with a higher compression in the two sides where the barrier impacts the pillars (Figure 6-13). The A-pillar provides higher resistance and hence compression of the barrier, however the redesign of the hinge details resulted in

smoother decelerations and more progressive and predictable energy absorption (Figure 6-12).

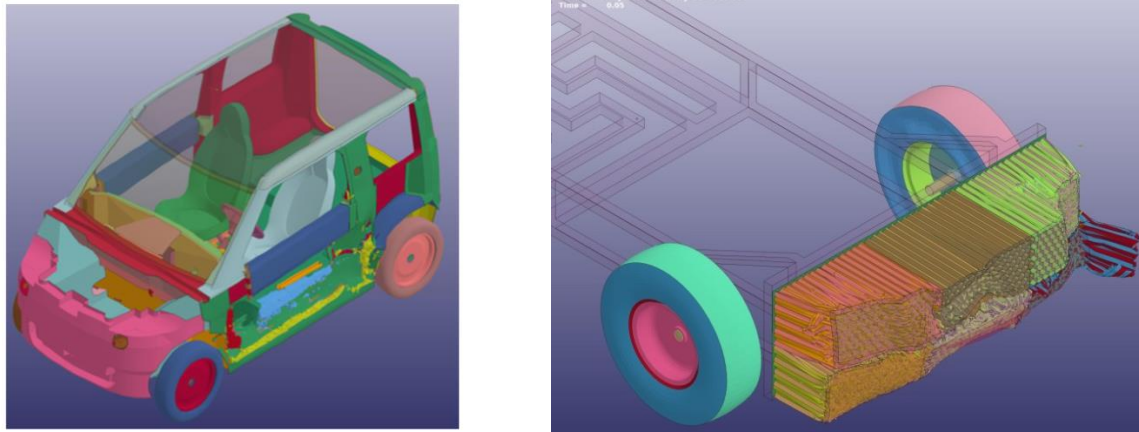


Figure 6-13: (a) Side impact damage of the final design of the Ecoshell Citi vehicle and (b) damage of the barrier after the impact

Design 2 is a significant improvement over the initial studies, with the side crash performance achieving acceptable results. The intrusion was restricted to 250mm, with very limited damage in the driver seat. The failure was controlled and progressive, without any failure or damage of any interior components not in contact with the barrier.

The energy curves extracted from the model of design 2 are depicted Figure 6-14. The impact results in acceleration of the vehicle towards the impact direction, which, after approximately 35msec equalizes with the velocity of the slowing barrier. After this stage, no more energy is absorbed by the vehicle and the barrier and car travel together. The total energy throughout the whole crash remains unmodified, showing energy balance and numerical stability through the simulation.

The significant improvement of the design over design 1 can be also observed through the comparison of the load curves (Figure 6-12). The load curve shows a plateau force between 150 to 200 kN, approximately 50 kN higher than design 1, explained through higher energy absorption of the material and structure. Further, the force-time history of the second design remains smooth through the sequence, without any peaks observed. The crash lasted about 50 msec.

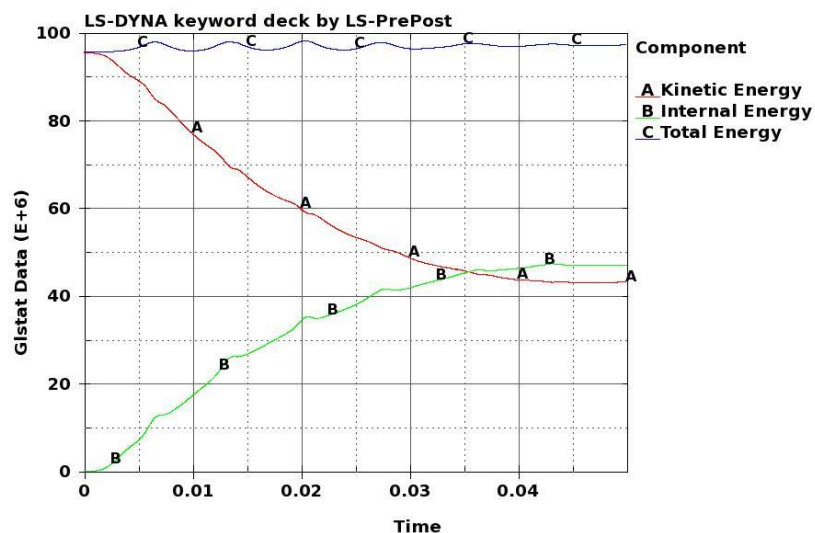


Figure 6-14: Energy time histories through the side impact of the final design iteration of the Ecoshell Citi Car

6.8 Conclusions

Very little numerical work is found in the literature on the mechanical performance of bio-composites and very little work is related to modeling, based mainly on generic assumptions and models initially created for man-made composites. The assumptions on the existing models do not realistically represent the nature of biocomposites, and cannot always predict the properties of natural fibre composites. In order to get close results, a number of correcting factors must be used to account for the increased cell wall density, the moisture, the non-perfect adhesion, and other factors related to the fibres, resin but also manufacturing and the different applications.

Further a large number of numerical tools and methods exist for the accurate simulation of traditional composites; however no work has been reported to date on how these models correlate with the response of natural fibre biocomposites in different loading and environmental conditions. Ls-Dyna material models Mat24 and Mat58 have been used and both show good correlation with tensile and impact testing. However, mat24 -as initially developed for metallic components- does not contain failure or damage. Mat58 realistically represents flax/PLA under both tensile and impact testing, and cracking and failure of the elements correlates well with tested samples.

Card Mat58 was used as a material for the setup of the Ecoshell model, and subjected to side crash testing. The material model was successfully implemented and helped through all the design stages to successfully assess the performance of flax/PLA used in most structural components of a whole vehicle structure.

Chapter 7. Conclusions and future work

In this study flax/PLA biocomposites prepared using a hot press moulding process, were studied to assess their potential use in structural and exterior automotive components. The interest of this work steered away from the well-studied chemical and structural composition of the constituents and their resulting composites, and targeted the understanding of the macro-mechanical behaviour of flax/PLA, i.e. its stress-strain response, damage accumulation, failure characteristics, strain rate dependency and the effect of environmental parameters such as temperature and moisture onto these properties. The special focus of this work was on the low velocity localised impact response, caused by stone impacts assuming the use of the material in exterior automotive components.

In addition, key in the design and development of such a vehicle and all the necessary structural components is the use of modelling techniques and FE analysis. The ability to accurately reproduce the macro-mechanical behaviour of the material under different loading conditions is needed, to provide the industry with the necessary tools to include the material into their design and development.

Part of this work was the link between the material studies and the modelling of biocomposites and focused on the assessment of different modelling methods and the capability of existing material models to predict the response of flax/PLA biocomposites. A case study was performed using these models to understand, develop

and improve the side crash performance of a superlight city car prototype developed by the European fp7 project Ecoshell.

From the results obtained in the individual studies in this work it can be concluded that:

- The strength and stiffness of flax/PLA was measured at 72 MPa and 13GPa respectively, indicating a very promising material to replace traditional choices in load bearing applications, such as CFRP and glass fibre panels. SEM micrographs confirm the poor interfacial adhesion between the fibres and matrix reported previously [1; 2; 11-13].
- The PLA matrix shows brittle characteristics, with an average failure strain of 1.5%. The stress-strain law is non-linear with the non-linearity introduced due to viscous behaviour of the material combined with a certain level of damage accumulation throughout the testing.
- DMA results show deterioration of the composite properties with a tan delta peak at around 74-76 °C. The flax fibres have a positive effect on the thermal response delaying the loss of stiffness to higher temperatures compared to that of pure PLA. The crystallinity of PLA was measured and found to be approximately 27%. Annealing above 100 °C for one hour brings that value to 30%, but analysis of tensile results of annealed specimens reveals a significant reduction of both the tensile strength and modulus.
- At 50 °C the stiffness is reduced 52% and the ultimate strength is also reduced significantly. At 110 °C the modulus reduces to approximately 5GPa with a remaining strength of 15.5 MPa. With increasing temperature the elongation at break increases. The failure characteristics remain brittle for the temperatures up to 65 °C, while at 110 °C high degradation of PLA is observed and the load seems to be carried through the fibres which progressively slip apart.
- Strain rate has an effect on the material and its viscous behaviour. Strength and modulus increase with increasing strain rates, while elongation at break reduces respectively.
- Flax/PLA samples were subjected to impact testing using a 20g projectile, at impact energies of 1, 4.5 and 6 J. The samples impacted at 1J did not show any visible damage or cracking, while in samples tested above 4.5J a cross-shaped

crack was visible in the back face (tensile face) of the sample with a visible indentation on the front face. Further, sample penetration was found to occur at approximately 16J impact energy.

- Load-time histories reveal the crack initiation as a drop of the acceleration derivative, hence a localized plateau of the force. The average maximum load recorded from the impacts was 3.6, 6.2 and 6.9 kN for impact energies of 1, 4.5 and 6 J respectively.
- The impact energy has no effect on the compressive modulus of the samples which remained constant at 20GPa. This was explained as the damage was localized and did not affect the in-plane properties, thus the loading was transferred through the unaffected areas. This resulted in progressive loss of strength as the impact energy was increasing.
- Good agreement with Fick's material models was found to be followed. The average percentage weight gain (saturation) for the immersed samples (room temperature) was 15%.
- Samples tested at higher temperatures did not show any visible cracks, but only micro-cracking and discoloration. Ultrasonic inspection revealed significant internal damage of the samples tested at 45 and 65°C.
- Samples initially submerged into water did not show any visible cracking but a significant deformation of the whole sample could be observed.
- The average maximum loads recorded were significantly reduced from the effect of both temperature and moisture.
- The impact energy absorbed during the impact increased with increasing testing temperature from 51% to 72% at 65°C. Higher moisture content also affected the energy absorbed to 73% for the samples with 5% water content; however this number did not increase further at higher moisture contents.
- FE analysis of flax/PLA under tensile and impact, predicted accurately within a 5% error the material behaviour, including loading time-histories, strength and material energies. Failure in the form of eroded elements was visible, but the models failed to accurately represent the failure shapes.

General Conclusions

Flax/PLA appears to be a good alternative to traditionally used man-made composites such as carbon or glass fibre reinforced composites offering high specific modulus and strength. The design however has to take into account the non-linear stress-strain behaviour of the material caused by material viscosity and internal damage accumulation. Main weakness of flax/PLA composites appears to be the environmental factor of temperature and moisture. This natural inherent of the constituents is the main limitation for their use in structural automotive components, and should be addressed.

The material response to localised stone impacts shows very promising results. Damage and cracking occurs only at impact velocities higher than 10m/sec impact and closer to 20m/sec (assuming an average stone size). Further, the material failure served to absorb the energy of each impact, without allowing penetration of the stone. This characteristic could be beneficial for the design of very light exterior components designed to protect expensive and critical parts. It is also important noting that the modulus after impact was unaffected and independent of the impact energy, ensuring a structure that can maintain its structural capacity until service or replacement.

Smearred property modelling (macro-scale) combined with detailed material testing for property selection, allows the accurate prediction of the structural behaviour of flax/PLA under different loading conditions. This predictive capability, together with 'clever' design of structures to use the material in its strengths, makes biocomposites now more than ever a viable choice for use in the automotive sector. The case study presented in this work supports the above argument showing a full vehicle design out of flax/PLA structural components. The specific properties of the material, its impactability and crashworthiness, make it an attractive new material option, in the constant effort of the automotive manufacturers to save weight but also create environmentally friendly vehicles.

Future work

Future studies should focus on the environmental disadvantages of flax/PLA, and study ways of tackling these weaknesses. Fibre and resin chemical modifications as well as additives have been widely reported as a method of improving the interfacial adhesion between the two composite constituents. It is now vital to focus these studies on the improvement of the stability of the materials with temperature and moisture. The effects of these material modifications on the structural response of the material i.e. the stress-strain behaviour, strain rate response, viscosity and damage, should then be revisited.

Further, especially as far as the automotive industry is concerned, it is vital to study the opportunities of repair after impacts and damage have occurred. Ways to repair locally the damaged areas without the need to replace whole components and keeping the structural performance unmodified and safe is critical.

A very interesting and necessary field of study is also that of fatigue and repetitive loading of biocomposites and flax/PLA. The fatigue characteristics have not been thoroughly studied, and the mechanical properties change (if any) under repetitive loading are not well understood. However these studies and their results are necessary for many applications.

Additionally, further development of the modelling techniques to incorporate the specific peculiarities of bio-composites (interfacial adhesion, porosity, non-uniform fibre dimensions, etc.) will be necessary as biocomposites find their way into more and more applications. Detailed design of components and very specific loading conditions will demand very accurate modelling that will require steering away from macro-scale modelling.

Achievements

Journal and conference Publications

1. **Nassiopoulos, E. and Njuguna, J.** (2015), "Thermo-mechanical performance of poly(lactic acid)/flax fibre-reinforced biocomposites", *Materials & Design*, vol. 66, Part B, no. 0, pp. 473-485.
2. **Nassiopoulos, E. and Njuguna, J.**, "Low velocity impact properties and strength after impact performance of flax/PLA biocomposites", *Composites*, 2015, Submitted
3. **Nassiopoulos, E., Abhyankar, H., Njuguna, J.**, "Structural flax/PLA biocomposites: understanding of their thermo-mechanical behaviour", *21st Annual International Conference on Composites or Nano Engineering (ICCE-21)*, Tenerife, Canary Islands, 2013
4. **Nassiopoulos, E., Njuguna, J.**, "Natural fibre biocomposites into structural vehicle components: Progress and challenges", (*SPE*) *EUROTECH 2011*, 14-15 November 2011, Barcelona, Spain
5. **Kalia, S., Dufresne, A., Cherian, B. M., Kaith, B. S., Avérous, L., Njuguna, J. and Nassiopoulos, E.** (2011), "Cellulose-Based Bio- and Nanocomposites: A Review", *International Journal of Polymer Science*, vol. 2011
6. **Zhu, J., Sauget, A., Nassiopoulos, E., Pizzi, A., Avril, C., Njuguna, J., Abyhankar, H.**, "Structural performances of flax reinforced composites from tannin resin and bio-epoxy", *Transport Research Arena*, Paris, 2014
7. **Zhu, J., Abhyankar, H., Nassiopoulos, E., Njuguna, J.**, "Tannin-based flax fibre reinforced composites for structural applications in vehicles", *IOP Conference Series Materials Science and Engineering*, 2012
8. **Jiying, F., Nassiopoulos, E., James Brighton, Alain De Larminat, James Njuguna**, 'New structural biocomposites for car applications' *Society of Plastics Engineers (SPE) EUROTECH 2011*, 14-15 November 2011, Barcelona, Spain
9. **Jiying, F., Nassiopoulos, E., James Njuguna**, "New structural biocomposites for car applications, Fibre crops: Agronomy and end uses workshop, Cambridge, UK, 16 Oct. 2011

10. **Kalia, S., Dufresne, A., Cherian, B. M., Kaith, B. S., Avérous, L., Njuguna, J. and Nassiopoulos, E.** (2011), "Cellulose-Based Bio- and Nanocomposites: A Review", *International Journal of Polymer Science*, vol. 2011.
11. **C. Avril, P. A. Bailly, J. Njuguna, E. Nassiopoulos, A. De Larminat,** "Development of flax-reinforced bio-composites for high-load bearing automotive parts", *ECCM15 - 15TH European Conference on Composite Materials, Venice, Italy, 24-28 June 2012*

Posters

1. **Nassiopoulos, E., Njuguna, J.,** 'Natural fibre Biocomposites for body-in-white, body panels and other structural components, 'Society of Plastics Engineers (SPE) EUROTECH 2011, 14-15 November 2011, Barcelona, Spain

Bibliography

- [1] Bledzki, A. K., Faruk, O. and V.E. Sperber (2006), "Cars from Bio-Fibres", *Macromolecular Materials and Engineering*, , no. 5, pp. 449-457.
- [2] Wambua, P., Ivens, J. and Verpoest, I. (2003), "Natural fibres: can they replace glass in fibre reinforced plastics?", *Composites Science and Technology*, vol. 63, no. 9, pp. 1259-1264.
- [3] Njuguna, J., Pielichowski, K. and Zhu, H. (2014), *Health and Environmental Safety of Nanomaterials, Polymer Nanocomposites and Other Materials Containing Nanoparticles*, 1st Edition ed, Elsevier, UK.
- [4] Kalia, S., Dufresne, A., Cherian, B. M., Kaith, B. S., Avérous, L., Njuguna, J. and Nassiopoulos, E. (2011), "Cellulose-Based Bio- and Nanocomposites: A Review", *International Journal of Polymer Science*, vol. 2011.
- [5] Official Journal of European Communities (2000), Directive 2000/53/EC of the European Parliament and of the Council (End-Of life vehicles), .
- [6] Bos H. (2004), *The potential of flax fibres as reinforcement for composite materials*.
- [7] Drzal, L. T., Mohanty, A. K. and Misra, M. "Bio-composite materials as alternatives to petroleum-based composites for automotive applications", *Composite Materials and Structures Center*, vol. Michigan State University, East Lansing, MI 48824.
- [8] Bledzki, A. K. and Gassan, J. (1999), "Composites reinforced with cellulose based fibres", *Progress in Polymer Science*, vol. 24, no. 2, pp. 221-274.
- [9] Nova Institute (2011), www.nova-institut.de, available at: www.nova-institut.de.
- [10] Karus, M., Ortmann, S., Gahle, C. and Pendarovski, C. (2006), "Use of natural fibres in composites for the German automotive production from 1999 till 2005", *Hurth : nova-Institute*, .

- [11] Biagiotti, J., Puglia, D. and Kenny, J. M. (2004), "A Review on Natural Fibre-Based Composites-Part I -- Structure, Processing and Properties of Vegetable Fibres", *Journal of Natural Fibers*, vol. 1, no. 2, pp. 37-68.
- [12] Summerscales, J., Dissanayake, N. P. J., Virk, A. S. and Hall, W. (2010), "A review of bast fibres and their composites. Part 1 – Fibres as reinforcements", *Composites Part A: Applied Science and Manufacturing*, vol. 41, no. 10, pp. 1329-1335.
- [13] Sparnins, E. (2006), *Mechanical properties of flax fibres and their composites* Lulea University of Technology : Division of Polymer Engineering, .
- [14] Njuguna J., Wambua P., Pielichowski K. and Kayvantash K. (2011), "Natural Fibre-reinforced polymer composites and nanocomposites for automotive applications", in *Cellulose Fibres: Bio- and Nano-Polymer Composites*, Springer.
- [15] Mohanty A.K., Misra M. and Drzal L.T. (eds.) (2005), *Natural Fibres, Biopolymers, and Biocomposites*, .
- [16] Nishino T. (2004), "Natural fibre sources", in *Green composites: Polymer composites and the environment*, .
- [17] Bos, H. L., Müssig, J. and van den Oever, M. J. A. (2006), "Mechanical properties of short-flax-fibre reinforced compounds", *Composites Part A: Applied Science and Manufacturing*, vol. 37, no. 10, pp. 1591-1604.
- [18] Bos, H., Van, D.O. and Peters, O., (2002), *Tensile and compressive properties of flax fibres for natural fibre reinforced composites*, Springer Netherlands.
- [19] Ku, H., Wang, H., Pattarachaiyakoo, N. and Trada, M. (2011), "A review on the tensile properties of natural fiber reinforced polymer composites", *Composites Part B: Engineering*, vol. 42, no. 4, pp. 856-873.
- [20] Kalia, S., Kaith, B. S. and Kaur, I. (2009), "Pretreatments of natural fibers and their application as reinforcing material in polymer composites:A review", *Polymer Engineering and Science*, vol. 49, no. 7, pp. 1253-1272.
- [21] Gomes, A., Goda, K. and Ohgi, J. (2004), "Effects of Alkali Treatment to Reinforcement on Tensile Properties of Curaua Fiber Green Composites", *JSME International Journal Series A*, vol. 47, no. No. 4 Special Issue on Green Composites, pp. 541-546.
- [22] Gassan, J. and Bledzki, A. K. (1999), "Alkali treatment of jute fibers: Relationship between structure and mechanical properties", *Journal of Applied Polymer Science*, vol. 71, no. 4, pp. 623-629.
- [23] Van de Weyenberg, I., Ivens, J., De Coster, A., Kino, B., Baetens, E. and Verpoest, I. (2003), "Influence of processing and chemical treatment of flax fibres on their composites", *Composites Science and Technology*, vol. 63, no. 9, pp. 1241-1246.

- [24] George, J., Sreekala, M. S. and Thomas, S. (2001), "A review on interface modification and characterization of natural fiber reinforced plastic composites", *Polymer Engineering & Science*, vol. 41, no. 9, pp. 1471-1485.
- [25] Li, X., Tabil, L. and Panigrahi, S., (2007), *Chemical Treatments of Natural Fiber for Use in Natural Fiber-Reinforced Composites: A Review*, Springer Netherlands.
- [26] Mishra, S., Mohanty, A. K., Drzal, L. T., Misra, M. and Hinrichsen, G. (2004), "A Review on Pineapple Leaf Fibers, Sisal Fibers and Their Biocomposites", *Macromolecular Materials and Engineering*, vol. 289, no. 11, pp. 955-974.
- [27] Gauthier, R., Joly, C., Coupas, A. C., Gauthier, H. and Escoubes, M. (1998), "Interfaces in polyolefin/cellulosic fiber composites: Chemical coupling, morphology, correlation with adhesion and aging in moisture", *Polymer Composites*, vol. 19, no. 3, pp. 287-300.
- [28] Kushwaha, P. K. and Kumar, R. (2011), "Influence of chemical treatments on the mechanical and water absorption properties of bamboo fiber composites", *Journal of Reinforced Plastics and Composites*, vol. 30, no. 1, pp. 73-85.
- [29] Heine, E. and HÄ¶cker, H. (1995), "Enzyme treatments for wool and cotton", *Review of Progress in Coloration and Related Topics*, vol. 25, no. 1, pp. 57-70.
- [30] Xie, Y., Hill, C. A. S., Xiao, Z., Militz, H. and Mai, C. (2010), "Silane coupling agents used for natural fiber/polymer composites: A review", *Composites Part A: Applied Science and Manufacturing*, vol. 41, no. 7, pp. 806-819.
- [31] Gassan, J. and Bledzki, A. K. (1999), "Effect of cyclic moisture absorption desorption on the mechanical properties of silanized jute-epoxy composites", *Polymer Composites*, vol. 20, no. 4, pp. 604-611.
- [32] International Year of Natural Fibres , www.naturalfibres2009.org/en/index.html, available at: www.naturalfibres2009.org/en/index.html.
- [33] Mohanty, A. K., Misra, M. and Hinrichsen, G. (2000), "Biofibres, biodegradable polymers and biocomposites: An overview", *Macromol.Mater.Eng.*, vol. 276-277, no. 1, pp. 1-24.
- [34] Liu, Q. and Hughes, M. (2008), "The fracture behaviour and toughness of woven flax fibre reinforced epoxy composites", *Composites Part A: Applied Science and Manufacturing*, vol. 39, no. 10, pp. 1644-1652.
- [35] John, M. J. and Anandjiwala, R. D. (2009), "Chemical modification of flax reinforced polypropylene composites", *Composites Part A: Applied Science and Manufacturing*, vol. 40, no. 4, pp. 442-448.
- [36] Garkhail S.K., Heinjenrath R.W.H. and Peijs T. (2000), "Mechanical Properties of Natural-Fibre-Mat-Reinforced Thermoplastics based on Flax Fibres and Polypropylene", *Applied Composite Materials*, vol. 7, pp. 351-372.

- [37] Baiardo, M., Zini, E. and Scandola, M. (2004), "Flax fibre–polyester composites", *Composites Part A: Applied Science and Manufacturing*, vol. 35, no. 6, pp. 703-710.
- [38] Maryudi, R. M., Yunus, A. H. N. and Abidin, M. H. (2009), "Synthesis and Characterization of Manganese Carboxylates", *Journal of Applied Sciences*, vol. 9, no. 17, pp. 3156-3160.
- [39] Soy info centre , *Henry Ford and His Employees: Work with Soy*, available at: http://www.soyinfocenter.com/HSS/henry_ford_and_employees.php.
- [40] Plackett, D., Løgstrup Andersen, T., Batsberg Pedersen, W. and Nielsen, L. (2003), "Biodegradable composites based on -polylactide and jute fibres", *Composites Science and Technology*, vol. 63, no. 9, pp. 1287-1296.
- [41] Garlotta, D. (2001), "A Literature Review of Poly(Lactic Acid)", *Journal of Polymers and the Environment*, vol. 9, no. 2, pp. 63-84.
- [42] Ray, S. S. and Ramontja, J. (2009), "Polylactide-Based Nanocomposites", in *Biodegradable Polymer Blends and Composites from Renewable Resources*, John Wiley & Sons, Inc., , pp. 389-413.
- [43] Tokoro, R., Vu, D., Okubo, K., Tanaka, T., Fujii, T. and Fujiura, T., (2008), *How to improve mechanical properties of polylactic acid with bamboo fibers*, Springer Netherlands.
- [44] Ochi, S. (2008), "Mechanical properties of kenaf fibers and kenaf/PLA composites", *Mechanics of Materials*, vol. 40, no. 4-5, pp. 446-452.
- [45] Shibata, M., Oyamada, S., Kobayashi, S. and Yaginuma, D. (2004), "Mechanical properties and biodegradability of green composites based on biodegradable polyesters and lyocell fabric", *Journal of Applied Polymer Science*, vol. 92, no. 6, pp. 3857-3863.
- [46] Pan, P., Zhu, B., Kai, W., Serizawa, S., Iji, M. and Inoue, Y. (2007), "Crystallization behavior and mechanical properties of bio-based green composites based on poly(L-lactide) and kenaf fiber", *Journal of Applied Polymer Science*, vol. 105, no. 3, pp. 1511-1520.
- [47] Espert, A., Vilaplana, F. and Karlsson, S. (2004), "Comparison of water absorption in natural cellulosic fibres from wood and one-year crops in polypropylene composites and its influence on their mechanical properties", *Composites Part A: Applied Science and Manufacturing*, vol. 35, no. 11, pp. 1267-1276.
- [48] Thwe, M. M. and Liao, K. (2003), "Durability of bamboo-glass fiber reinforced polymer matrix hybrid composites", *Composites Science and Technology*, vol. 63, no. 3-4, pp. 375-387.

- [49] Pavithran C., Mukherjee P.S. and Brahmakumar M. (1991), "Coir-glass Intermingled Fibre Hybrid Composites", *Journal of Reinforced Plastics and Composites*, vol. 10, pp. 91-101.
- [50] Tobias BC. (1993), "Tensile and Impact behaviour of natural fibre-reinforced composite materials", in Chandra T., D. A. K. (ed.) *The Minerals, Metals and Materials Society*, .
- [51] Mueller H. D. (2004), "Improving the Impact Strength of Natural Fibre Reinforced Composites By Specifically Designed Material and Process Parameters", *IJN Winter*, .
- [52] De Bruijn J.C.M. (2000), "Natural Fibre Mat Thermoplastic Products from a Processor's Point of View", *Applied Composite Materials*, vol. 7, pp. 415-420.
- [53] Sparnins, E. (2006), *Mechanical properties of flax fibers and their composites* (unpublished PhD thesis thesis), Division of Polymer Engineering , Department of Materials and Manufacturing Engineering, Lulea University of Technology, Sweden.
- [54] S.W., T. (ed.) (2008), *Strength & Life of Composites*, Composites Design Group, Department of Aeronautics & Astronautics, Stanford University, Stanford.
- [55] A.R., B. and J., R. (2005), *Fundamentals of fibre reinforced composite materials*, Institute of physics Publishing, London.
- [56] Hull, D. and Clyne, T. W. (1996), *An introduction to composite materials*, 2nd edition ed, Press Syndicate of the University of Cambridge, Cambridge.
- [57] Greve, L. and Pickett, A. K. (2006), "Modelling damage and failure in carbon/epoxy non-crimp fabric composites including effects of fabric pre-shear", *Composites Part A: Applied Science and Manufacturing*, vol. 37, no. 11, pp. 1983-2001.
- [58] M., F. (2006), *Damage and failure modelling of carbon and glass 2D braided composites* Cranfield University, .
- [59] Chang, F. K. and Chang, K. Y. (1987), "A progressive damage model for laminated composites containing stress concentrations", *Journal of Composite Materials*, vol. 21, no. 9, pp. 834-855.
- [60] Tsai, S. W. and Wu, E. M. (1971), "A general theory of strength for anisotropic materials", *Journal of Composite Materials*, vol. 5, pp. 58-80.
- [61] Gol'denblat, I. and Kopnov, V. A. (1966), "Strength of glass reinforced plastic in the complex stress state", *Polymer Mechanics*, vol. 1, pp. 54-60.
- [62] Hinton, M. J., Kaddour, A. S. and Soden, P. D. (2002), "A comparison of the predictive capabilities of current failure theories for composite laminates, judged against experimental evidence", *Composites Science and Technology*, vol. 62, no. 12-13, pp. 1725-1797.

- [63] Z., H. (1980), "Failure criteria for unidirectional fibre composites", *ASME Journal of Applied Mechanics*, vol. 47, no. 2, pp. 329-334.
- [64] Hinton, M. J. and Soden, P. D. (1998), "Predicting failure in composite laminates: the background to the exercise", *Composites Science and Technology*, vol. 58, no. 7, pp. 1001-1010.
- [65] C.G., D., P.P., C. and C.A., R. (2005), "Failure Criteria for FRP Laminates", *Journal of Composite Materials*, vol. 39, pp. 323.
- [66] Ladeveze, P. and LeDantec, E. (1992), "Damage modelling of the elementary ply for laminated composites", *Composites Science and Technology*, vol. 43, no. 3, pp. 257-267.
- [67] L., G. (2005), *Damage and failure modelling of carbon/epoxy non-crimp fabric composites* Cranfield University, .
- [68] Rijswijk, K., Brouwer, W. D. and Beukers, A. (2001), "Application of Natural Fibre Composites", *Structures and Materials Laboratory Faculty of Aerospace Engineering Delft University of Technology*, .
- [69] Composites Europe 2011 - blog, *Composites Europe*, available at: <http://blog.composites-europe.com/tag/natural-fibre-reinforced-plastics/>.
- [70] Holbery, J. and Houston, D. (2006), "Natural-fiber-reinforced polymer composites in automotive applications", *JOM Journal of the Minerals, Metals and Materials Society*, vol. 58, no. 11, pp. 80-86.
- [71] Oksman, K., Skrifvars, M. and Selin, J. -. (2003), "Natural fibres as reinforcement in polylactic acid (PLA) composites", *Composites Science and Technology*, vol. 63, no. 9, pp. 1317-1324.
- [72] Bax, B. and Müssig, J. (2008), "Impact and tensile properties of PLA/Cordenka and PLA/flax composites", *Composites Science and Technology*, vol. 68, no. 7-8, pp. 1601-1607.
- [73] Ahmed, J., Zhang, J. X., Song, Z. and Varshney, S. K. (2009), "Thermal properties of polylactides - Effect of molecular mass and nature of lactide isomer", *Journal of Thermal Analysis and Calorimetr*, vol. 95, no. 3, pp. 957-964.
- [74] Cao, X., Mohamed, A., Gordon, S. H., Willett, J. L. and Sessa, D. J. (2003), "DSC study of biodegradable poly(lactic acid) and poly(hydroxy ester ether) blends", *Thermochimica Acta*, vol. 406, no. 1-2, pp. 115-127.
- [75] Oksman, K., Wallström, L., Berglund, L. A. and Filho, R. D. T. (2002), "Morphology and mechanical properties of unidirectional sisal? epoxy composites", *Journal of Applied Polymer Science*, vol. 84, no. 13, pp. 2358-2365.

- [76] Varna, J., Rozite, L., Joffe, R. and Pupurs, A. (2012), "Non-linear behaviour of PLA based flax composites", *Plastics, Rubber and Composites*, vol. 41, no. 2, pp. 49-60.
- [77] Gehring, F., Bouchart, V., Dinzart, F. and Chevrier, P. (2012), "Microstructure, mechanical behaviour, damage mechanisms of polypropylene/short hemp fibre composites: Experimental investigations", *Journal of Reinforced Plastics and Composites*, vol. 31, no. 22, pp. 1576-1585.
- [78] Baley, C., Morvan, C. and Grohens, Y. (2005), "Influence of the Absorbed Water on the Tensile Strength of Flax Fibers", *Macromolecular Symposia*, vol. 222, no. 1, pp. 195-202.
- [79] Van de Velde, K. and Baetens, E. (2001), "Thermal and Mechanical Properties of Flax Fibres as Potential Composite Reinforcement", *Macromolecular Materials and Engineering*, vol. 286, no. 6, pp. 342-349.
- [80] Mouti, Z. (2012), *Localised Low Velocity Impact Performance of Short Glass Fibre Reinforced Polyamide 66 Oil Pans* (unpublished PhD thesis), Cranfield University, Cranfield.
- [81] Zhou, Y. and Mallick, P. K. (2002), "Effects of temperature and strain rate on the tensile behavior of unfilled and talc-filled polypropylene. Part II: Constitutive equation", *Polymer Engineering & Science*, vol. 42, no. 12, pp. 2461-2470.
- [82] Dhakal, H., Zhang, Z. and Richardson, M. (2006), "Effect of water absorption on the mechanical properties of hemp fibre reinforced unsaturated polyester composites", *Composites Science and Technology*, vol. 67, no. 7-8, pp. 1674-1683.
- [83] Nair, G. R., Liplap, P., Gariepy, Y. and Raghavan, G. S. V. (2011), "Microwave Drying of Flax Fibre at controlled Temperatures", *Journal of Agricultural Science & Technology B*, vol. 1, no. 12b, pp. 1103.
- [84] Stamboulis, A., Baillie, C. A. and Peijs, T. (2001), "Effects of environmental conditions on mechanical and physical properties of flax fibers", *Composites Part A: Applied Science and Manufacturing*, vol. 32, no. 8, pp. 1105-1115.
- [85] Li, Z. and Lambros, J. (2001), "Strain rate effects on the thermomechanical behavior of polymers", *International Journal of Solids and Structures*, vol. 38, no. 20, pp. 3549-3562.
- [86] Omar, M. F., Md Akil, H., Ahmad, Z. A., Mazuki, A. A. M. and Yokoyama, T. (2010), "Dynamic properties of pultruded natural fibre reinforced composites using Split Hopkinson Pressure Bar technique", *Materials & Design*, vol. 31, no. 9, pp. 4209-4218.
- [87] Bledzki, A. K., Faruk, O. and Sperber, V. E. (2006), "Cars from Bio-Fibres", *Macromolecular Materials and Engineering*, vol. 291, no. 5, pp. 449-457.

- [88] Nassiopoulou, E. and Njuguna, J. (2015), "Thermo-mechanical performance of poly(lactic acid)/flax fibre-reinforced biocomposites", *Materials & Design*, vol. 66, Part B, no. 0, pp. 473-485.
- [89] Cantwell, W. J. and Morton, J. (1991), "The impact resistance of composite materials — a review", *Composites*, vol. 22, no. 5, pp. 347-362.
- [90] Wright, P. and Matthews, T. (2001), *Formula 1 Technology*, Society of Automotive Engineers, 400 Commonwealth Dr, Warrendale, PA, 15096, USA, URL:<http://www.sae.org/technical/books/R-230><http://www.sae.org>.
- [91] Gassan, J. (2002), "A study of fibre and interface parameters affecting the fatigue behaviour of natural fibre composites", *Composites Part A: Applied Science and Manufacturing*, vol. 33, no. 3, pp. 369-374.
- [92] Yoganandan, N. and Pintar, F. A. (2005), "Responses of side impact dummies in sled tests", *Accident Analysis & Prevention*, vol. 37, no. 3, pp. 495-503.
- [93] Zhao, H. and Gary, G. (1998), "Crushing behaviour of aluminium honeycombs under impact loading", *International Journal of Impact Engineering (UK)*, vol. 21, no. 10, pp. 827-836.
- [94] Alimuzzaman, S., Gong, R. H. and Akonda, M. (2013), "Impact Property of PLA/Flax Nonwoven Biocomposite", *Materials Science*, vol. 2013.
- [95] Padaki, V. N., Alagirusamy, R. and Deopura, B. L. (2008), "Low velocity impact behaviour of textile reinforced composites", *Indian Journal of Fibre and Textile Research*, vol. 33, pp. 189-202.
- [96] Richardson, M. O. W. and Wisheart, M. J. (1996), "Review of low-velocity impact properties of composite materials", *Composites Part A: Applied Science and Manufacturing*, vol. 27, no. 12, pp. 1123-1131.
- [97] Bartus, S. D. and Vaidya, U. K. (2005), "Performance of long fiber reinforced thermoplastics subjected to transverse intermediate velocity blunt object impact", *Composite Structures*, vol. 67, no. 3, pp. 263-277.
- [98] Lee, S. F. and Swallowe, G. M. (2004), "Direct measurement of high rate stress-strain curves using instrumented falling weight and high-speed photography", *The Imaging Science Journal*, vol. 52, pp. 193-201.
- [99] Young, W. C. and Budynas, R. G. (2001), *Roark's Formulas for Stress and Strain*, 7 edition ed, McGraw-Hill Professional.
- [100] Young, D. (1939), "Clamped rectangular plates with a central concentrated load", *ASME Paper A-114, Journal of Applied Mechanics*, vol. 6, no. 3.
- [101] Timoshenko, S. and Woinowsky-Krieger, S. (1959), "Theory of Plates and Shells", *2nd Edition, McGraw-Hill*, .

- [102] Petrucci, R., Nisini, E., Ghelli, D., Santulli, C., Puglia, D., Sarasini, F., Minak, G. and Kenny, J. M. (2012), "Mechanical and impact characterisation of hybrid composites laminates based on flax, hemp, basalt and glass fibres produced by vacuum infusion", *ECCM15, 15th European Conference on Composite Materials*, vol. Venice, Italy.
- [103] Santulli, C., Janssen, M. and Jeronimidis, G. (2005), "Partial replacement of E-glass fibers with flax fibers in composites and effect on falling weight impact performance", *Journal of Materials Science*, vol. 40, pp. 3581-3585.
- [104] Sevkat, E., Liaw, B., Delale, F. and Raju, B. B. (2009), "Drop-weight impact of plain-woven hybrid glass-graphite/toughened epoxy composites", *Composites Part A: Applied Science and Manufacturing*, vol. 40, no. 8, pp. 1090-1110.
- [105] Sanchez-Saez, S., Barbero, E., Zaera, R. and Navarro, C. (2005), "Compression after impact of thin composite laminates", *Composites Science and Technology*, vol. 65, no. 13, pp. 1911-1919.
- [106] Prichard, J. C. and Hogg, P. J. (1990), "The role of impact damage in post-impact compression testing", *Composites*, vol. 21, no. 6, pp. 503-511.
- [107] Chow, C. P. L., Xing, X. S. and Li, R. K. Y. (2007), "Moisture absorption studies of sisal fibre reinforced polypropylene composites", *Composites Science and Technology*, vol. 67, no. 2, pp. 306-313.
- [108] Lin, Q., Zhou, X. and Dai, G. (2002), "Effect of hydrothermal environment on moisture absorption and mechanical properties of wood flour-filled polypropylene composites", *Journal of Applied Polymer Science*, vol. 85, no. 14, pp. 2824-2832.
- [109] Stamboulis, A., Baillie, C. A. and Peijs, T. (2001), "Effects of environmental conditions on mechanical and physical properties of flax fibers", *Composites Part A: Applied Science and Manufacturing*, vol. 32, no. 8, pp. 1105-1115.
- [110] Assarar, M., Scida, D., El Mahi, A., Poilâne, C. and Ayad, R. (2011), "Influence of water ageing on mechanical properties and damage events of two reinforced composite materials: Flax-fibres and glass-fibres", *Materials & Design*, vol. 32, no. 2, pp. 788-795.
- [111] Espert, A., Vilaplana, F. and Karlsson, S. (2004), "Comparison of water absorption in natural cellulosic fibres from wood and one-year crops in polypropylene composites and its influence on their mechanical properties", *Composites Part A: Applied Science and Manufacturing*, vol. 35, no. 11, pp. 1267-1276.
- [112] Zhu, J., Zhu, H., Njuguna, J. and Abhyankar, H. (2013), "Recent Development of Flax Fibres and Their Reinforced Composites Based on Different Polymeric Matrices", *Materials*, vol. 6, no. 11, pp. 5171-5198.

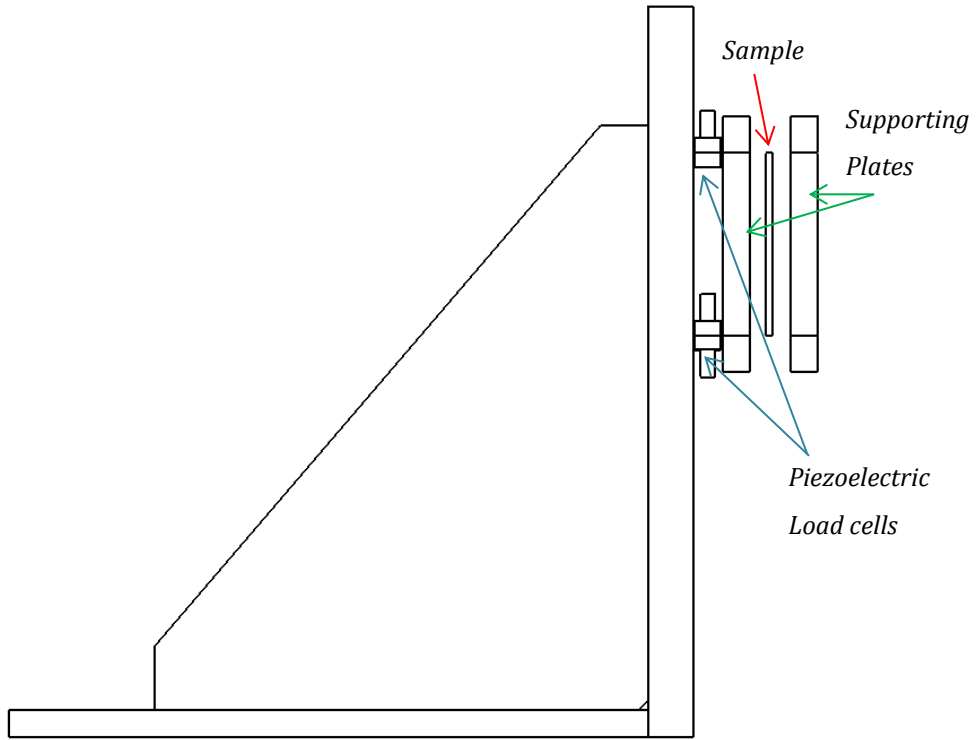
- [113] Nassiopoulos, E. and Njuguna, J. "Low velocity impact properties and strength after impact performance of flax/PLA biocomposites", *Not yet published*, .
- [114] Le Duigou, A., Davies, P. and Baley, C. (2009), "Seawater ageing of flax/poly(lactic acid) biocomposites", *Polymer Degradation and Stability*, vol. 94, no. 7, pp. 1151-1162.
- [115] Ndazi, B. S. (2011), "Characterization of hydrolytic degradation of polylactic acid/rice hulls composites in water at different temperatures", *expresspolymlett: eXPRESS Polymer Letters*, vol. 5, no. 2, pp. 119-131.
- [116] Alimuzzaman, S., Gong, R. H. and Akonda, M. (2014), "Biodegradability of nonwoven flax fiber reinforced polylactic acid biocomposites", *Polymer Composites*, vol. 35, no. 11, pp. 2094-2102.
- [117] Giridhar, J., Kishore and Rao, R. M. V. G. K. (1986), "Moisture Absorption Characteristics of Natural Fibre Composites", *Journal of Reinforced Plastics and Composites*, vol. 5, pp. 141.
- [118] Girisha, C., Sanjeevamurthy and Srinivas, G. R. (2012), "Sisal/Coconut Coir Natural Fibers – Epoxy Composites: Water Absorption and Mechanical Properties", *International Journal of Engineering and Innovative Technology*, vol. 2, no. 3, pp. 166.
- [119] Taib, M. R., Ramarad, S., Ishak, M. Z. A. and Todo, M. (2008), "Water absorption and tensile properties of kenaf bast fibre plasticized poly lactic acid biocomposites", *Proceedings of the Polymer Processing Society, 24th Annual Meeting*, vol. PPS-24.
- [120] Osman, E., Vakhguelt, A., Sbarski, I. and Mutasher, S. (2011), "Water absorption behaviour and its effect on the mechanical properties of Kenaf natural fibre unsaturated polyester composites", *18th International Conference on composite materials*, .
- [121] La Mantia, F. P. and Morreale, M. (2011), "Green composites: A brief review", *Composites Part A: Applied Science and Manufacturing*, vol. 42, no. 6, pp. 579-588.
- [122] Mohanty, A.K., Misra, M. and Drzal, L.T., (2002), *Sustainable Bio-Composites from Renewable Resources: Opportunities and Challenges in the Green Materials World*, Springer Netherlands.
- [123] European Commission, F. P. (2015), *Development of new light high-performance environmentally benign composites made of bio-materials and bio-resins for electric car application*, available at: http://cordis.europa.eu/project/rcn/97556_en.html (accessed 04/25).
- [124] Cox, H. L. (1952), "The elasticity and strength of paper and other fibrous materials", *British Journal of Applied Physics*, vol. 3, no. 3, pp. 72.

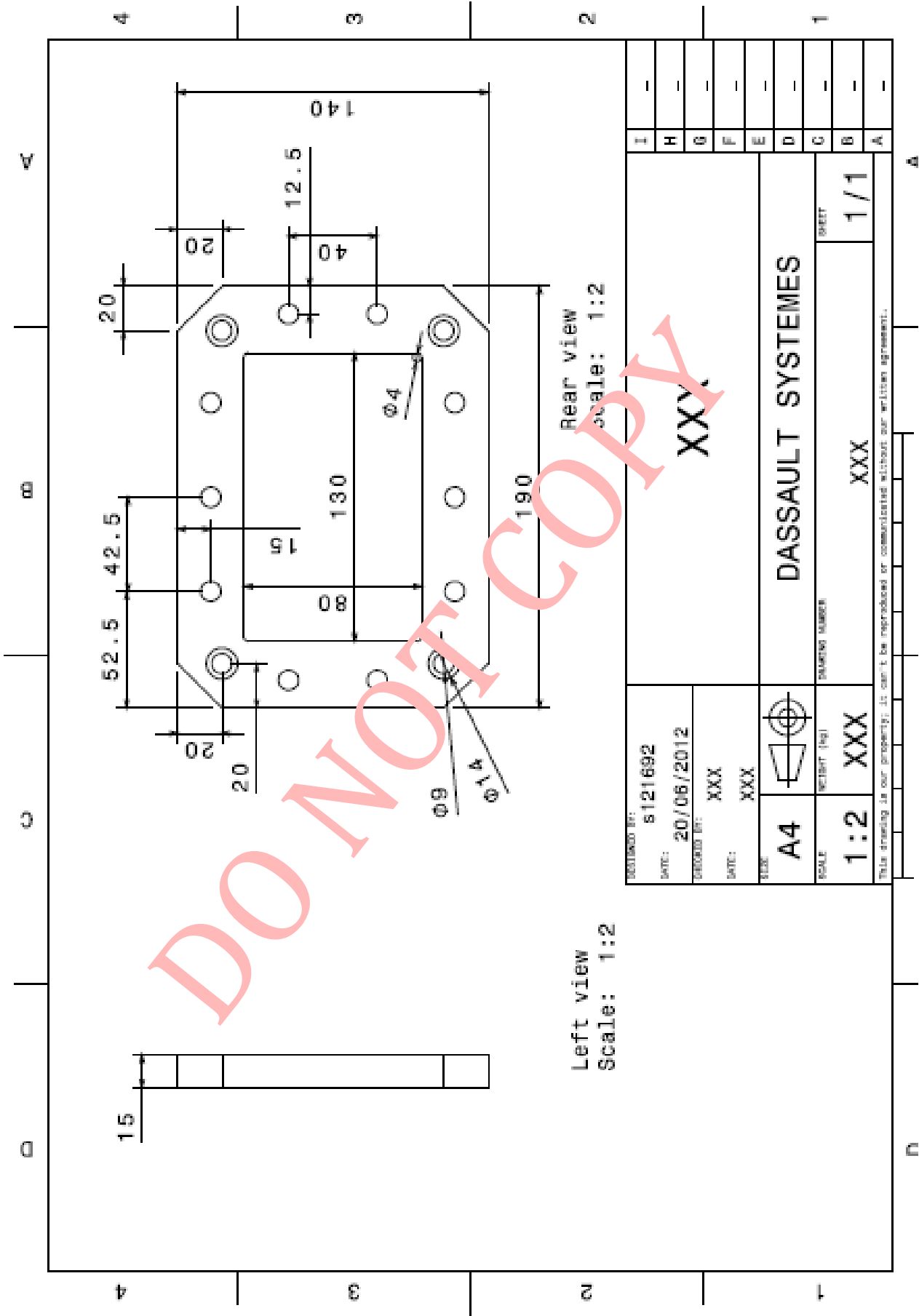
- [125] Oever, v., Bos, H. L. and van Kemenade, M. (2000), "Influence of the Physical Structure of Flax Fibres on the Mechanical Properties of Flax Fibre Reinforced Polypropylene Composites", *Applied Composite Materials*, vol. 7, no. 5, pp. 387-402.
- [126] Summerscales, J., Dissanayake, N., Virk, A. and Hall, W. (2010), "A review of bast fibres and their composites. Part 2 – Composites", *Composites Part A: Applied Science and Manufacturing*, vol. 41, no. 10, pp. 1336-1344.
- [127] Madsen, B., Thygesen, A. and Lilholt, H. (2009), "Plant fibre composites – porosity and stiffness", *Composites Science and Technology*, vol. 69, no. 7-8, pp. 1057-1069.
- [128] Madsen, B. (2004), *Properties of Plant Fibre Yarn Polymer Composites - An Experimental Study* Technical University of Denmark, Department of Civil Engineering, .
- [129] Madsen, B. and Lilholt, H. (2003), "Physical and mechanical properties of unidirectional plant fibre composites—an evaluation of the influence of porosity", *Composites Science and Technology*, vol. 63, no. 9, pp. 1265-1272.
- [130] Lamy, B. and Baley, C. (2000), "Stiffness prediction of flax fibers-epoxy composite materials", *Journal of Materials Science Letters*, vol. 19, no. 11, pp. 979-980.
- [131] Li, Y., Mai, Y. and Ye, L. (2000), "Sisal fibre and its composites: a review of recent developments", *Composites Science and Technology*, vol. 60, no. 11, pp. 2037-2055.
- [132] Virk, A. S. (2010), *Numerical models for natural fibre composites with stochastic properties* PhD Thesis, Faculty of Science and Technology, University of Plymouth;, .
- [133] Kelly, A. and Tyson, W. R. (1965), "Tensile properties of fibre-reinforced metals: Copper/tungsten and copper/molybdenum", *Journal of the Mechanics and Physics of Solids*, vol. 13, no. 6, pp. 329-350.
- [134] Facca, A. G., Kortschot, M. T. and Yan, N. (2007), "Predicting the tensile strength of natural fibre reinforced thermoplastics", *Composites Science and Technology*, vol. 67, no. 11-12, pp. 2454-2466.
- [135] Laura Peponi, Jerico Biagiotti, Jose M. Kenny and Inaki Mondragon (2008), "Statistical Analysis of the Mechanical Properties of Natural Fibres and Their Composite Materials. II. Composite Materials", *Polymer Composites*, , pp. 321-325.
- [136] Andersons, J., Poriķe, E. and Spārniņš, E. (2009), "The effect of mechanical defects on the strength distribution of elementary flax fibres", *Composites Science and Technology*, vol. 69, no. 13, pp. 2152-2157.
- [137] Facca, A. G., Kortschot, M. T. and Yan, N. (2006), "Predicting the elastic modulus of natural fibre reinforced thermoplastics", *Composites Part A: Applied Science and Manufacturing*, vol. 37, no. 10, pp. 1660-1671.

- [138] LS-DYNA (2007), "Keyword User's Manual, Version 971", *Livermore, Livermore Software Technology Corporation*, .
- [139] Hallquist, J. O. (2006), "LS-DYNA Theory Manual", *Livermore, Livermore Software Technology Corporation*, .
- [140] Schweizerhof, K., Weimar, K., Munz, T. and Rottner, T. (1998), "Crashworthiness analysis with enhanced composite material models in LS_DYNA - Merits and limits", *LS-DYNA World Conference, Detroit, Michigan, USA*, .
- [141] "EuroNCAP, Crash Test and Assessment ", (2004), vol. Protocols (www.euroncap.com).
- [142] Nassiopoulos, E. (2010), *Side impact protection systems (SIPS) for World Rally Championship cars (WRC)* Cranfield University, Cranfield.
- [143] Marklund, E, *Modeling the Mechanical Performance of Natural Fiber Composites*, Doctoral thesis, Lulea University of technology, Department of Applied physics and mechanical engineering, 2007

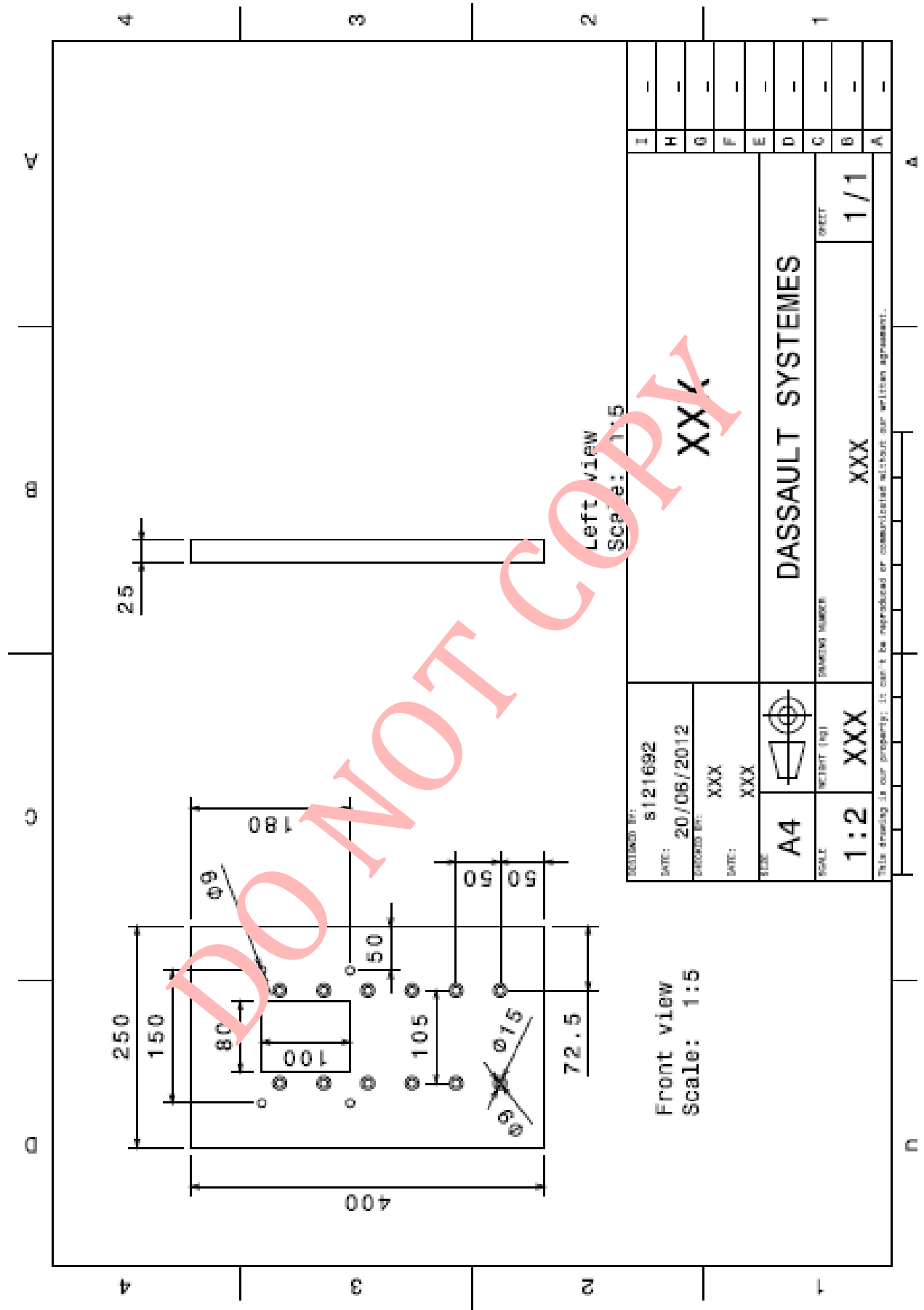
Appendix A

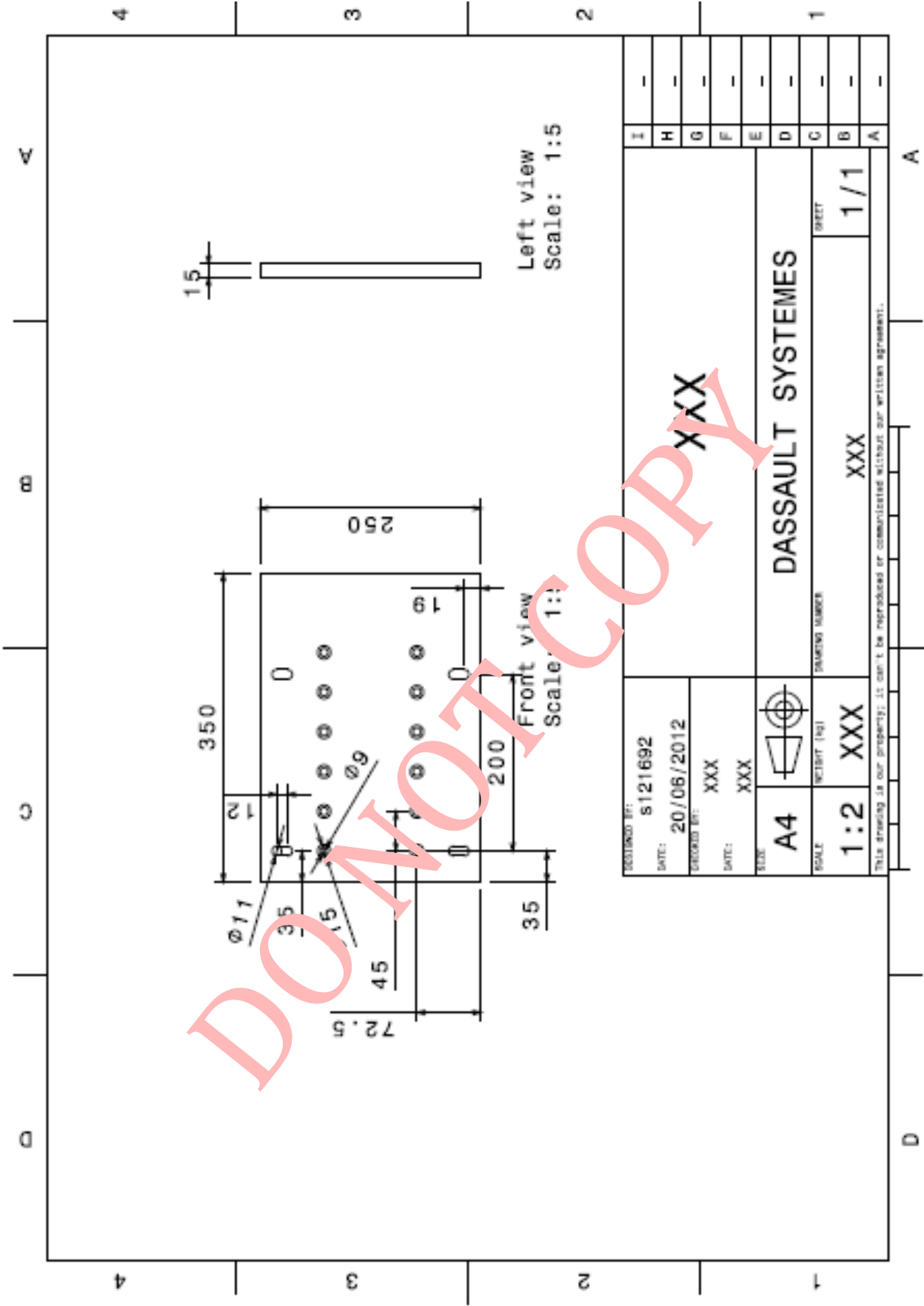
Localised impact fixture design





DO NOT COPY





Appendix B

Composite Modelling

The theories below have been developed for the intra-laminar failure of initially unidirectional materials. Each of the above criteria gives the prediction of lamina strength in one of the principal directions, with a different approach and degree of focus on the failure modes, and using different approximations.

Table 7-1: Most famous failure criteria for composite macroscopic modelling

Criterion	Comments
Maximum stress	More applicable for brittle modes of failure of the material, and does not take into account any stress interactions
Maximum strain (Hart-Smith)	Stress interactions
CHANG-CHANG	Very similar to Puck
PUCK	Separate criteria for matrix and fibre controlled failure Distinguishes three different matrix failure modes Tension and compression. Combines transverse tension-shear and compression-shear failure Fibre failure and inter-fibre failure modes
TSAI-HILL	Adaptation of the Hill criterion for anisotropic ductile metals to orthotropic composites No distinction between tensile and compressive strengths No strain rate effect
TSAI-WU	Quadratic failure criterion Continuous failure envelope Interaction of all stress components in one criterion Accounts differences between tension and compression No strain rate effect The Tsai-Wu form can only apply to moderately anisotropic systems
HASHIN	Separate criteria for matrix and fibre controlled failure Accounts differences between tension and compression Initially developed for 2D unidirectional, but modifications make it work also for other materials. In 3D the maximum stress criteria is used for the transverse normal stress component

The Chang-Chang model [59] is a stress failure criterion that distinguishes between matrix and fibre failure with combined tension and shear stresses. The initial model was designed for a 2D failure criterion for unidirectional composite lamina and arbitrary oriented ply laminates. It can be, however, modified and used for non-unidirectional composites.

Matrix failure:

$$\left(\frac{\sigma_{22}}{Y_T}\right)^2 + \frac{\frac{\tau_{12}^2}{2G_{12}} + \frac{3}{4}a\tau_{12}^4}{\frac{S_{12}^2}{2G_{12}} + \frac{3}{4}aS_{12}^4} = e_M^2, \quad (1)$$

where α is a constant to be determined experimentally, and Y_T and S_{12} are the transverse tensile strength and the in-situ lamina shear strength respectively. The matrix failure criterion states that when in a lamina the stresses σ_{22} and τ_{12} satisfy the above equation ($e_M \geq 1$), matrix cracking occurs. For the case of linear elastic behaviour $a=0$ and equation 10 can be simplified as follows:

$$\left(\frac{\sigma_{22}}{Y_T}\right)^2 + \left(\frac{\tau_{12}}{S_{12}}\right)^2 = e_M^2 \quad (2)$$

Fibre failure:

$$\left(\frac{\sigma_{11}}{X_T}\right)^2 + \frac{\frac{\tau_{12}^2}{2G_{12}} + \frac{3}{4}a\tau_{12}^4}{\frac{S_{12}^2}{2G_{12}} + \frac{3}{4}aS_{12}^4} = e_f^2 \quad (3)$$

The fibre failure criterion states that when in a lamina the stresses σ_{11} and τ_{12} satisfy the criterion ($e_f \geq 1$) the lamina fails either by fibre cracking or fibre matrix shearing. With $a=0$, the equation can be again simplified.

Tsai-Wu [54; 60] is a generally easy criterion to apply, with again quadratic failure which considers the total strain energy (both distortion energy and dilatation energy) for predicting failure and distinguishes between compressive and tensile failure strengths. The Tsai-Wu failure criterion is more a mathematical than a physical concept, or as often referred to just a 'curve fitting' model. As a specialization of the general quadratic failure criterion proposed by Gol'denblat and Kopnov [61], its general form is a potential function, expandable into a power series, as shown below.

$$F_{ij}\sigma_i\sigma_j + F_i\sigma_i = 1, \quad (4)$$

where $i, j=1,2,\dots,6$ and F_i, F_{ij} are functions of the strength parameters of the material. For an orthotropic or transversely isotropic material in two dimensional stress states, equation 14 can take the form:

$$\frac{\sigma_{11}^2}{X_T X_c} + \frac{X_c - X_T}{X_T X_c} \sigma_{11} + \frac{\sigma_{22}^2}{Y_T Y_c} + \frac{Y_c - Y_T}{Y_T Y_c} \sigma_{22} + \frac{2\beta \sigma_{11} \sigma_{22}}{\sqrt{X_T X_c Y_T Y_c}} = \begin{cases} \geq 1 & \text{failure} \\ < 1 & \text{no failure} \end{cases} \quad (5)$$

The form and values of the interaction term (F_{12} , described here in the last term of the equation above), would usually require a biaxial test, which is usually very difficult to perform. However, an empirical form is used, as described above, with β being in the range $-1 \leq \beta \leq 0$. Other failure criteria, such as the Tsai-Hill or Hoffman [54; 62], share the exact same background, with the only difference on the interaction parameter (F_{12}).

$$\left(\frac{\sigma_{22}}{Y_c Y_T}\right)^2 + \left(\frac{\tau_{12}}{S_{12}}\right)^2 + \frac{(Y_c - Y_T)\sigma_{22}}{Y_c Y_T} = \begin{cases} \geq 1 & \text{failure} \\ < 1 & \text{no failure} \end{cases} \quad (6)$$

Hashin [63] introduced a quadratic criterion with four failure modes, including fiber and matrix failure criteria, which distinguish tensile and compressive failure [62; 64]. Although the Hashin criteria were developed for unidirectional laminates, they have been also successfully applied to progressive failure analyses of laminates [65]. The criterion can be extended to three dimensional problems, where the maximum stress criterion is used for the transverse normal stress component. The failure modes included in Hashin's criteria are as follows:

Tensile fibre failure:

$$\left(\frac{\sigma_{11}}{X_T}\right)^2 + \frac{\tau_{12}^2 + \tau_{13}^2}{S_{12}^2} = \begin{cases} \geq 1 & \text{failure} \\ < 1 & \text{no failure} \end{cases} \quad (7)$$

Compressive fibre failure:

$$\left(\frac{\sigma_{11}}{X_c}\right)^2 = \begin{cases} \geq 1 & \text{failure} \\ < 1 & \text{no failure} \end{cases} \quad (8)$$

Tensile matrix failure:

$$\left(\frac{\sigma_{22}+\sigma_{33}}{Y_T}\right)^2 + \frac{\tau_{23}^2-\sigma_{22}\sigma_{33}}{S_{23}^2} + \frac{\tau_{12}^2+\tau_{13}^2}{S_{12}^2} = \begin{cases} \geq 1 & \text{failure} \\ < 1 & \text{no failure} \end{cases} \quad (9)$$

Compressive matrix failure:

$$\left[\left(\frac{Y_c}{2S_{23}}\right)^2 - 1\right] \left(\frac{\sigma_{22}+\sigma_{33}}{Y_c}\right) + \frac{(\sigma_{22}+\sigma_{33})^2}{4S_{23}^2} + \frac{\tau_{23}^2-\sigma_{22}\sigma_{33}}{S_{23}^2} + \frac{\tau_{12}^2+\tau_{13}^2}{S_{12}^2} = \begin{cases} \geq 1 & \text{failure} \\ < 1 & \text{no failure} \end{cases} \quad (10)$$

Apart from the above criteria, many other criteria are available in the open literature, together with many attempts to clarify and collect them. Analytical description of these theories can be found in composite handbooks and several publications.

Damage

The formation of failure (crack) in a lamina is referred to as “first failure”, while the material behaviour beyond this point as “post failure” behaviour. Damage mechanics aim to describe the material response in the post failure region, caused by the evolving damage state. “Damage” or “damaging” is called the degradation of the elastic properties of a composite governed by gradual accumulation of micro-cracks, which cause material softening, but do not lead immediately to failure in a macro-level. The study of damage mechanics is of no interest when the target is static elastic and in the case of the design of components with appropriate strength and stiffness for a particular job. On the other hand, however, when impact performance and crashworthiness of materials is studied, the effect of damaging cannot be neglected, and its accurate prediction is necessary.

Damage mechanics can be studied at the macro-, meso- or micro- scale [55]. However, the macro-scale fails to exactly represent the damaging causes. The meso-scale approach, when the ply becomes the basic unit, seems to be the most promising, as property degradation generally appears inside the plies as transverse cracking and fibre breakage, or between the plies as delamination. Specific damage mechanisms at the

microscopic level, such as fibre/matrix debonding, or matrix cracking, are not individually identified, but are considered as stiffness loss and plastic strain accumulation. Many theories have been developed, two of which are the Chang-Chang damage model, and the theory of Ladevèze.

Chang and Chang [59] proposed a model based on their failure criterion. The model is a property reduction model developed for 2 dimensional composite laminates with arbitrary ply orientation. The mathematical approach is based on the Weibull distribution with an exponential form as presented below.

$$\frac{E_x^d}{E_x} = \exp\left[-\left(\frac{A}{A_0}\right)^\beta\right] \quad (11)$$

$$\frac{G_x^d}{G_x} = \exp\left[-\left(\frac{A}{A_0}\right)^\beta\right], \quad (12)$$

where E_x^d, G_x^d are the reduced (degraded) tensile and shear moduli respectively, A is the damage zone predicted by the failure criteria, and A_0 is the fibre failure interaction zone associated with the measured ply tensile strength. The parameter β is the Weibull shape parameter for the degradation of the specific property.

The Ladevèze model [66] makes use of scalar damage functions, d_{ij} , that take values from 0, for no damage, to 1 for the fully damage properties. These functions are introduced as multipliers into the stiffness (K) or the compliance matrix ($C=K^{-1}$), in order to soften the matrix modulus – tensile and shear – of the material. The compliance matrix for a thin transversely orthotropic material looks then as follows:

$$[C] = \begin{bmatrix} C_{11}^0 & \nu_{21}^0 C_{11}^0 & 0 & 0 & 0 \\ \nu_{21}^0 C_{11}^0 & C_{22}^0(1 - d_{22}) & 0 & 0 & 0 \\ 0 & 0 & G_{12}^0(1 - d_{12}) & 0 & 0 \\ 0 & 0 & 0 & G_{23}^0(1 - d_{12}) & 0 \\ 0 & 0 & 0 & 0 & G_{12}^0(1 - d_{12}) \end{bmatrix} \quad (13)$$

For the parameters d_{ij} Ladevèze [57; 66; 67] assumed a linear damage function, according to which:

$$d_{ij} = f(\bar{Y}) = \begin{cases} \frac{\bar{Y} - \bar{Y}_{22}^0}{\bar{Y}_{22}^c} & \text{if } (\bar{Y} > \bar{Y}_{22}^0) \\ \mathbf{0} & \text{otherwise} \end{cases} \quad (14)$$

where \bar{Y} is a coupling expression describing shear and transverse damage progression. This expression is based on two individual damaging functions, extracted from partial derivation of the damaged elastic work.

$$\bar{Y}(t) = \sup_{\tau \leq t} (\sqrt{Y_{12}(\tau) + bY_{22}(\tau)}) \quad (15)$$

$$Y_{12} = \frac{1}{2} \{ \mathbf{G}_{12}^0 [(\boldsymbol{\gamma}_{12}^e)^2 + (\boldsymbol{\gamma}_{13}^e)^2] + \mathbf{G}_{23}^0 (\boldsymbol{\gamma}_{23}^e)^2 \} \quad (16)$$

$$Y_{22} = \frac{1}{2} \mathbf{C}_{22}^0 (\langle \boldsymbol{\nu}_{12}^0 \boldsymbol{\varepsilon}_{11}^e + \boldsymbol{\varepsilon}_{22}^e \rangle_+)^2 \quad (17)$$

Appendix C

PCB 208C05 Load Cell Specifications

Appendix C

FE Modeling – Software selection

In this thesis, LS-DYNA was used for the static and dynamic modeling, using mainly a macroscopic approach, where the composite material was treated as a homogenous material.

The FE (Finite Element) code LS-DYNA is designed to solve large deformation structural dynamics. The main solution methodology is based on explicit time integration, while an implicit solver is currently available. LS-DYNA has a library of over 200 material models, including metals, plastics, foams, honeycombs and fluids, a large variety of elements, including beams, shells and solids, and a large number of contact algorithms to simulate impact interactions (sliding with friction, gaps, etc.). It appeals strongly to the automotive industry, because of its specialist modelling features like the airbags, spot welds, seatbelts and numerous material failure methods that enable detailed crashworthy analysis. For these reasons, and for its ability to perform both explicit and implicit analysis, LS-DYNA is among the best options for non-linear dynamic simulations; hence it is used in this work.

A wide range of material models for composite materials are available in LS-DYNA, each with a number of differences and approximations. Table 7-2 summarizes the available models.

All LSDYNA models are based on the macro-scale approach, with the possibility to include failure modes and damage from the meso-scale. MAT 22 and MAT 54 provides Chang-Chang fiber and matrix failure modes. Material MAT 54 describes anisotropic, linear elastic behavior, followed by nonlinearities introduced from various damage criteria. Failure due to out of plane shear and normal stresses is neglected. MAT 58 is based on the Hashin criteria and continuum damage mechanics. It is implemented only for shell elements and does not consider strain rate effects. However, this material model can be used in the initial design stage due to rather small amount of material properties and input information needed. MAT 59, is the only elasto-plastic material, but it does not support strain rate effects or damage. MAT 161 is a composite lamina model based on 3D stresses field, which can be used to effectively simulate fiber failure, matrix damage and delamination behavior. In order to account for the experimentally observed nonlinear and rate dependent behavior, a general rate dependent progressive failure model has been developed. Disadvantages of this material model are the fact that

it applies only for solid elements and needs a quite large number of material properties input, not easily accessed by standard material testing. MAT 161 needs also the purchase of a special license to be available with LSDYNA.

Table 7-2: Available composite models in LS-DYNA

Material Model		Shell elements	Solid elements	Strain rate	Damage	Behaviour	Failure Criteria
Code	Name						
MAT 22	Composite Damage	✓	✓			elastic	Chang-Chang
MAT 54	Enhanced Composite Damage	✓			✓	elastic	Chang-Chang
MAT 55	Enhanced Composite Damage	✓			✓	elastic	Tsai-Wu
MAT 58	Laminated composite Fabric	✓			✓	elastic	Hashin
MAT158	Rate sensitive composite Fabric	✓		✓	✓	elastic	Hashin
MAT 59	Composite Failure	✓	✓			elasto-plastic	Similar to Tsai-Wu
MAT 116	Composite Layup					elastic	No failure
MAT 117	Composite Matrix	✓				elastic	No failure
MAT 118	Composite Direct	✓				elastic	No failure
MAT 161	Composite MSC		✓	✓	✓		Hashin (delamination)

As pre-processor, ANSA software was used. ANSA is a powerful pre-processing tool that provides all the necessary functionalities for full-model build up, from computer-aided design (CAD) data to ready-to-run solver input file, in a single integrated environment. It provides a variety of data import options to facilitate the treatment of models, built with different software, as well as several input cards, organized in different template options to realize models for a wide range of solvers (NASTRAN, LS-DYNA, Abaqus and others). All CAD files and drawings were designed in this work using CATIA v5.